Coordination Chemistry Reviews 253 (2009) 1759–1792

Contents lists available at ScienceDirect

Coordination Chemistry Reviews

journal homepage: www.elsevier.com/locate/ccr

Review

Aliphatic and aromatic carboxylate divalent metal coordination polymers incorporating the kinked and hydrogen-bonding capable tethering ligand 4,4′-dipyridylamine

Robert L. LaDuca*

Lyman Briggs College and Department of Chemistry, Michigan State University, East Lansing, MI 48825, USA

Contents

ARTICLE INFO

Article history:
Received 26 July 2008
Accepted 18 January 2009
Available online 31 January 2009

Keywords:
Coordination polymer
Dicarboxylate
Aliphatic
Aromatic
Dipyridylamine
Crystal structure
Magnetism
Luminescence
Interpenetration
Self-penetration

ABSTRACT

Numerous functional coordination polymer solids with diverse topologies have been constructed using the rigid rod tethering ligand 4,4′-bipyridine (4,4′-bpy). In contrast, the underlying structural topologies of coordination polymers based on the related diimine 4,4′-dipyridylamine (dpa) are often significantly different, due to its kinked donor disposition and hydrogen-bonding capability. In this review we discuss many of the divalent metal carboxylate/dpa dual-ligand coordination polymer phases recently prepared in our laboratory. One-, two- and three-dimensional structures with varying degrees of interpenetration have been observed; several unprecedented self-penetrated network topologies were generated. Synergistic interactions between metal coordination geometry, carboxylate donor disposition and binding mode and hydrogen bonding patterns mediated by the central amine of the dpa ligands play an important role in structure direction in this coordination polymer system.

1. Introduction

Over the past decade, a focused research effort has been extended towards the synthesis and characterization of metal–organic coordination polymers because of their potential utility in hydrogen storage [1], molecular shape-selective

* Correspondence address: Lyman Briggs College, E-30 Holmes Hall, Michigan State University, East Lansing, MI 48825, USA. Tel.: +1 517 432 2268.
E-mail address: laduca@msu.edu.

0010-8545/$ – see front matter © 2009 Elsevier B.V. All rights reserved.
doi:10.1016/j.ccr.2009.01.025

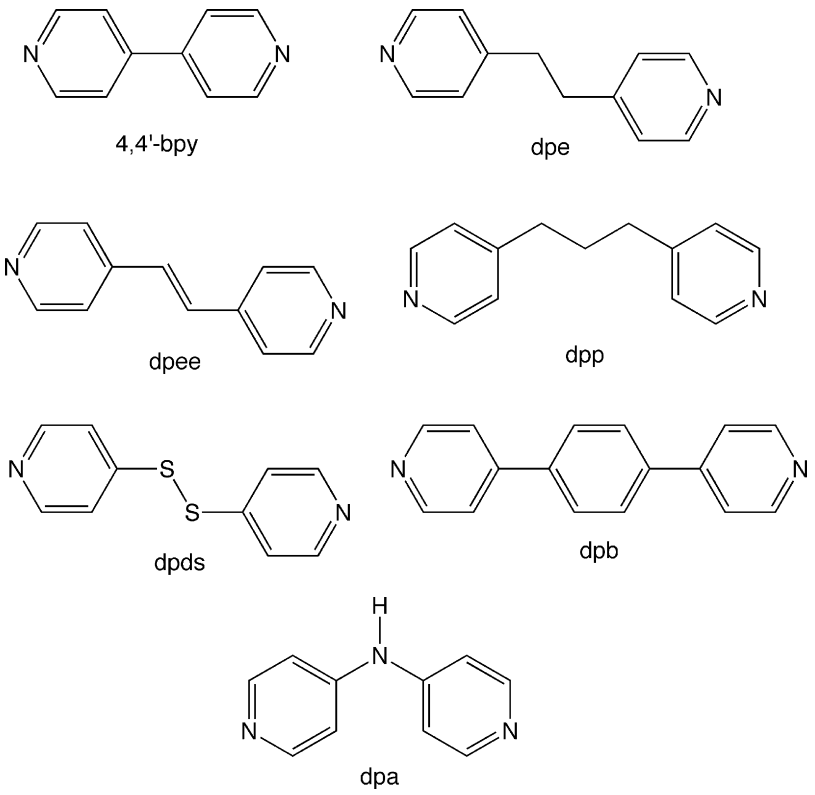

Scheme 1.

separations [2], ion exchange [3], catalysis [4], non-linear optics [5], and luminescent applications [6]. Most of the phases within this burgeoning genre of materials contain multitopic anionic carboxylate ligands, which can covalently conjoin cationic metal nodes while simultaneously supplying the necessary charge balance for the construction of neutral phases. Thus, the incorporation of porosity-curtailing counterions can be avoided, maximizing the potential for the preparation of a functional open-framework coordination polymer material. Despite the thousands of structurally characterized coordination polymers reported in the literature, deliberate design of particular structural motifs tailored to specific end-use applications remains a desired yet elusive goal. Exploratory synthesis continues to be the driving force for the discovery of novel structural types and intriguing structure–property relationships.

An extremely diverse range of structural motifs occurs within the purview of multitopic carboxylate-based coordination polymer solids, predicated on the disposition of the donor atoms within the organic moieties, conformational changes within flexible side chains, and critically, the coordination geometry preferences of the specific metal cations employed. The structural diversity and property applications of coordination polymers have been recently expanded by the incorporation of the neutral tethering diimine 4,4′-bipyridine (4,4′-bpy) [7–9]. For example, the 2D phase {[Zn(isophthalate)(4,4′-bpy)(H_2O)]·1.5H_2O} [8a] and the double layered solid {[Zn(isophthalate)(4,4′-bpy)$_2$(H_2O)][Zn(isophthalate)(4,4′-bpy)]·0.25 H_2O} [8b] have potential use as blue luminescent materials. Intriguingly, the interpenetrated 3D coordination polymer [Zn(terephthalate)(4,4′-bpy)$_{0.5}$] can chromatographically separate branched and linear hydrocarbons [2b], garnering the interest of petrochemical industry.

A plethora of coordination polymers incorporating 4,4′-bpy has been prepared, bringing Zaworotko to remark that it is "the C–C bond of crystal engineering" [10]. A variety of other dipodal nitrogen-base tethering co-ligands have also been utilized in expanding the scope of coordination polymer structure types (Scheme 1), such as di-4-pyridylethane (dpe) [11], di-4-pyridylethylene (dpee) [12], di-4-pyridylpropane (dpp) [13], 4,4′-dipyridyldisulfide (dpds) [14] and 1,4-di-4-pyridylbenzene (dpb) [15]. Nevertheless, dipyridyl linking ligands with short, hydrogen-bonding capable tethers, such as 4,4′-dipyridylamine (dpa), have not been as extensively studied as neutral scaffolds for the construction of divalent metal dicarboxylate coordination polymers.

For about a decade our group has been investigating the synthesis and characterization of coordination polymers containing dpa, which can be relatively easily prepared by the thermally induced coupling of pyridine and 4-aminopyridine with PCl_3 [16]. In contrast to 4,4′-bpy, dpa possesses a kinked disposition of its terminal nitrogen donor atoms as well as a potential hydrogen bonding point of contact, allowing it to aggregate coordination polymer subunits via supramolecular as well as covalent interactions.

Our first exploratory synthetic forays with dpa involved the preparation of mixed metal molybdates and vanadates [17–20]. For example, {[$CuMoO_4$(dpa)$_2$]·2H_2O}$_n$ possesses unique 2D copper molybdate layers strutted by dpa tethers [14], and [$NiMoO_4$(dpa)$_2$] has a "starburst" 3D structure formed by molybdate-linked cationic [Ni(dpa)$_2$]$_n^{2n+}$ layers [20]. The coordination polymer chemistry of dpa has been extended into monovalent silver and divalent cadmium oxoanion and pseudohalide systems by Hanton and colleagues [21–23]. Over the past three years we have focused our synthetic investigations on divalent metal carboxylate coordination polymers incorporating dpa, wherein metal coordination geometry, carboxylate binding mode and conformation, and dpa-based covalent and supramolecular hydrogen bonding patterns all play a synergistic role in structure direction. This review intends to summarize our recent successes in preparing one-, two- and three-

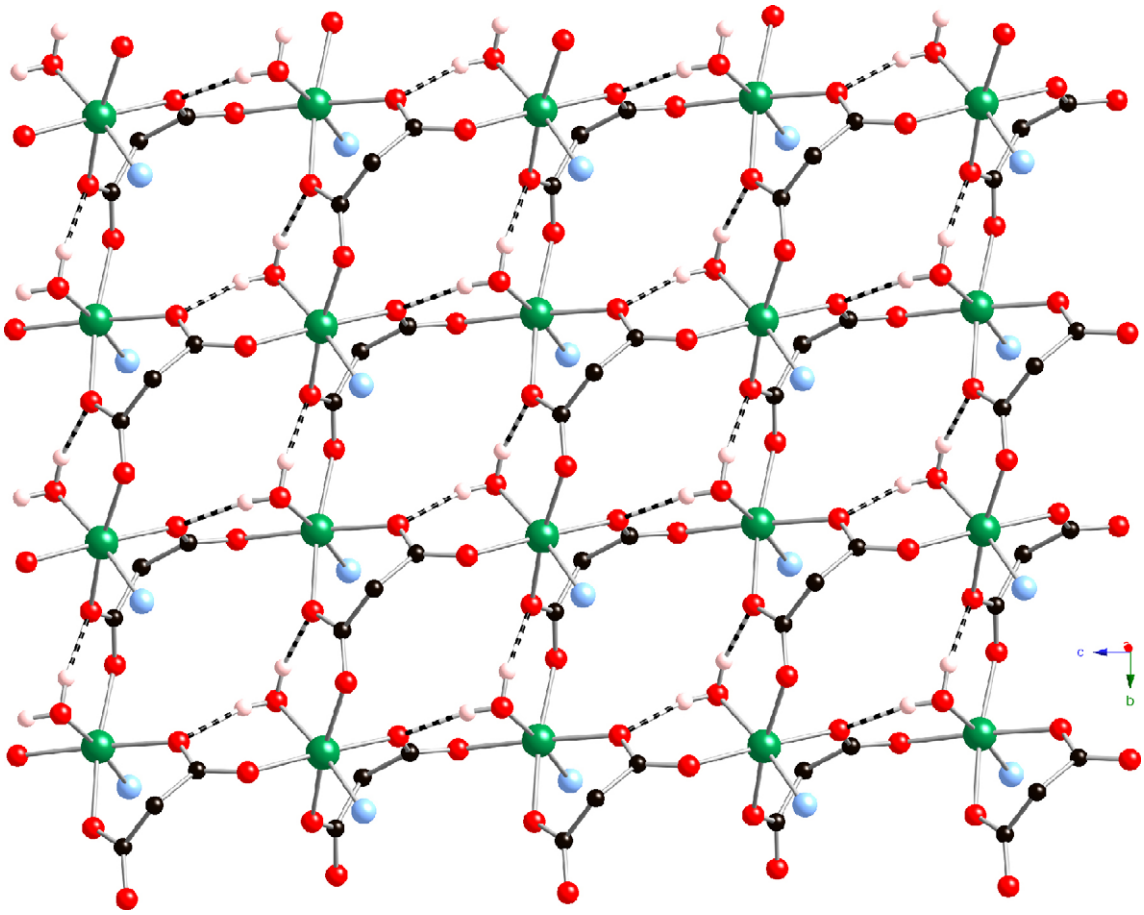

Fig. 1. View down *a* of the (4,4)-grid-like $[Ni_2(malonate)_2(H_2O)]_n$ layer motif in **1–Ni**. A similar pattern exists in **1–Co**. Hydrogen bonding is indicated as dashed lines. Adapted from Ref. [24].

dimensional divalent metal carboxylate coordination polymers built from 4,4′-dipyridylamine, many with rare or unprecedented structural topologies, and some with tantalizing hints of functional behavior.

2. Aliphatic dicarboxylate dpa-containing coordination polymers

2.1. Malonate/dpa coordination polymers

Hydrothermal reaction of a mixture of cobalt or nickel chloride, malonic acid, and dpa generated a pair of isostructural coordination polymers with a general formulation of $\{[M_2(malonate)_2(dpa)(H_2O)_2]\cdot 2H_2O\}$ (M = Co, **1–Co**; M = Ni, **1–Ni**) [24] as violet and green crystals, respectively. X-ray diffraction showed that the coordination geometry in both **1–Co** and **1–Ni** is a distorted $\{MO_5N\}$ octahedron, where the equatorial planes contain two mutually *cis* oxygen atoms belonging to a 1,3-chelating malonate ligand, and two other mutually *cis* oxygen atoms, each part of two other malonate ligands. The coordinated water molecule and the nitrogen donor from the dpa ligand occupy the *trans* axial positions.

The 1,3-chelating malonate ligand results in $\{MOC_3O\}$ "boat"-conformation six-membered rings. Each of the other two malonate oxygen atoms not involved in chelation connects to a different cobalt atom. Therefore each individual malonate ligand is exotridentate. In turn, each metal atom conjoins to three sets of two others through the carboxylate bridges of the malonate ligands to

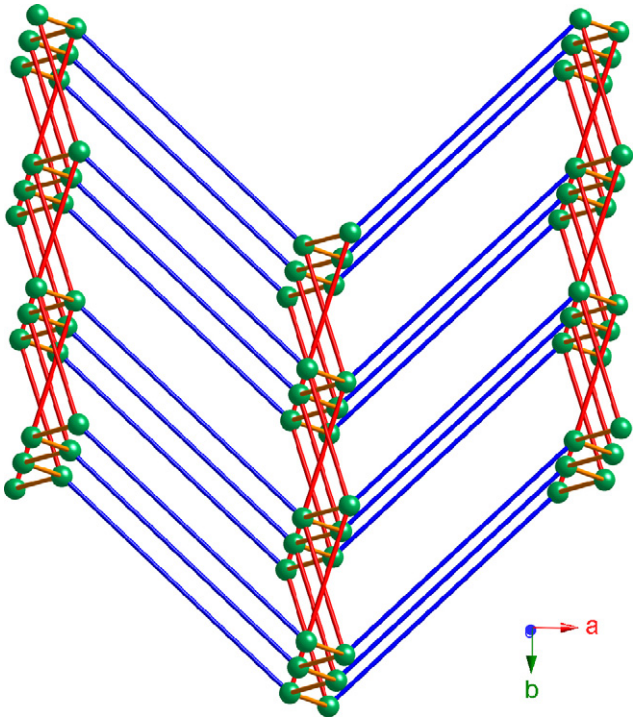

Fig. 2. Network perspective of the 5-connected 3D $4^4 6^6$ topology **sqp** coordination polymer connectivity in **1–Co** and **1–Ni**. Adapted from Ref. [24].

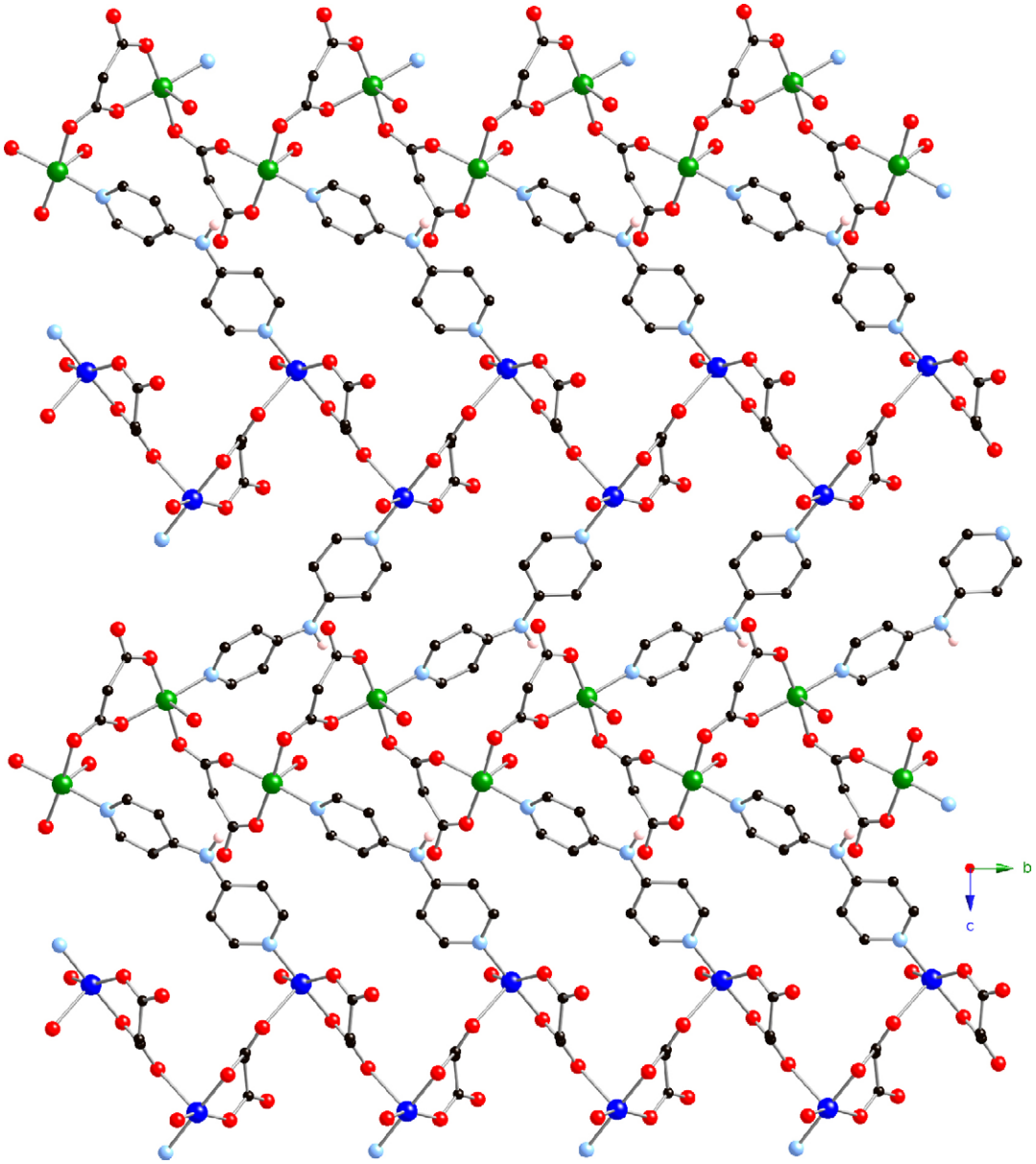

Fig. 3. Face-on view of a $[Cu_2(malonate)_2(dpa)(H_2O)_2]_n$ 2D layer in **2**. Adapted from Ref. [27].

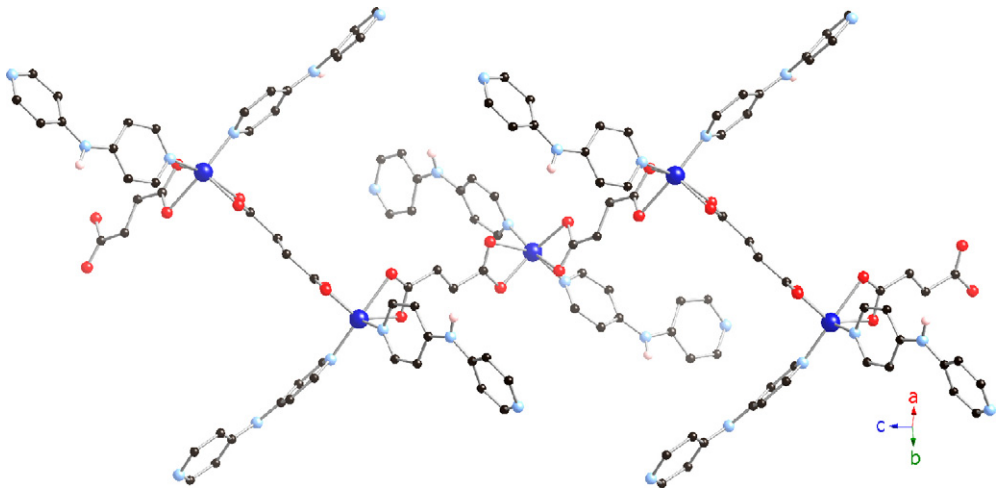

Fig. 4. A single neutral $[Co(suc)(dpa)_2]_n$ threefold helix in **3**. Adapted from Ref. [33].

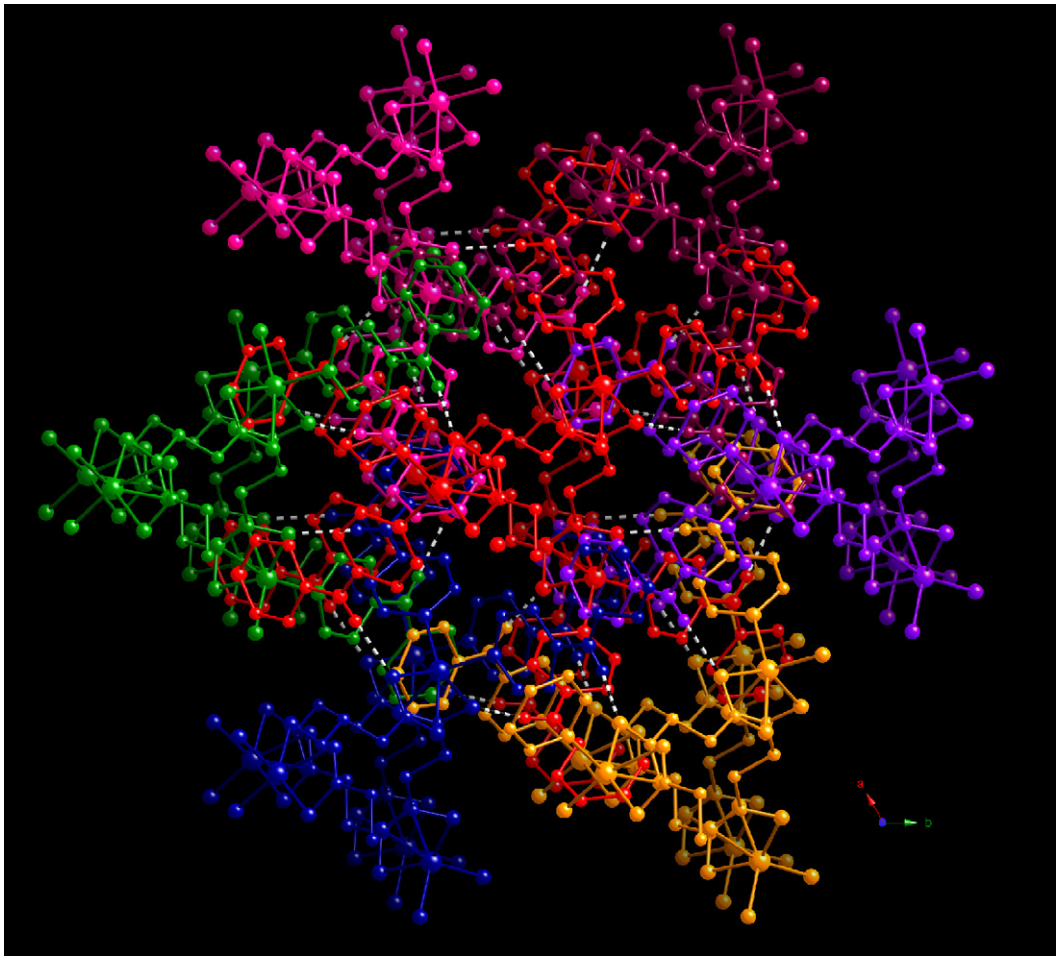

Fig. 5. View down *c* of **3** showing hydrogen bonding between neighboring helical chain motifs as dashed lines. Adapted from Ref. [33].

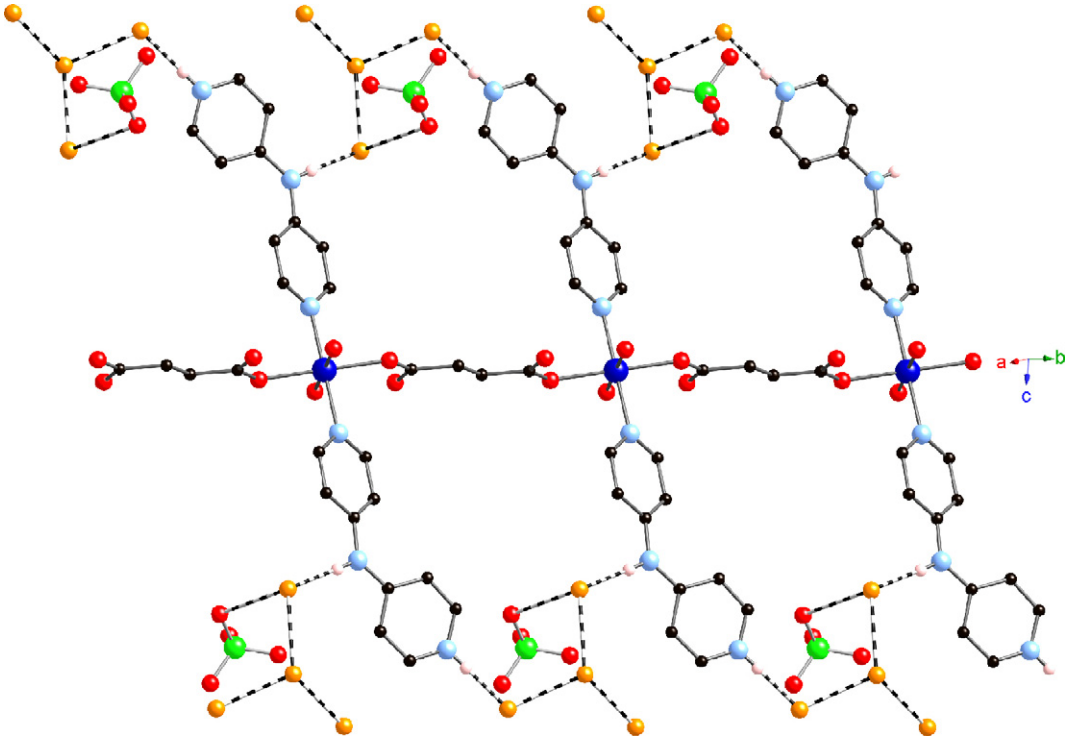

Fig. 6. A single chain motif in **4**, with neighboring perchlorate ions and water molecules of crystallization shown. Hydrogen bonding is indicated as dashed lines. Adapted from Ref. [35].

construct a ruffled 2D (4,4)-grid-like $[M_2(malonate)_2(H_2O)_2]_n$ layer motif (Fig. 1).

The 2D $[M_2(malonate)_2(H_2O)_2]_n$ layers are stacked in an *ABAB* pattern and are covalently linked by means of the dipodal dpa tethering ligands, establishing a 5-connected 3D coordination polymer net with 4^46^6 topology in each case (**sqp** lattice, Fig. 2). Interestingly, the dpa ligands in **1–Co** and **1–Ni** adopt twisted conformations in response to the supramolecular environment, resulting in crystallization in the acentric space group *Aba2*. In contrast, the 4,4′-bpy analog of **1–Co**, which also adopts a **sqp** lattice, crystallizes in a centrosymmetric space group because of the lack of the central kink in the imine tether [25]. The central amine groups of the dpa ligands in **1–Co** and **1–Ni** engage in hydrogen bonding to the water molecules of crystallization, held within incipient voids in the structures comprising 12.9 and 14.0% of the unit cell volumes, respectively.

Although their structures are very similar, the variable temperature magnetic susceptibility behavior of **1–Co** and **1–Ni** are quite different. The data for **1–Co** and **1–Ni** were both fit to Lines' expression for a 2D quadratic lattice [26]. For **1–Co**, the value of J was $-1.05(8)\,cm^{-3}$, indicating intralayer antiferromagnetic coupling. On the other hand the unpaired spins in **1–Ni** couple in a ferromagnetic fashion ($J = 0.289(1)\,cm^{-3}$). The divergent magnetic behavior was ascribed to population of different magnetic *d* orbitals.

While a copper malonate/dpa phase could not be prepared via hydrothermal techniques, slow diffusion of an aqueous solution of copper malonate with an ethanolic solution of dpa at room temperature resulted in the deposition of blue blocks of $\{[Cu_2(malonate)_2(dpa)(H_2O)_2]\cdot H_2O\}$ (**2**) [27]. Although the stoichiometry of **2** is virtually identical to that of **1–Co** and **1–Ni**, its structure and dimensionality are different because of the alteration of the coordination environment at the divalent metal ion.

The structure of **2** contains two different $[Cu(malonate)]_n$ chains. One consists of very distorted ($\tau = 0.34$ [28]) $\{CuO_4N\}$ square pyramids linked by bis-bridging malonate ligands in an *anti–anti* binding mode. The other consists of virtually ideal $\{CuO_4N\}$ square pyramids linked by bis-bridging malonate ligands in a *syn–anti* binding mode. These chain patterns alternate and are linked by bridging dpa ligands to form a 2D (6,3) herringbone layer (Fig. 3). Compound **2** represents only the second observed case of two different copper malonate bridging modes in the same coordination polymer [29]. The 4,4′-bpy analog of **2** is also a 2D coordination polymer, but with a much more common (4,4)-grid topology [30].

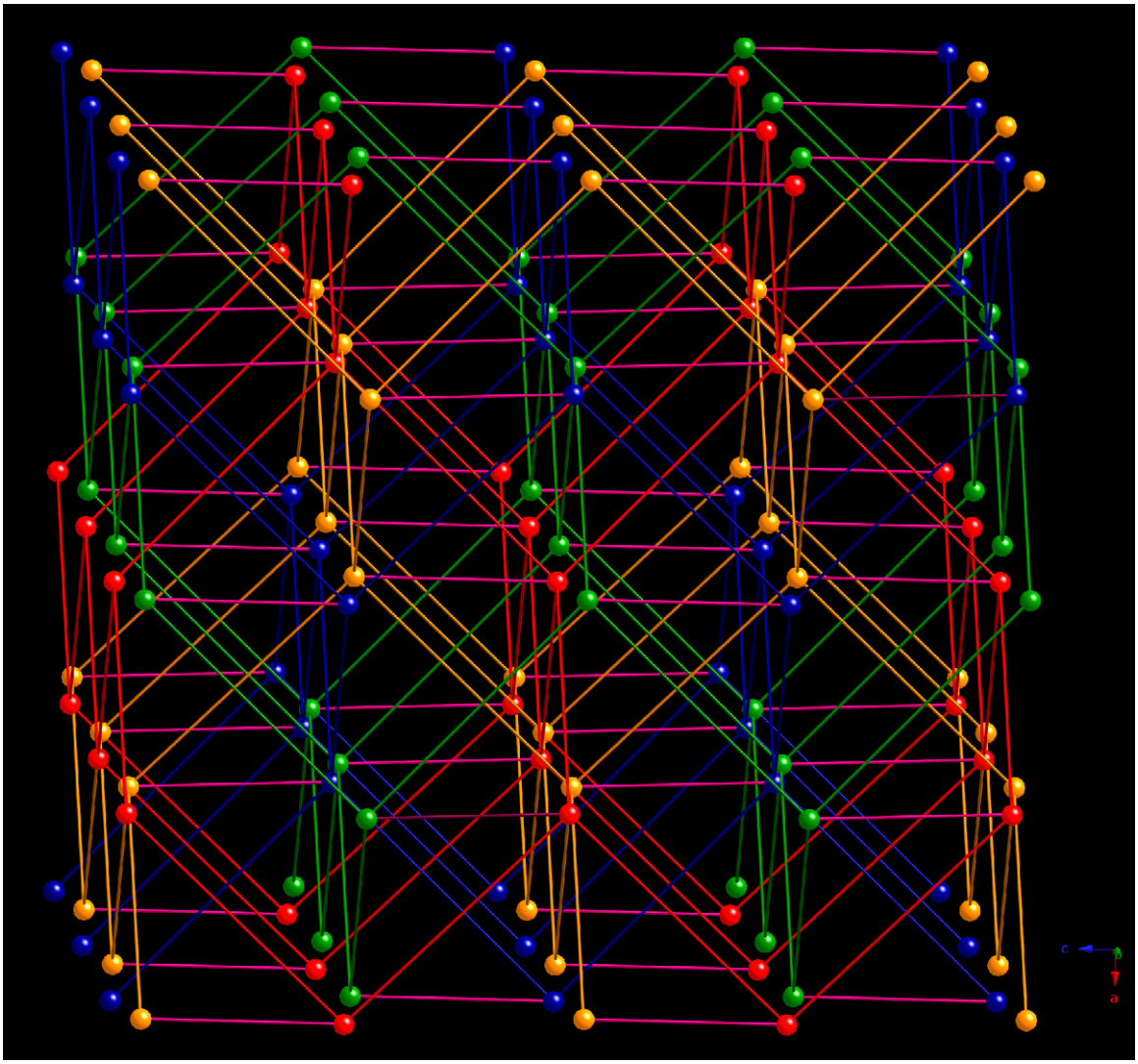

Fig. 7. Framework perspective of **5** showing the quadruply interpenetrated $[Ni(dpa)_2]_n^{2n+}$ diamondoid lattices linked into a self-penetrated cationic 6^{10} 5-connected network through succinate ligands. Each lattice is shown in a different color. Linking succinate groups are shown in pink. Chloride ions occupying the incipient voids are omitted for clarity. Adapted from Ref. [33].

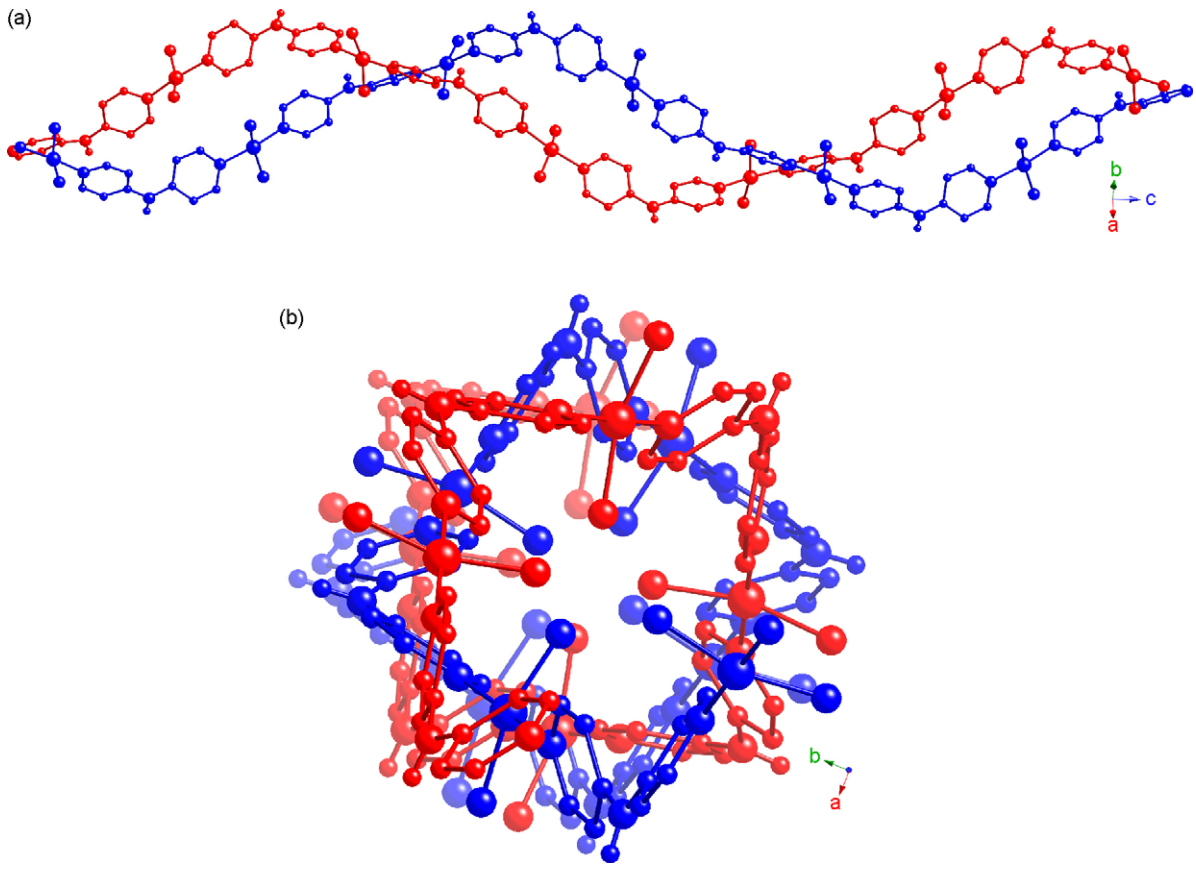

Fig. 8. (a and b) Side-on and end-on perspectives of a double $[Cu(dpa)]_{2n}^{4n+}$ fourfold helix in **6**. Adapted from Ref. [33].

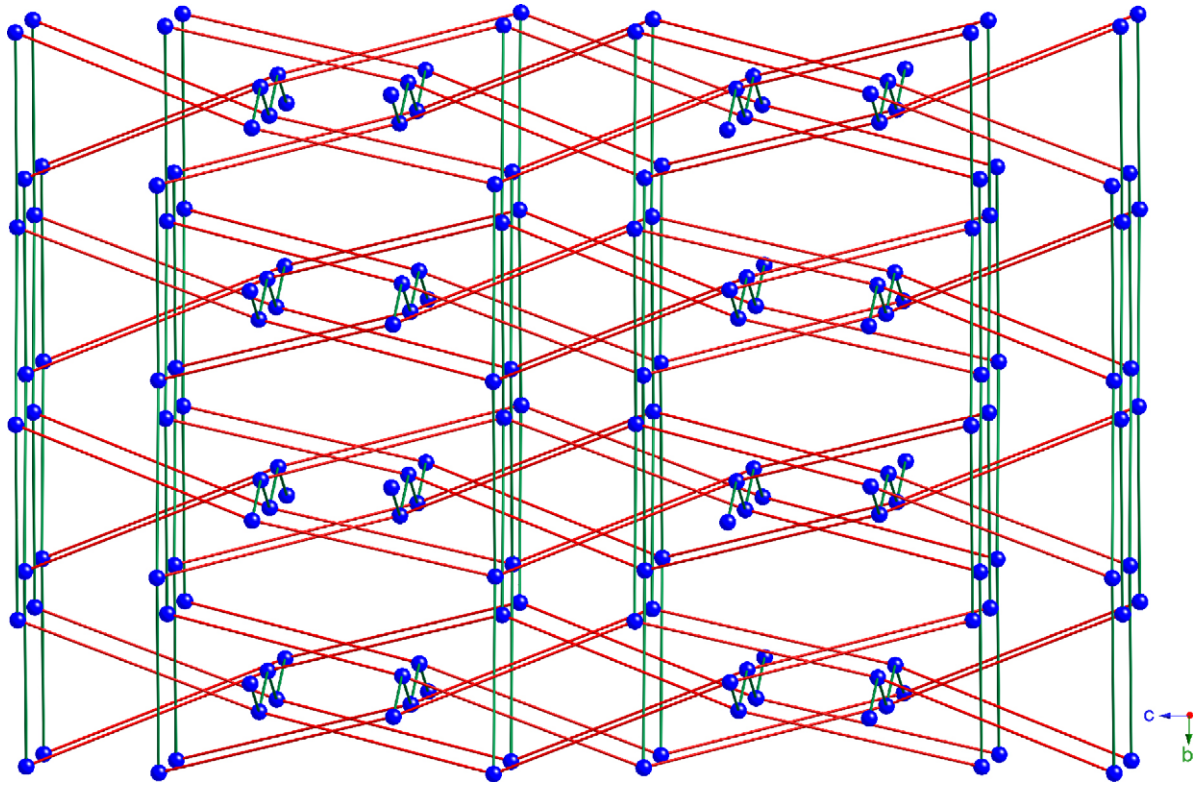

Fig. 9. Framework perspective of the doubly interpenetrated $6^5 8$ topology $CdSO_4$-type structure of **6**. Adapted from Ref. [33].

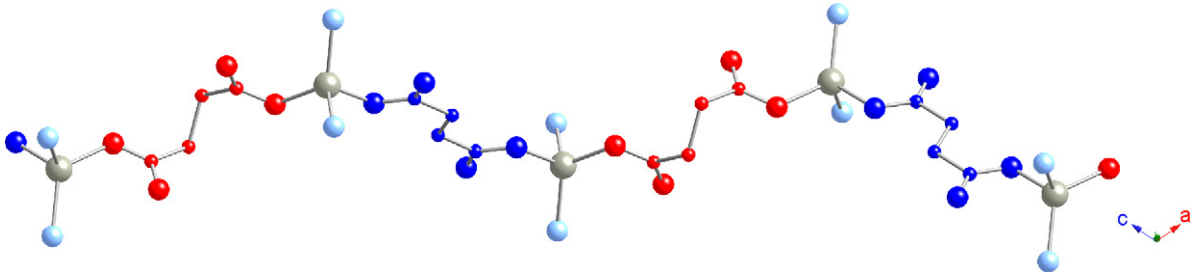

Fig. 10. A single $[Zn(suc)]_n$ chain motif in **7**. The *gauche* and *anti* conformation succinate ligands are in red and blue, respectively. Adapted from Ref. [33].

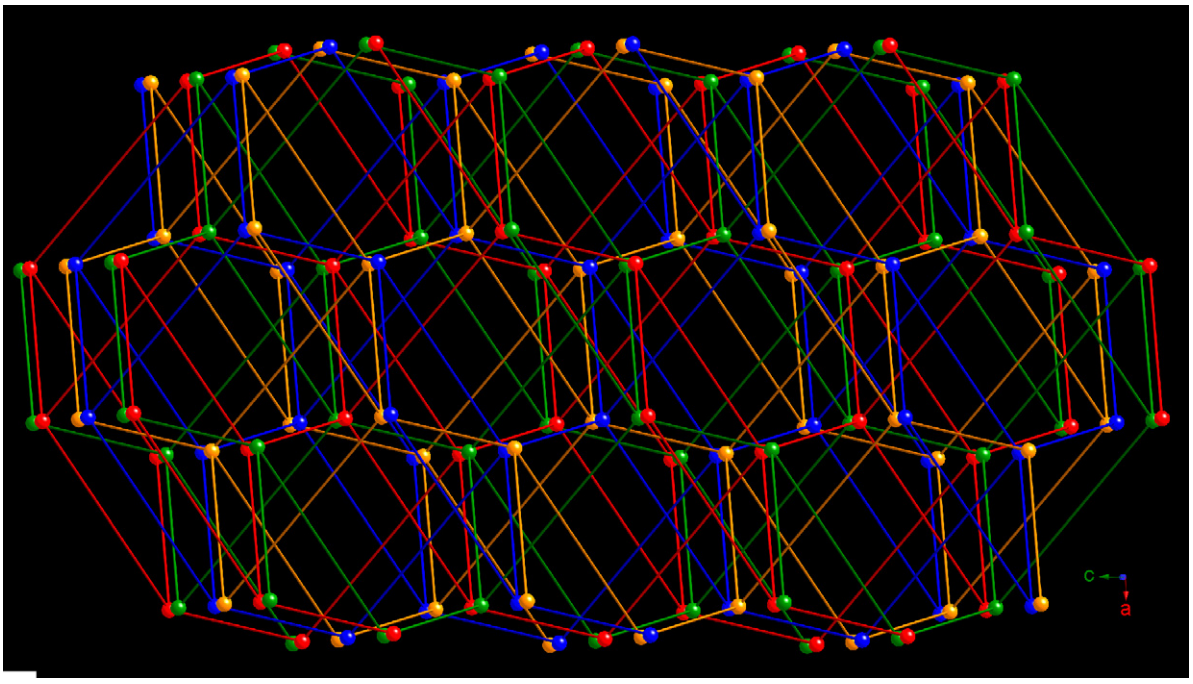

Fig. 11. A view down *c* of the quadruply interpenetrated $SrAl_2$ network structure of **7**. Adapted from Ref. [33].

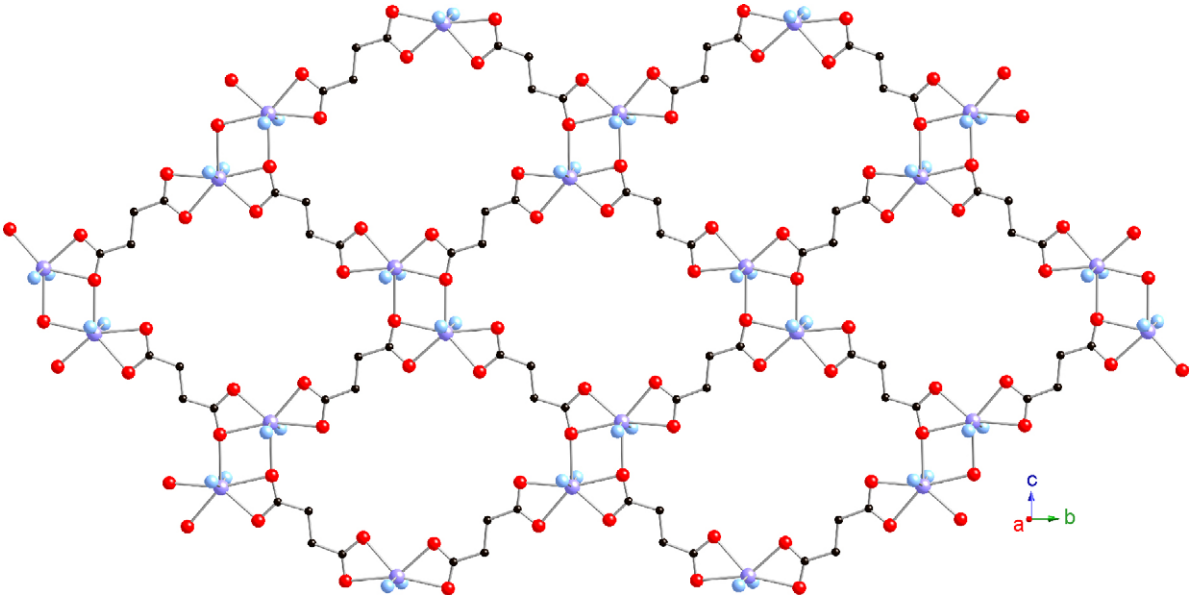

Fig. 12. Face-on view of a single $[Cd(suc)]_n$ layer in **8**. Adapted from Ref. [33].

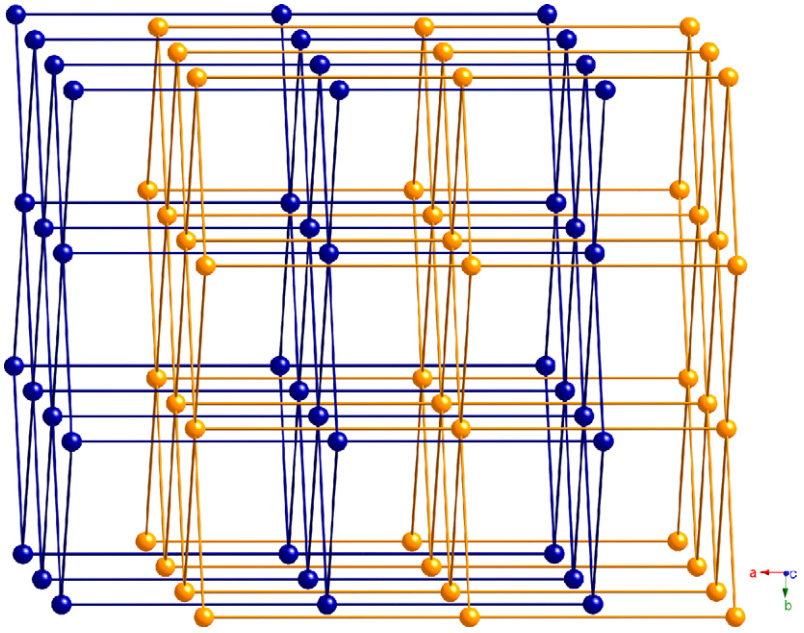

Fig. 13. Framework perspective of **8**, highlighting the doubly interpenetrated α-Po 6-connected networks. The centroid of each Cd_2O_2 dimeric unit is represented as the connecting node. Adapted from Ref. [33].

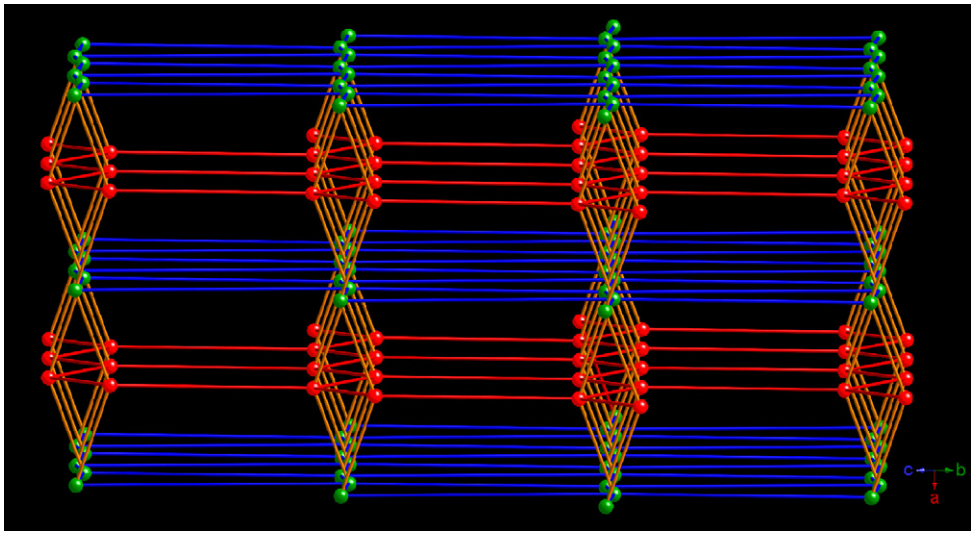

Fig. 14. Framework perspective of the $(4^6 6^4)(4^{10}6^5)$ (5,6)-connected binodal network in **9**. Adapted from Ref. [35].

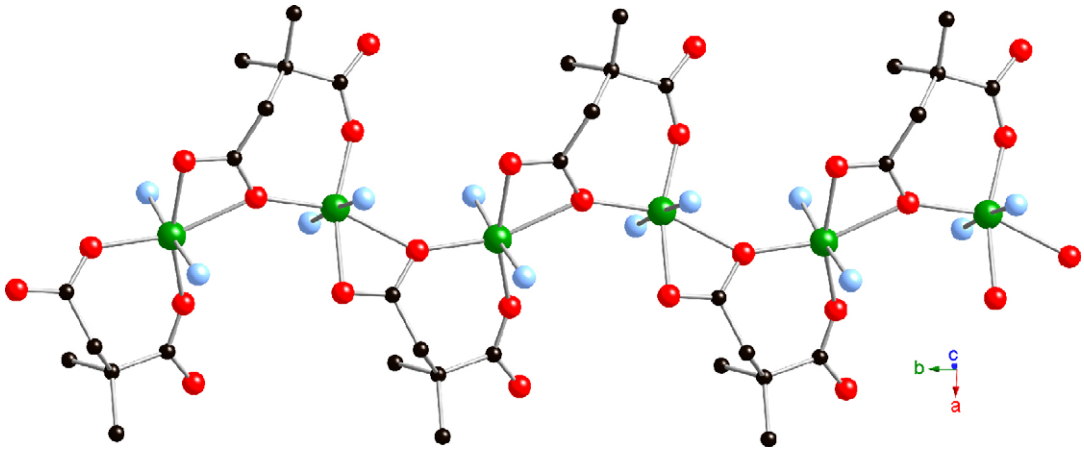

Fig. 15. A single 1D $[Ni(dms)]_n$ ribbon in **11**. Adapted from Ref. [32].

The magnetic susceptibility data of **2** was modeled using the method of Baker [31] for a 1D Heisenberg chain, yielding a J value of 0.64(1) cm^{-3} indicative of ferromagnetic coupling. Based on comparison to other copper malonate coordination polymer systems, it is plausible that the majority of the observed ferromagnetic coupling in **2** can be attributed to the *syn–anti* bridging malonate ligands within one type of $[Cu(malonate)]_n$ chain in **2**. These bridge equatorial sites on neighboring $\{CuO_4N\}$ square pyramids, thereby maximizing interaction between the magnetic d_{x2-y2} orbitals [32].

2.2. Succinate/dpa coordination polymers

Hydrothermal treatment of a mixture of the appropriate metal chloride or nitrate salt with succinic acid and dpa afforded a family of succinate/dpa coordination polymers, whose structures depend synergistically on the coordination geometry at the divalent metal, the binding and bridging modes of the dicarboxylate ligand, the conformation of the succinate (suc) moiety, and occlusion of any anionic species within the lattice [33].

$[Co(suc)(dpa)_2]$, **3**, was prepared via hydrothermal reaction of cobalt chloride, dpa and succinic acid. It possesses a $\{CoO_4N_2\}$ distorted octahedral coordination environment, in which the *cis* nitrogen donors belong to two different monodentate dpa ligands. Pendant, unprotonated dpa ligands have been previously observed only in the polyoxomolybdate cluster complex $\{[(H_2dpa)_2][Mo_8O_{26}(dpa)_2]\}$ [34]. Adjacent cobalt atoms are linked by bischelating succinate tethers in *anti* conformation to form a threefold helix motif (Fig. 4). Each $[Co(suc)(dpa)_2]$ helix donates hydrogen bonds from its dpa central amine N–H subunits to carboxylate oxygen atoms in three other chains, and accepts hydrogen bonds at its own carboxylate oxygen atoms from dpa amine groups in three other neighboring chains. Thus, each individual helix in **3** is supramolecularly conjoined to six others, arranged in a homochiral hexagonal pattern around the "central" helix (Fig. 5). If cobalt perchlorate was used as a starting material instead, the 1D chain polymeric phase $\{[Co(suc)(Hdpa)_2(H_2O)_2](ClO_4)_2{\cdot}7.5H_2O\}_n$ (**4**) was obtained. Here, bismonodentate *anti* conformation suc ligands permit formation of straight cationic chains (Fig. 6), unlike the coiled helices caused by bischelating *anti* conformation suc ligands in **3**. The pendant dpa ligands in this case are protonated, with interstitial perchlorate ions providing the necessary charge balance [35].

The nickel congener of this family, $\{[Ni(dpa)_2(suc)_{0.5}]Cl\}$ (**5**), also exhibits an octahedral coordination sphere. However the $\{NiN_4O_2\}$ environment results in a dramatically different dimensionality and structure from that seen in **3** and **4**. Within the structure of **5**, fourfold interpenetrated cationic $[Ni(dpa)_2]_n^{2n+}$ diamondoid lattices (6^6 topology) are observed, similar to those in the dpa/oxoanion 3D phase $\{Ni(dpa)_2(SO_4)(H_2O)]{\cdot}2H_2O\}$ [20]. In **5**, bischelating succinate anions in a *gauche* conformation bridge nickel atoms in different $[Ni(dpa)_2]_n^{2n+}$ diamondoid nets thereby creating a 5-connected self-penetrated cationic framework (Fig. 7). This network is the first example of a uniform 6^{10} topology (long vertex symbol $6_3.6_3.6_3.6_3.6_3.6_3.6_3.6_3.6_3.6_3$) and opens a new vista in the creation of self-penetrated coordination polymer nets. It can even be considered a regular (6,5) lattice.

Moving to a square planar coordination geometry by use of the Jahn-Teller active divalent copper ion in this system resulted in the crystallization of $\{[Cu(suc)(dpa)]{\cdot}0.5H_2O\}$ (**6**). In this material neutral 1D $[Cu(suc)]_n$ fourfold helices are formed by the linkage of $\{CuN_2O_2\}$ square planar coordination spheres by bis(monodentate) succinate dianions in a modified *anti* conformation. The $[Cu(suc)]_n$ helices then intertwine to form double helix motifs (Fig. 8). These are then conjoined by tethering dpa ligands into a rare twofold interpenetrated $CdSO_4$ structure type (6^58 topology) (Fig. 9).

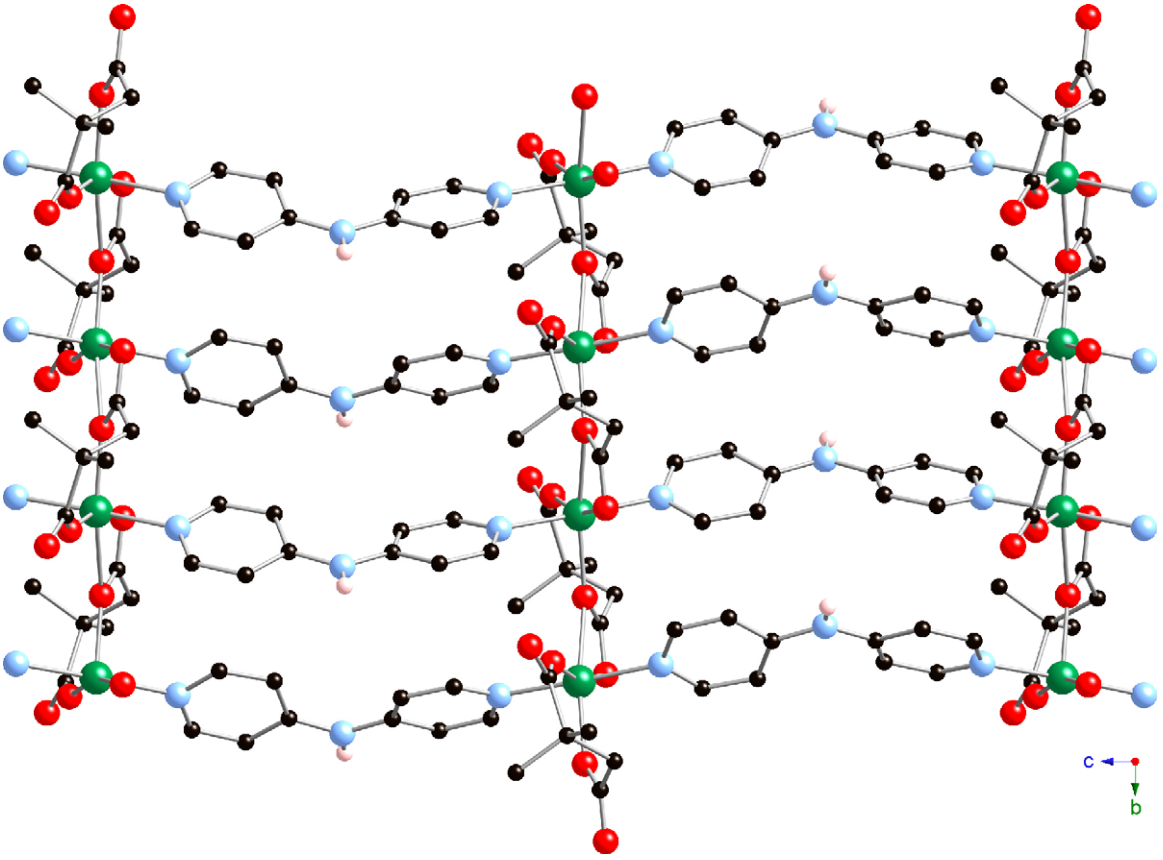

Fig. 16. The (4,4) rectangular grid layer structure of **11**. Adapted from Ref. [32].

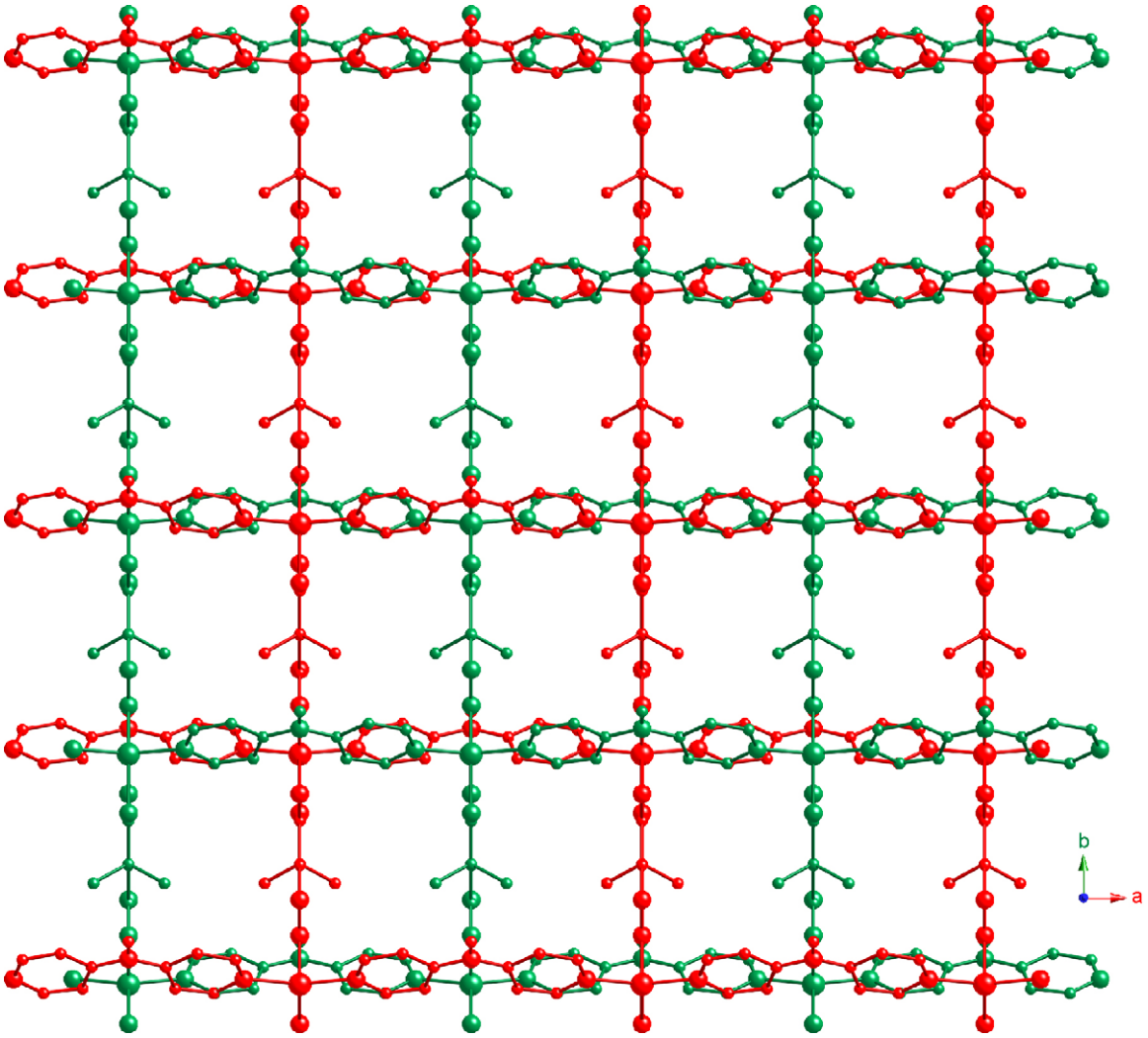

Fig. 17. The doubly interpenetrated (4,4) layer structure of **12**. Adapted from Ref. [32].

{[Zn(suc)(dpa)]·H_2O} (**7**) exhibits a tetrahedral {ZnN_2O_2} coordination sphere linked into undulating $[Zn(suc)]_n$ chains by bis(monodentate) suc ligands. The Zn···Zn contact distances in these chains alternate between 8.30 and 8.80 Å, because of alternating *gauche* and *anti* succinate conformations (Fig. 10). The $[Zn(suc)]_n$ chains are connected into a 3D coordination polymer framework as in **5** and **6**. However, the linkage of the tetrahedral nodes in **7** results in an uncommonly encountered fourfold interpenetrated $SrAl_2$ network (4^26^38 topology) (Fig. 11).

Use of the larger d^{10} divalent Cd ion allowed preparation of {[Cd(suc)(dpa)]·H_2O} (**8**) featuring [CdO_5N_2] pentagonal bipyramidal coordination, with suc oxygen donors situated in the equatorial plane and dpa nitrogen donors oriented in a *trans* fashion in the axial positions. The structure of **8** is built from flat $[Cd(suc)]_n$ layers, formed by the linkage of cadmium ions through exotridentate succinate ligands in *anti* conformation (Fig. 12). These layers may also be construed as coplanar aggregations of atom-sharing {Cd_2O_2} and {CdOCO} four-membered rings and 28-membered {$CdOC_4O$}$_4$ elliptical circuits. The $[Cd(suc)]_n$ layers are strutted by dpa ligands to construct a doubly interpenetrated α-Po primitive cubic topology (Fig. 13), a pattern seen in a few other aliphatic α,ω-dicarboxylate coordination polymers incorporating either 4,4′-bpy [36] or dpee [12a].

While compound **8** was prepared using cadmium nitrate, the hydrothermal reaction of cadmium perchlorate with succinic acid and dpa resulted in a 3D coordination polymer with a structural topology noticeably different from that of **8** [35]. {[$Cd_3(suc)_{2.5}(dpa)_2$](ClO_4)}, **9**, displays a cationic binodal (5,6)-connected net with an unprecedented (4^66^4)($4^{10}6^5$) topology. The complex structure of compound **9** is built from [Cd_3(*gauche*-suc)$_2$] grid-like layer motifs strutted both by *anti*-suc and dpa tethers. The topology of **9** can be simplified as pillared, alternating rectangular and hexagonal layers (Fig. 14).

2.3. Substituted succinate/dpa coordination polymers

In order to probe the effect of alkyl group substitution on the conformation of the succinate ligands and the resulting coordination polymer structures, similar synthetic procedures to those used for **3**–**9** were undertaken employing

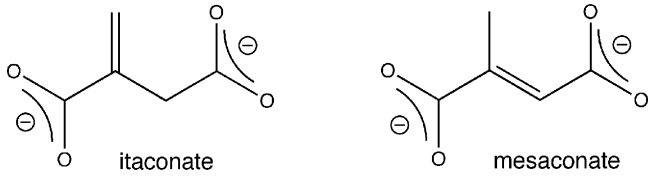

Scheme 2.

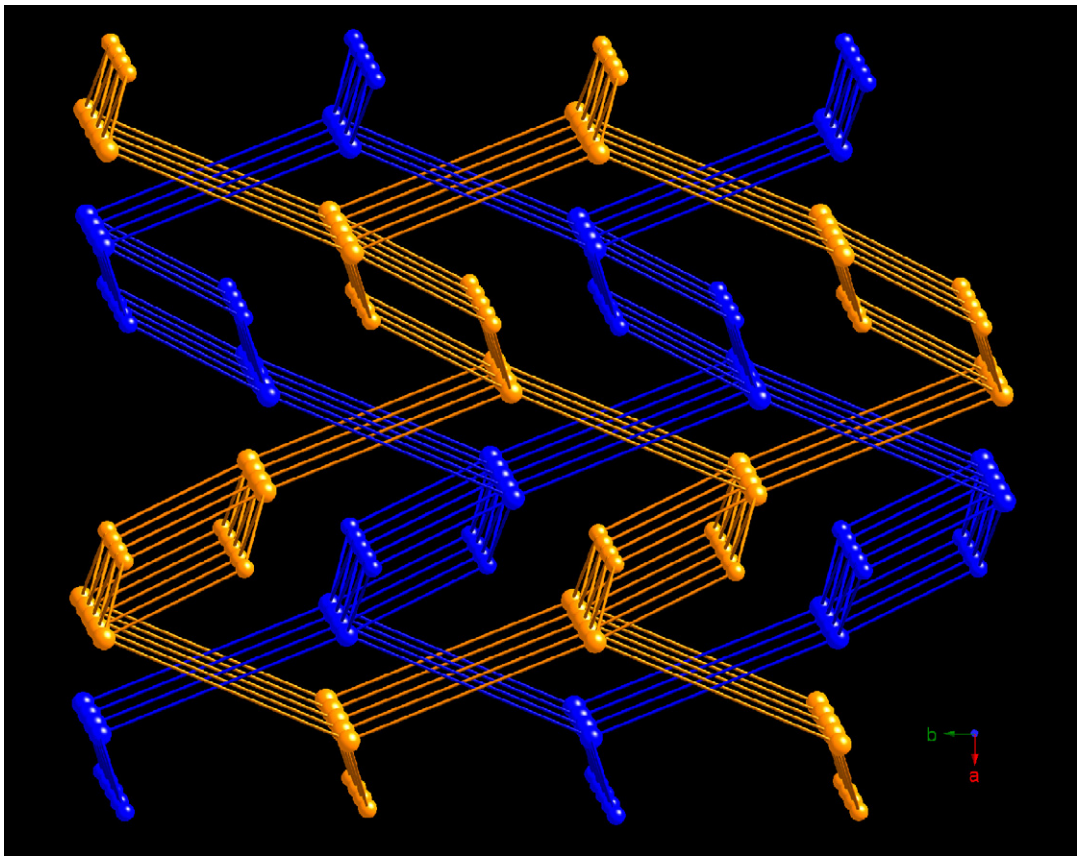

Fig. 18. Framework perspective of the doubly interpenetrated binodal (3,5)-connected 3D $(4^26)(4^26^58^3)$ supramolecular network in **12**.

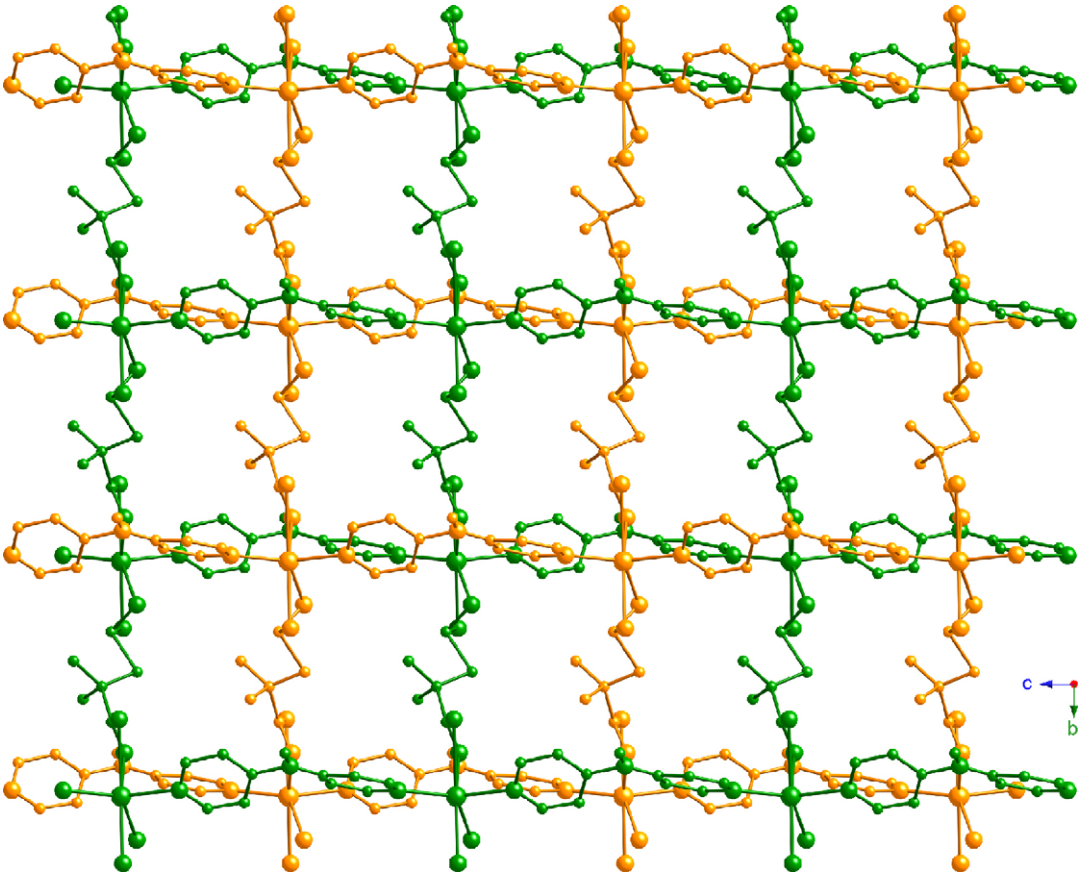

Fig. 19. The doubly interpenetrated 2D layer structure of **13**. All of the methyl groups within the dms ligands point towards the left of the figure. Adapted from Ref. [32].

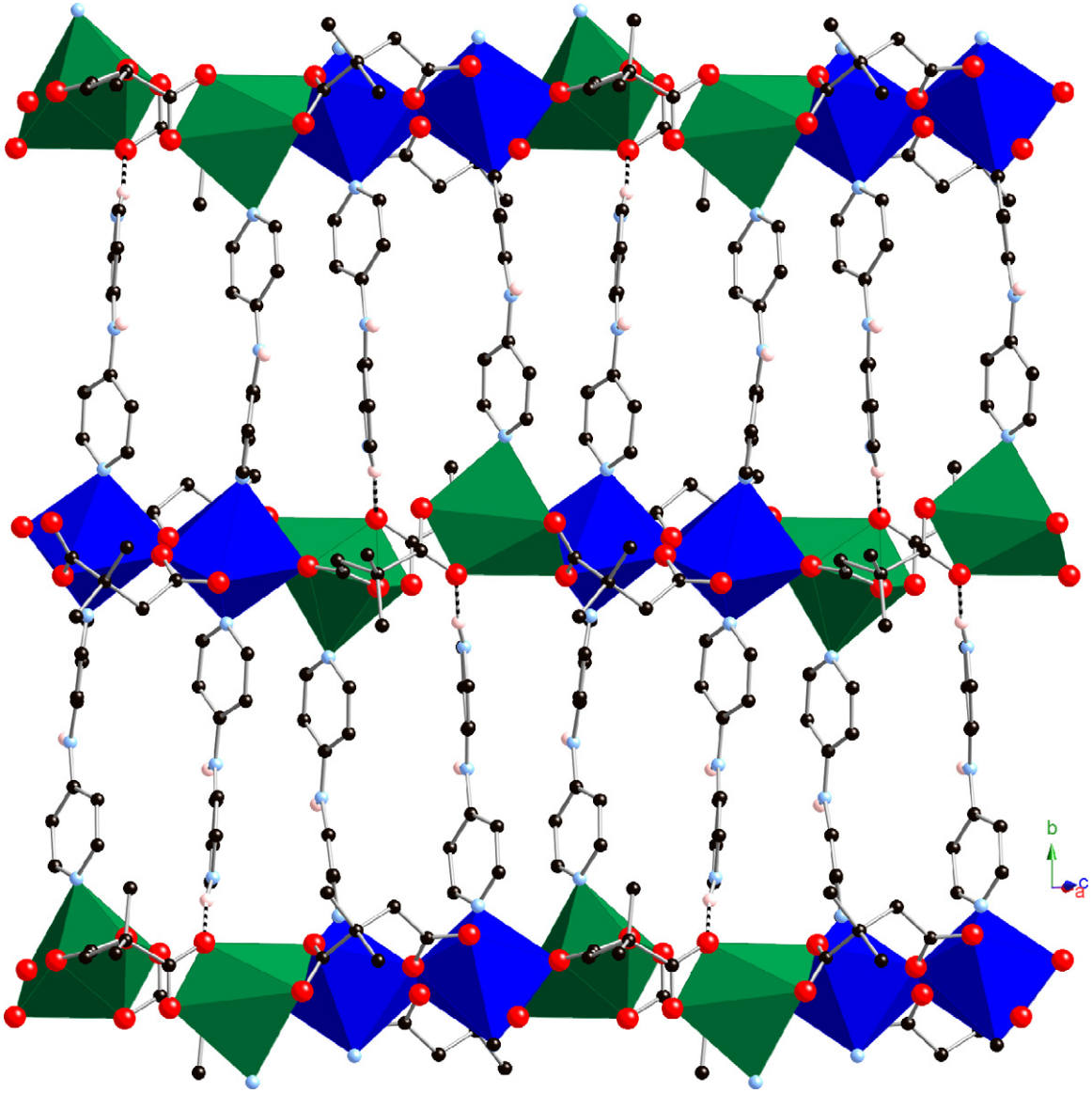

Fig. 20. A single (6,3) hexagonal grid $[Cd_2(dmsuc)_2(dpa)(Hdpa)]_n^{n+}$ cationic layer in **14**. Hydrogen bonding is shown as dashed lines. Adapted from Ref. [35].

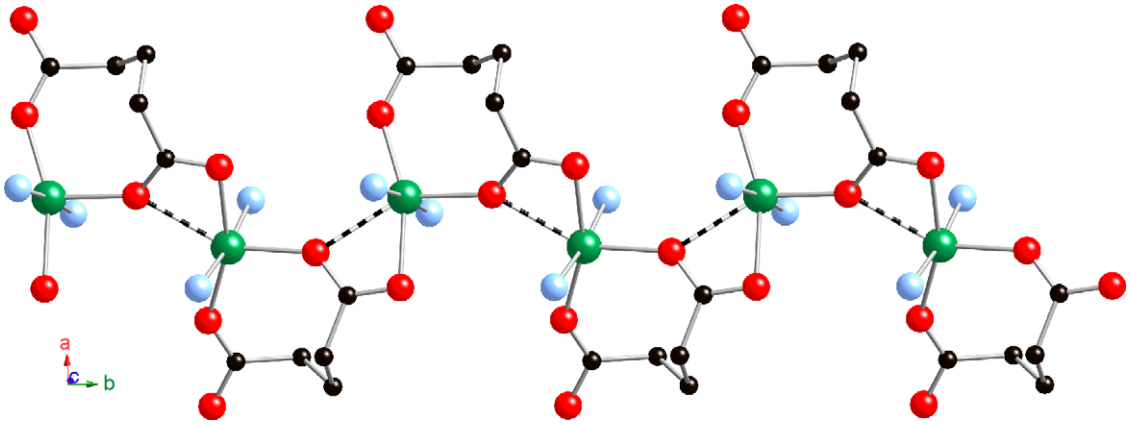

Fig. 21. The 1D $[M(glu)]_n$ ribbon motif in **16**–**18**. Semi-ligation is indicated as dashed lines. Adapted from Ref. [41].

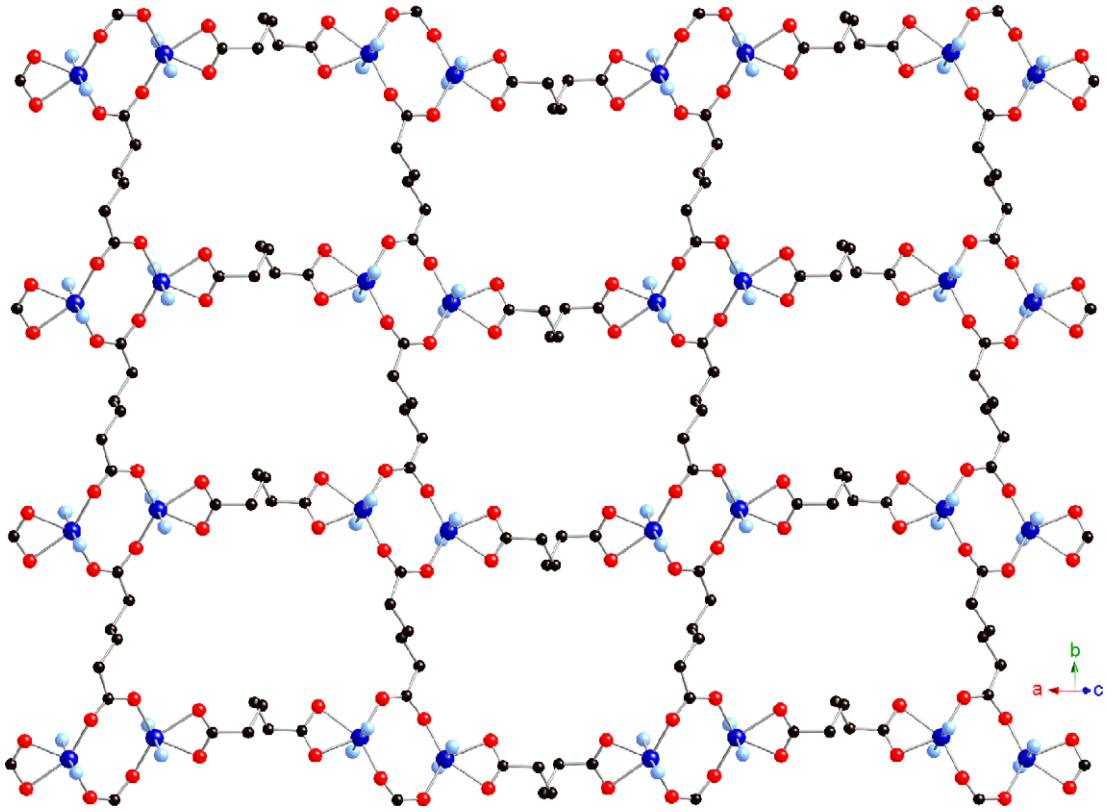

Fig. 22. View down (1 0 1) of a neutral $[Co_2(\mu_2\text{-adp})(\mu_4\text{-adp})]_n$ layer in **20**. Adapted from Ref. [43].

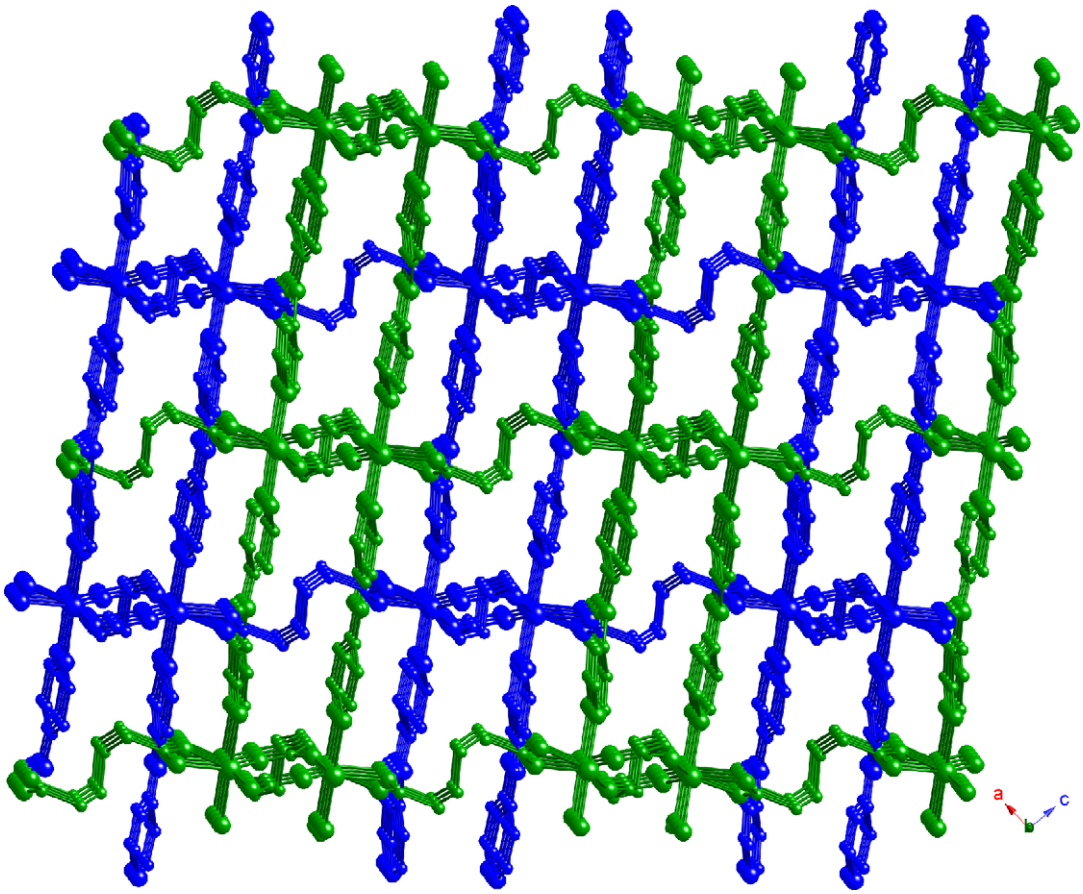

Fig. 23. Twofold interpenetration of 3D networks in **20** and **21**. Adapted from Ref. [43].

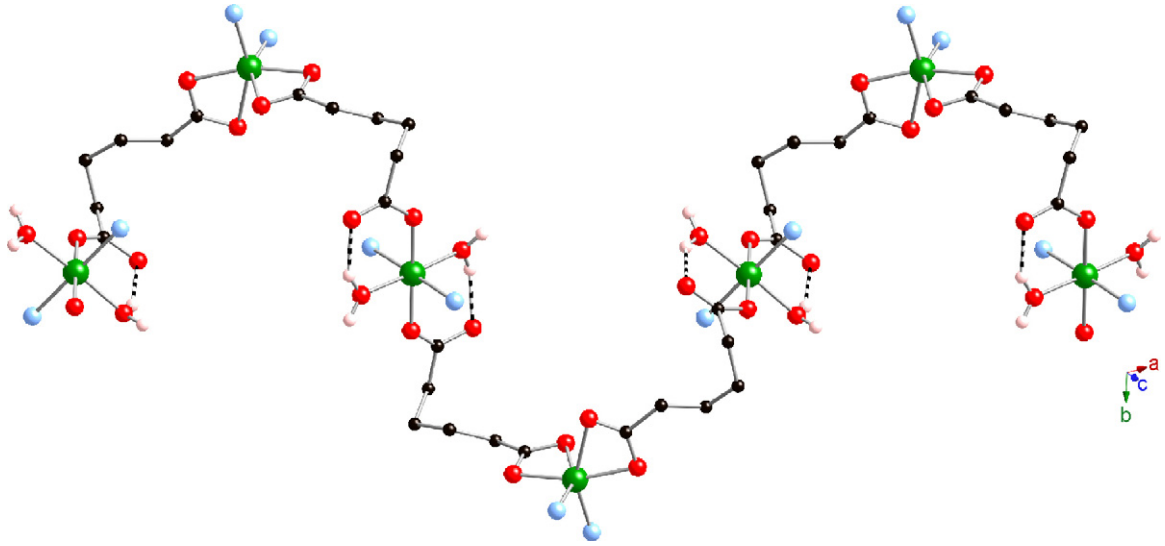

Fig. 24. A 1D zig-zag 1D $[Ni(adp)]_n$ pattern in **22**. Hydrogen bonding is indicated as dashed lines. Adapted from Ref. [43].

2,2-dimethylsuccinic acid (H_2dms). Four oxoanion-free coordination polymers of formulation [M(dms)(dpa)] (M = Co, **10**; M = Ni, **11**; M = Cu, **12**; M = Cd, **13**) [37] and a perchlorate containing phase $\{[Cd_2(dmsuc)_2(dpa)(Hdpa)](ClO_4)\cdot 6H_2O\}_n$ (**14**) were prepared and characterized. All five materials manifested different structures from each other, from their unsubstituted succinate derivatives [33], and from related phases incorporating 4,4′-bpy [38].

Compound **10**, prepared by the hydrothermal reaction of cobalt chloride, H_2dms and dpa, contains $[Co(dms)]_n$ chains formed by distorted *anti* conformation dms ligands in a bis(monodentate) binding mode connecting tetrahedrally coordinated Co atoms, in striking contrast to the octahedral coordination observed in **3**. The chain subunits also wind around a crystallographic twofold screw axis, a significant structural difference from the threefold helices observed in its unsubstituted congener. It is certainly plausible that the steric encumbrance of the *gem*-dimethyl substituents forces a lower coordination geometry at cobalt and prevents the helical subunits from winding more tightly. The $[Co(dms)]_n$ chains are further linked by tethering dpa ligands to construct a 3D fourfold interpenetrated 4^26^38 $SrAl_2$ topology, closely related to that seen in the tetrahedrally coordinated zinc-containing phase **7**.

Octahedral $\{NiO_4N_2\}$ coordination geometry in **11** results in a decrease from 3D to 2D dimensionality, with *gauche* conformation dms ligands in an exotridentate binding mode connecting nickel atoms into a 1D $[Ni(dms)]_n$ chain motif featuring a repeating 1D $(Ni–O–)_n$ ribbon (Fig. 15). The $[Ni(dms)]_n$ chains are linked into 2D by dpa ligands, thereby forming a (4,4)-rectangular grid (Fig. 16). These in turn stack in an *ABAB* pattern by means of

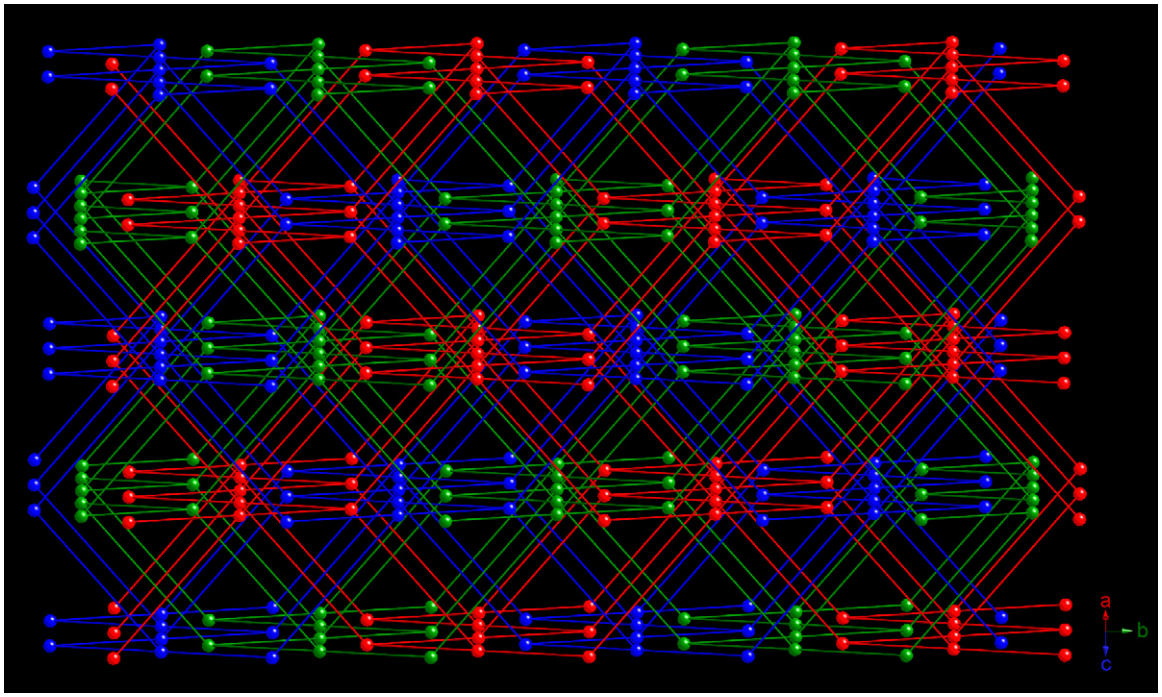

Fig. 25. A simplified representation of the unique threefold interpenetrated PtS network in **22**. Adapted from Ref. [43].

dpa-mediated hydrogen bonding to construct the overall 3D superstructure of **11**. Variable temperature magnetic susceptibility data for **11** were fit to Hatfield's polynomial expression for a 1D chain of $S = 1$ ions [39], revealing the presence of antiferromagnetic coupling ($J = -28.2(2)\,cm^{-1}$) along the 1D $(Ni–O–)_n$ ribbons. Spin canting due to anisotropy at the d^8 nickel centers results in a dramatic increase in the $\chi_m T$ product at low temperature.

In **12**, the copper atom manifests a $[CuN_2O_3]$ coordination sphere, best described as a distorted square pyramid with a τ value of 0.16. The coordination geometry differs from that in the unsubstituted analog **6**, again resulting in decrease in coordination polymer dimensionality. Compound **12** therefore adopts a doubly interpenetrated (4,4)-grid structural motif (Fig. 17) based on $[Cu(dms)]_n$ chains built from bis(monodentate) *anti* conformation dms ligands, linked by dpa tethers. Hydrogen bonding interactions between the dpa amine groups and unligated carboxylate oxygen atoms result in a novel twofold interpenetrated (3,5)-connected supramolecular network with $(4^26)(4^26^58^3)$ topology, considering the copper atoms and the dpa central nitrogen atoms as connecting nodes (Fig. 18).

Compound **13** displays $[CdO_4N_2]$ octahedral coordination at cadmium, but exhibits a doubly interpenetrated (4,4) grid structure very similar to that of **12**. Closer examination of the structure, however, illustrates that all of the methyl groups in the dms ligands point in the same direction (Fig. 19). The subtle shift from an idealized *anti* conformation in the dms ligands in **13**, provoked by the additional carboxylate coordination, results in an acentric structure. The added steric requirements of the dms ligands in **13** instigate the formation cadmium dicarboxylate chains at the expense of the layers seen in its unsubstituted analog **8**. Once again, employing dms instead of succinate resulted in an overall reduction in coordination polymer dimensionality. The 2D topology of **13** differs dramatically from the 3D $CdSO_4$ network (6^58 topology) seen in its 4,4′-bpy analog, $\{[Cd(dms)(4,4'\text{-bpy})(H_2O)_2]\cdot H_2O\}_n$ [38], although both materials crystallize in acentric space groups. Using cadmium perchlorate as the starting material resulted in **14**, which displays a 2D (6,3) herringbone lattice, wherein protonated $Hdpa^+$ ligands project into the pseudo-hexagonal apertures within the layers (Fig. 20) [35]; these pendant ligands prevent the interpenetration seen in the perchlorate-free analog **13**. Interstitial perchlorate anions are situated between the layers.

Irradiation of solid-state samples of **13** and **14** with ultraviolet light causes a blue-violet visible light emission ($\lambda_{max} = 350$ nm). As with other mixed-ligand d^{10} metal coordination polymer systems [6], the emissive behavior likely arises from ligand-centered π–π^* electronic transitions within the molecular orbital manifolds of the aromatic diimine tethers.

In order to examine further the substituent effects in this system, an attempt was made to produce a zinc/dpa coordination polymer based on isaconate, which has a doubly bound terminal methylene unit at the 2-position of a succinate chain. To our surprise, *in situ* isomerization of the isaconate unit had occurred, generating the internal alkenyl mesaconate ligand (Scheme 2) [40]. This transformation appears to be the first reported example of terminal-to-internal alkene isomerization during a coordination polymer self-assembly. The resulting compound [Zn(mesaconate)(dpa)]$_n$ (**15**) presents an acentric twofold interpenetrated (4,4) grid structural pattern very similar to that of **13**, despite tetrahedral coordination at zinc. Compound **15** also undergoes blue-violet luminescence upon irradiation with ultraviolet

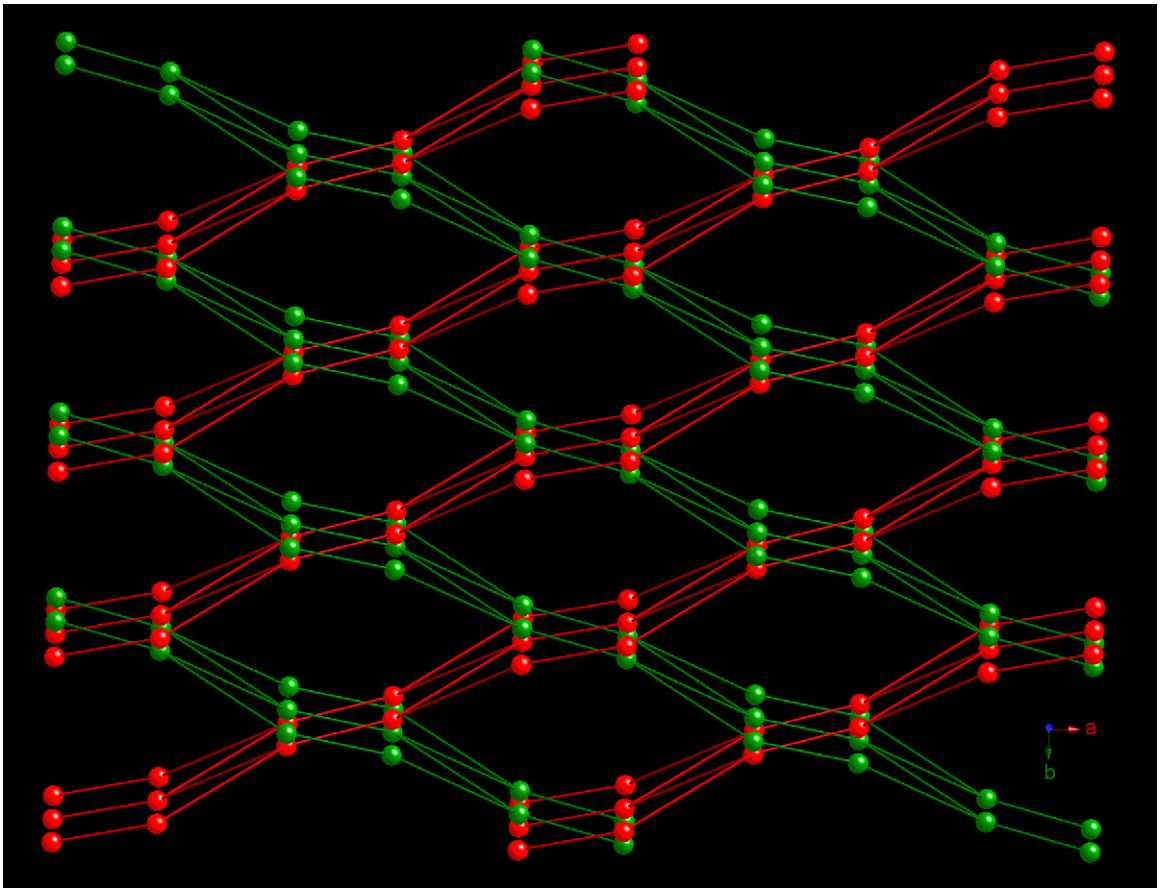

Fig. 26. Framework view of mutually inclined interpenetrated (6,3) layer motifs in **23**. Zn atoms are shown as spheres while the organic tethers are drawn as rods. Adapted from Ref. [43].

light. The 2D structure of **15** contrasts greatly with the fourfold interpenetrated 3D $SrAl_2$ network seen in its unsubstituted analog **7**, perhaps induced by the restricted rotation about the C=C double bond in the mesaconate ligand.

2.4. Glutarate/dpa coordination polymers

Several divalent metal coordination polymers constructed using glutarate (glu) and dpa ligands were synthesized and structurally characterized, all with a stoichiometry of $[M(glu)(dpa)]_n$. As in the succinate materials **3**–**9**, coordination geometry at the metal exerts an important structure directing effect, although with less skeletal diversity. $[Co(glu)(dpa)]_n$ (**16**), $[Ni(glu)(dpa)]_n$ (**17**) and $[Cu(glu)(dpa)]_n$ (**18**) all adopt a rectangular (4,4)-grid 2D lattice very similar to that seen in **11** [41]. All of the complexes **16**–**18** contain similar 1D $[M(glu)]_n$ chain motifs, wherein neighboring metal atoms are linked by *syn–anti* bridging carboxylates with the assistance of weaker semi-ligation (Fig. 21). Differences among the variable temperature magnetic behavior (antiferromagnetic coupling for **17** ($J = -0.28(1)\,cm^{-1}$) and **18** ($J = -0.33(1)\,cm^{-1}$), ferromagnetic coupling combined with zero field splitting ($J = 14(1)\,cm^{-1}$, $D = 30(1)\,cm^{-1}$) for **16**) can be ascribed to variances in magnetic orbital population and electronic configuration.

Changing the coordination number about the metal resulted in an increase in coordination polymer dimensionality from 2D to 3D. $[Cd(glu)(dpa)]_n$ (**19**) forms a twofold interpenetrated primitive cubic structure [42] very similar to its *anti*-succinate-only derivative **8**. Within the structure of **19**, dimeric {CdOCOCdO} units are linked into 2D by *anti-anti* and *anti-gauche* conformation glu ligands to form $[Cd_2(glu)_2]_n$ layers. In turn these connect into a 6-connected lattice via the dpa tethering ligands.

2.5. Adipate/dpa coordination polymers

Hydrothermal combination of metal nitrates or chlorides with adipic acid (H_2adp) and dpa resulted in four different coordination polymers falling into three different structure types [43,44]. $[Co(adp)(dpa)]_n$ (**20**) [43] and $[Cd(adp)(dpa)]_n$ (**21**) [44] both contain octahedrally coordinated metal atoms and similar 2D $[M(adp)]_n$ layered motifs (Fig. 22). In **20** and **21**, each metal atom connects to a neighboring metal atom via a bischelating

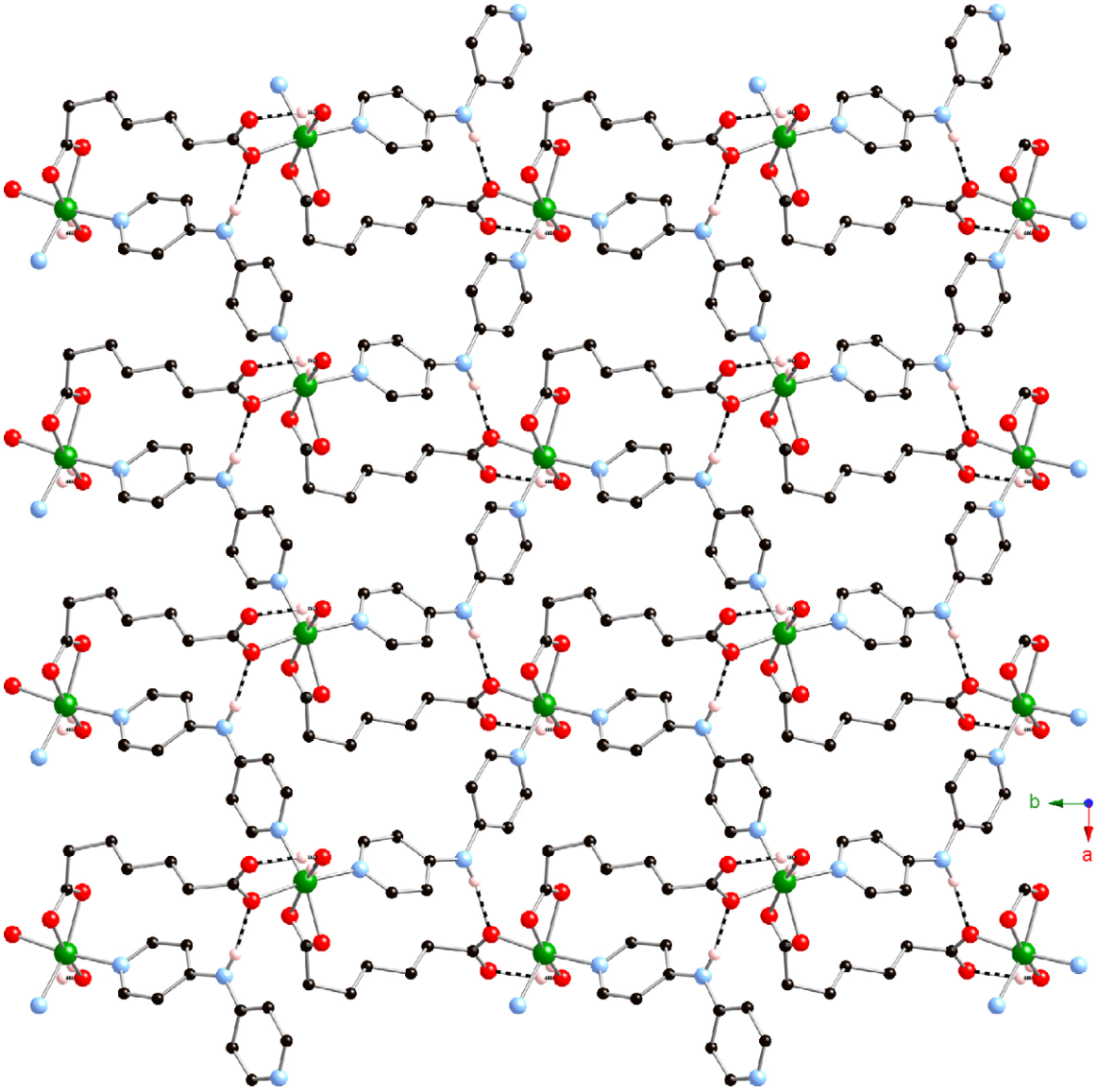

Fig. 27. Face-on view of a $[Ni(pim)(dpa)(H_2O)]_n$ 2D layer in **24**. Hydrogen bonding mediated by the dpa ligands is shown as dashed lines. Adapted from Ref. [45].

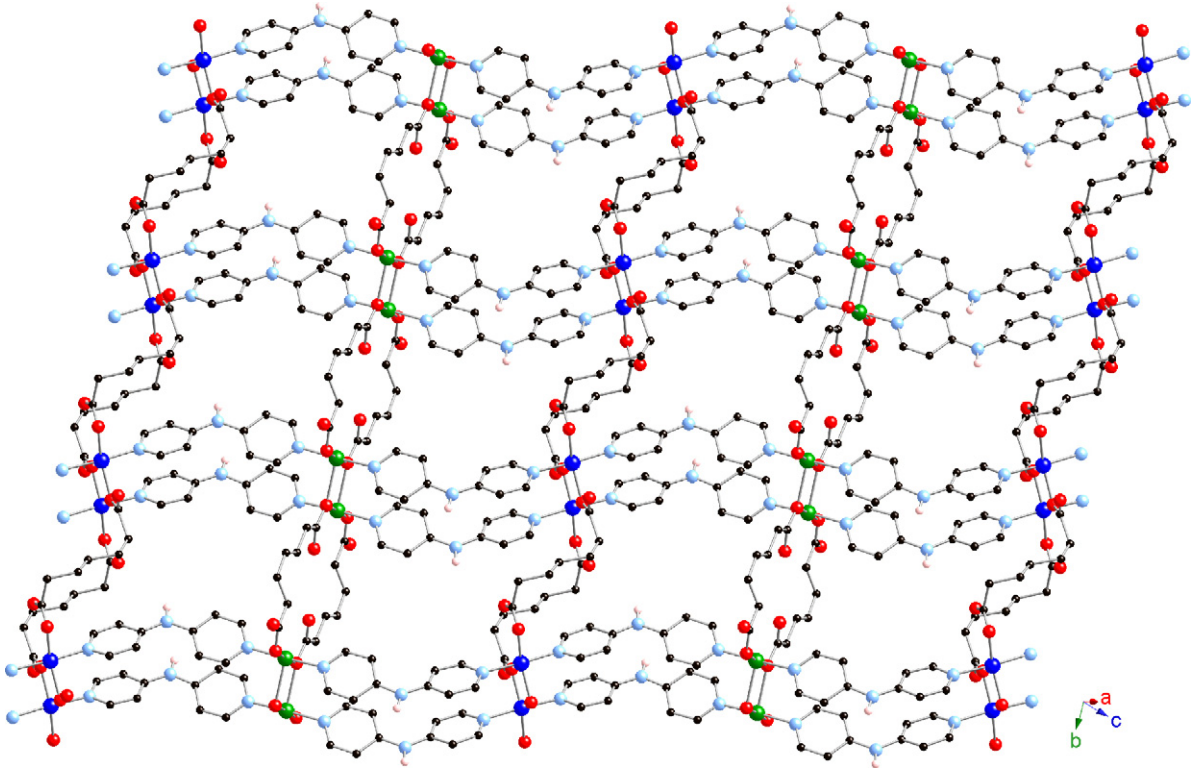

Fig. 28. A 2D slab motif in **25**, formed from the junction of parallel 1D $[Cu_2(pim)_2]_n$ ribbons and $[Cu(pim)]_n$ double chains through dpa tethers. Adapted from Ref. [45].

bis-bridging adp ligand in a very twisted *gauche-gauche-gauche* conformation. Each metal atom further connects to five others through two different exotetradentate adp ligands in an "S"-shaped *gauche-anti-gauche* conformation. Dinuclear $\{MOCO\}_2$ kernels are built from the bridging of two nearest neighbor metal atoms through carboxylate termini on two different *gauche-anti-gauche* adp ligands. The variable temperature magnetism of **20** follows Curie-Weiss behavior in the range 100–300 K with $\Theta = -3.3$ K, indicative of antiferromagnetic interactions within its $\{CoOCO\}_2$ units. The $[M(adp)(dpa)]_n$ layers in **20** and **21** are linked into a 3D primitive cubic 6-connected lattice by tethering dpa ligands. The incipient void space in one net allows interpenetration of a second identical net, promoted by supramolecular hydrogen bonding between the dpa amines in one net and carboxylate oxygen atoms in the other (Fig. 23).

$[Ni(adp)(dpa)(H_2O)_2]_n$ (**22**) also possesses $\{MO_4N_2\}$ octahedral coordination environments, as in **20** and **21**. However, there are two distinct types of coordination environment in **22**, with *cis* nitrogen donors in one and *trans* nitrogen donors in the other. As a result a serpentine 1D $[Ni(adp)]_n$ pattern is formed (Fig. 24), where the nickel atoms are linked by chelating/monodentate bis-bridging adp ligands in a "hairpin" *anti-gauche-gauche* conformation. The dipodal dpa ligands connect the 1D $[Ni(adp)]_n$ units into a 3D binodal PtS "cooperite" network with 4^28^4 topology. The long span of the adipate and dpa ligands permit significant incipient void spaces within a single net, allowing interpenetration of two other identical PtS-type nets (Fig. 25). As of this writing, compound **22** is the unique example of a threefold interpenetrated PtS network.

$[Zn(adp)(dpa)]\cdot H_2O$ (**23**) presents mutually inclined interpenetrated 2D graphitic layers consisting of neutral dimeric $[Zn_2(\mu_2\text{-adp})_2]$ kernels conjoined by dipodal dpa ligands. Contrasting with **19–22**, where the adipate ligands serve to propagate the extended crystal structures, the adipate anions adopt a "staple-shaped" *gauche-anti-gauche* conformation and simply connect neighboring Zn atoms to form "0D" neutral dinuclear units. The dpa tethers connect these units into (6,3) 2D honeycomb nets; parallel layers from two different sets mutually interpenetrate at a 43.4° angle (Fig. 26). Compounds **21** and **23** manifested blue light emission under ultraviolet excitation. Compound **23** undergoes a reversible structural reorganization upon dehydration/rehydration cycles between the original orthorhombic structure and a different orthorhombic phase.

2.6. Longer aliphatic dicarboxylate/dpa coordination polymers

Extension of the aliphatic chains resulted in the divalent metal/dpa system resulted in ladder, grid, double slab, and three-dimensional network coordination polymers, different in all cases from the shorter dicarboxylates discussed above. $[Ni(pim)(dpa)(H_2O)]_n$ (**24**) (pim = pimelate) exhibited undulating

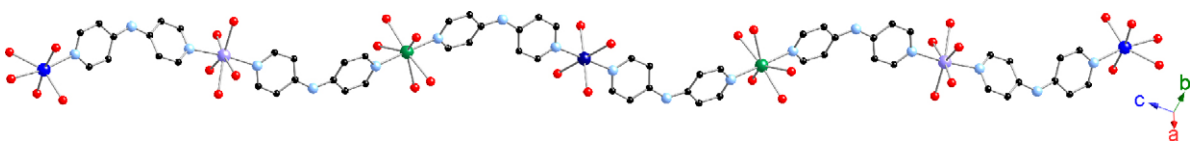

Fig. 29. A $[Cd_7(dpa)_6(H_2O)_2]_n$ *pseudo*-1D oligomer in the structure of **26**. Adapted from Ref. [44].

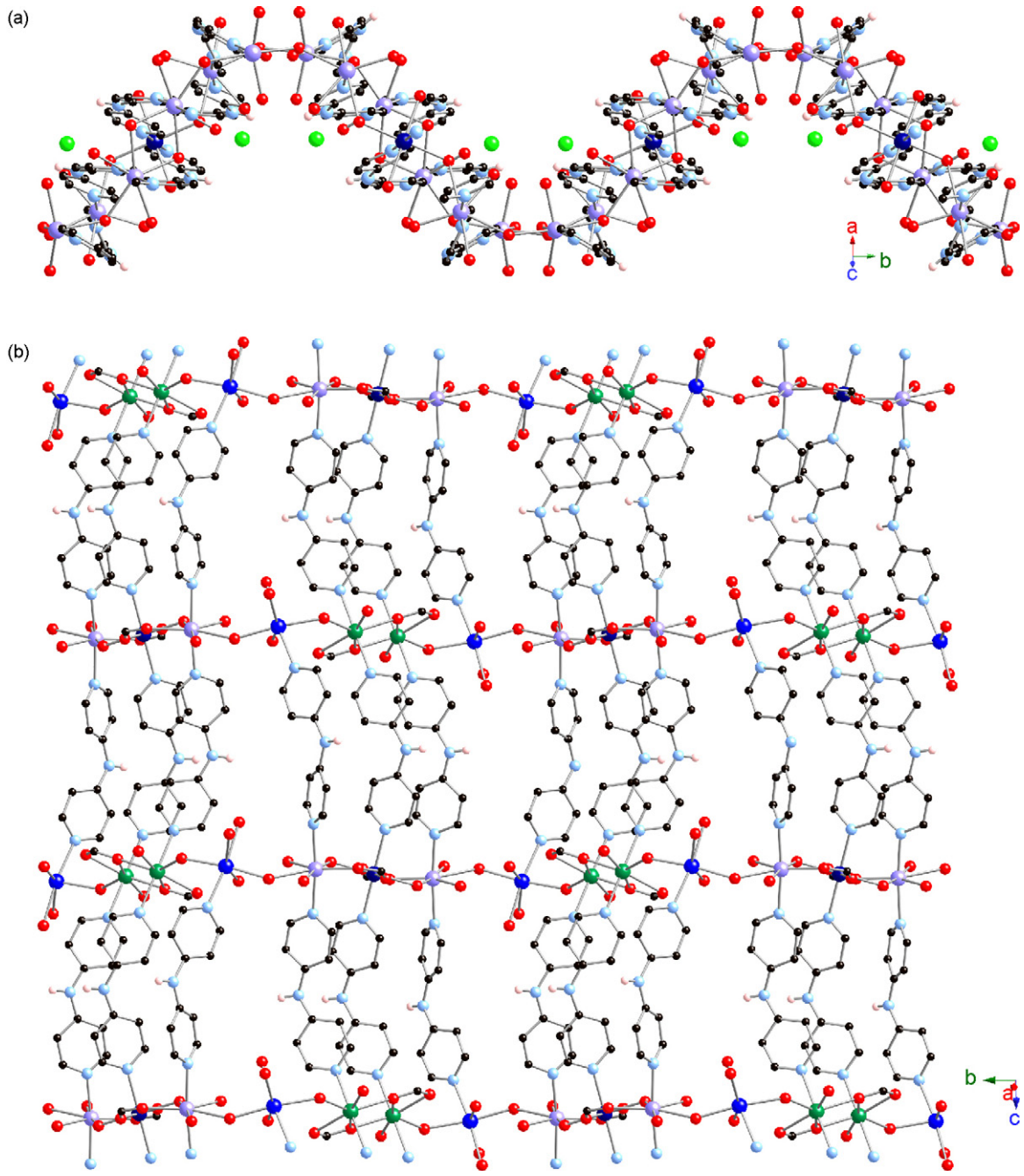

Fig. 30. An undulating 2D layer motif within the structure of **26**: (A) side view; (B) face view. Isolated spheres in (A) represent the perchlorate ion positions. Adapted from Ref. [44].

1D $[Ni(pim)]_n$ chains fostered by the *anti-gauche-gauche-gauche* conformation of the bis(monodentate) dicarboxylate ligands [45]. These are aggregated into a (4,4) rhomboid grids (Fig. 27) in which hydrogen bonding between the dpa amine functional group and unligated carboxylate oxygen atoms provide additional structure direction.

The copper pimelate congener in this system, $\{[Cu_2(pim)_2(dpa)_2]\cdot 5H_2O\}_n$ (**25**) [45], possesses crystallographically distinct $[Cu(pim)]_n$ chains and $[Cu_2(pim)_2]_n$ ribbons formed by bis(monodentate) pimelate ligands in *gauche-anti-anti-gauche* and *anti-gauche-anti-anti* conformations, respectively. These 1D motifs are connected in an alternating fashion by dpa tethers to form the 2D slab structure of **25** (Fig. 28). The dinuclear $\{Cu_2O_2\}$ units within the 1D motifs exhibit some weak ferromagnetic interactions. The intralayer and interlayer regions within the structure of **25** occupy 17.9% of the crystal volume. These incipient voids are filled by discrete water molecule chains in a rare D(8) morphological classification [46], with a connectivity pattern resembling that of 2,7-dimethyloctane.

The cadmium pimelate entry in the system of dpa-containing coordination polymers proved to be the most structurally complex in this system [44]. The structure of $\{[Cd_7(pim)_6(dpa)_6(H_2O)_2](ClO_4)_2\cdot 6H_2O\}_n$ (**26**) is based on $[Cd_7(dpa)_6(H_2O)_2]_n$ *pseudo*-1D oligomers (Fig. 29) linked into a striking undulating 2D layer through bridging pimelate oxygen atoms and carboxylate units (Fig. 30). A complex

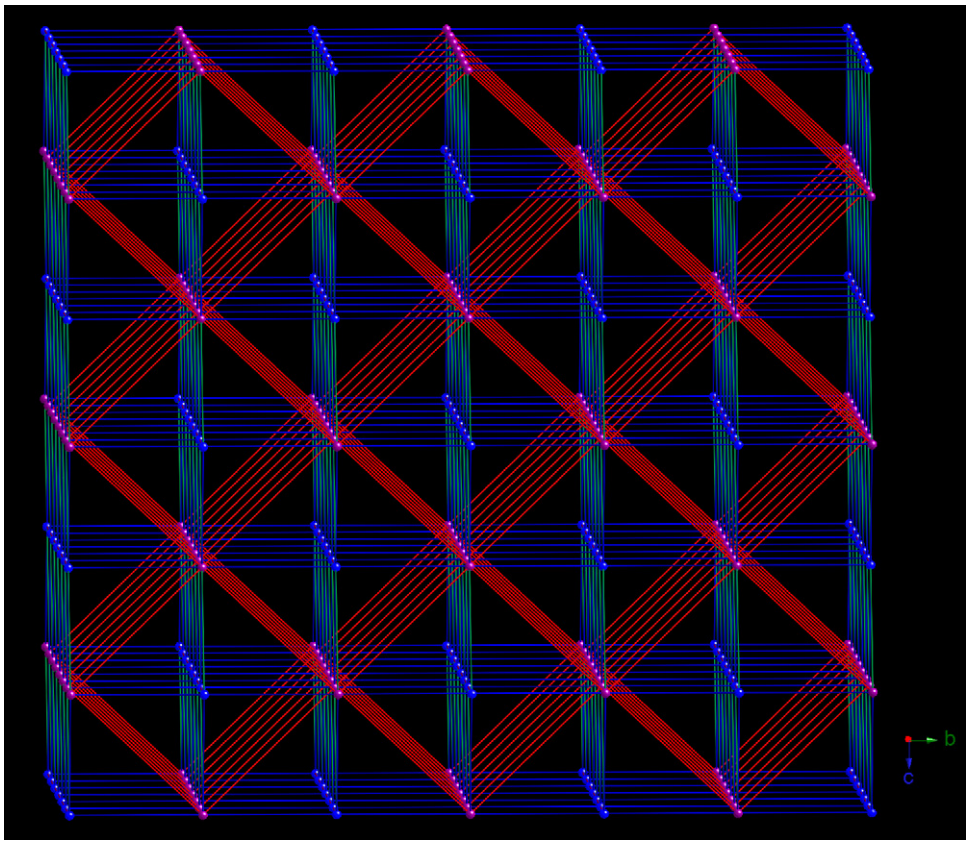

Fig. 31. A schematic view of the unprecedented (8,10)-connected self-penetrated lattice in **26**. Adapted from Ref. [44].

cationic self-penetrated (8,10)-connected 3D structure with $(3^8 4^{14} 5^4 6^2)(3^{10} 4^{18} 5^{14} 6^3)$ topology (Fig. 31) is formed from the aggregation of the wave-like layer motifs via pim ligands in three different conformations, with unligated perchlorate anions and water molecules filling the solvent-accessible void of 13.7% of the crystal volume. To the best of our knowledge, the (8,10)-connectivity of **2** represents the highest connected binodal self-penetrated lattice reported to date.

Reaction of copper(II) chloride with suberic acid and dpa under acidic hydrothermal conditions afforded $[Cu(dpa)(sub)_{0.5}Cl]$ (**27**, sub = suberate), which manifested a simple 1D ladder structure (Fig. 32) whose "rungs" are constructed by *gauche-anti-anti-anti-gauche* conformation sub ligands [47]. Hydrogen bonding patterns mediated by the dpa central amine and long range Cu···Cl interactions act in tandem to promote the pseudo-3D structure of **27**.

The cobalt suberate derivative, $[Co(sub)(dpa)(H_2O)]_n$, (**28**) appeared on first glance to possess a common (4,4) rhomboid grid structure. However crystallographic disorder within the suberate ligands (*gauche-anti-anti-gauche-gauche* and *anti-anti-anti-gauche-gauche* conformations in a 60:40) ratio revealed the presence of two intersecting types of idealized layers with differing suberate conformations (Fig. 33a and b). As a result the structure of **28** is best described on average as a *4-connected* 3D "ligand-vacancy" primitive cubic lattice (Fig. 34) [48].

To date, the nine-carbon azelate (aze) ligand is the longest aliphatic α,ω-dicarboxylate that we have been able to incorporate in a transition metal/dpa coordination polymer. $[Cu(aze)(dpa)(H_2O)]\cdot 3H_2O$ (**29**) presents a (4,4) 2D grid morphology with square pyramidally coordinated copper centers conjoined via dpa and *gauche-anti-anti-anti-anti-gauche* conformation aze ligands (Fig. 35) [47]. Interlamellar hydrogen bonding between the dpa central amine and unligated carboxylate oxygen atoms provides the impetus for aggregation into the *pseudo*-3D structure. Acyclic water molecule trimers in **29** are anchored to the coordination polymer backbone by additional hydrogen bonding mechanisms.

Similar "ligand-vacancy" 3D primitive cubic lattices as that seen in **28** are evident for $[Co(aze)(dpa)(H_2O)]_n$ (**30–Co**) and $[Ni(aze)(dpa)(H_2O)]_n$ (**30–Ni**) [49]. Seven-coordination at the larger cadmium ion in $[Cd(aze)(dpa)(H_2O)]_n$ (**31**) results in a relatively

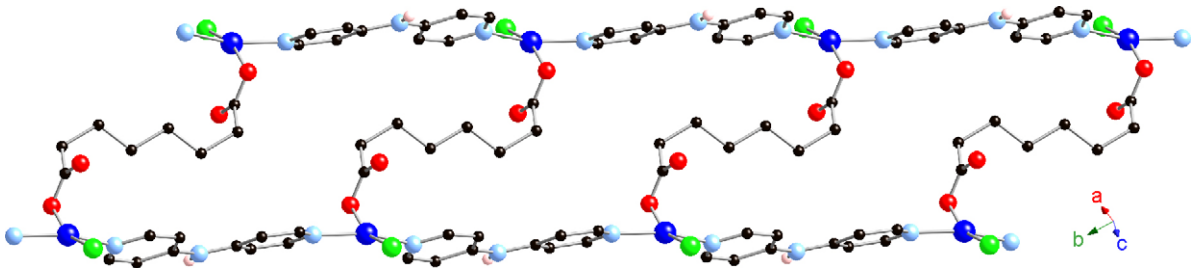

Fig. 32. The 1D ladder structure of **27**. Adapted from Ref. [47].

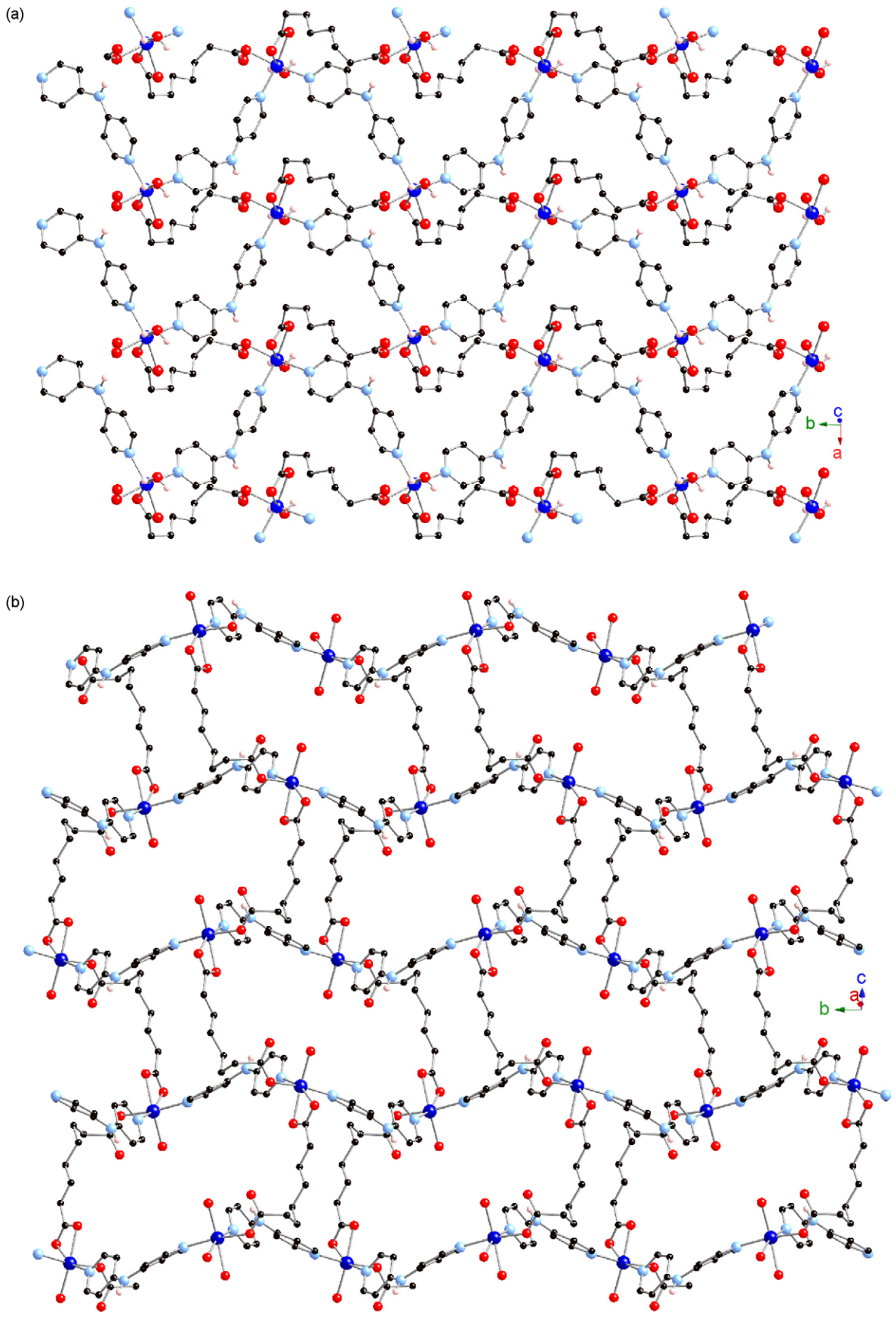

Fig. 33. The two idealized conformationally distinct layer motifs in **28**, shown in a face-on perspective (a) major component, (b) minor component. Adapted from Ref. [43].

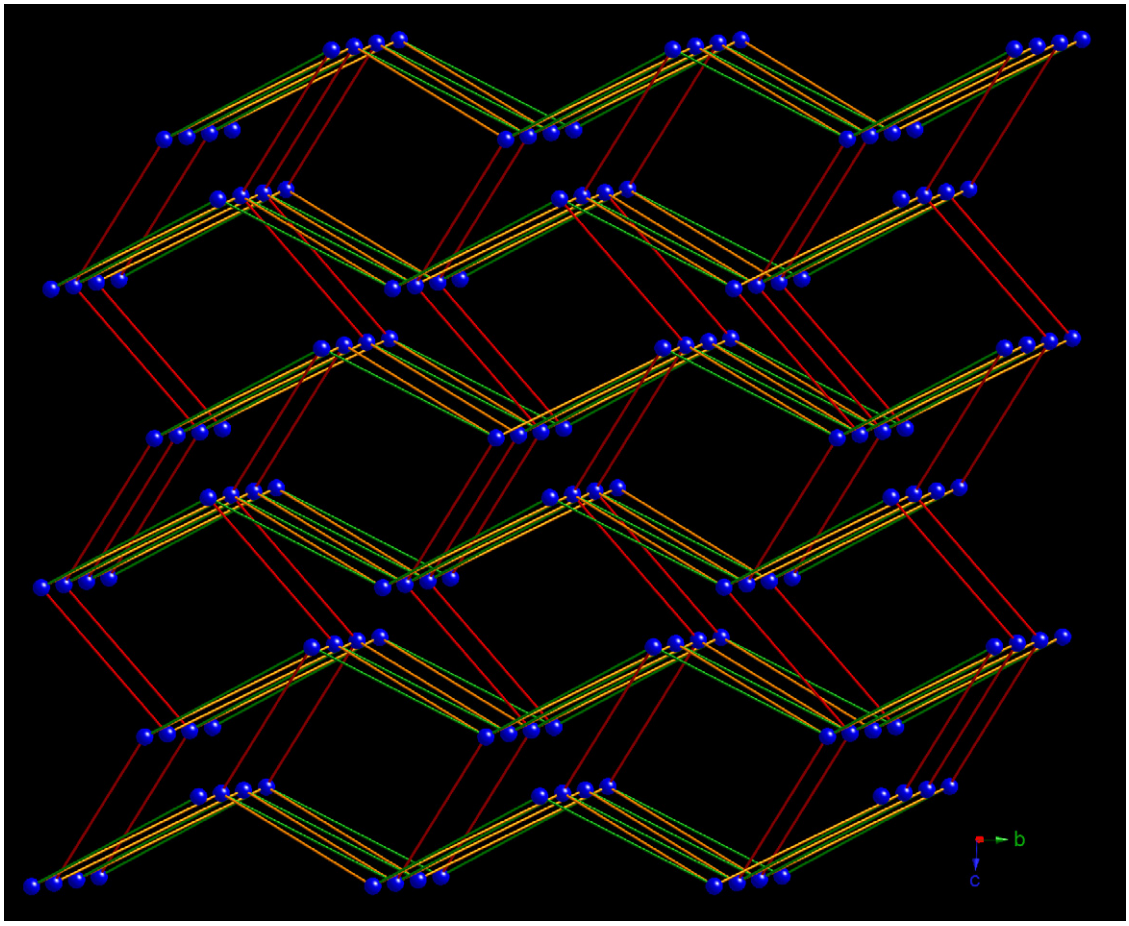

Fig. 34. The "ligand-vacancy" 3D primitive cubic lattice of **28**. Adapted from Ref. [48].

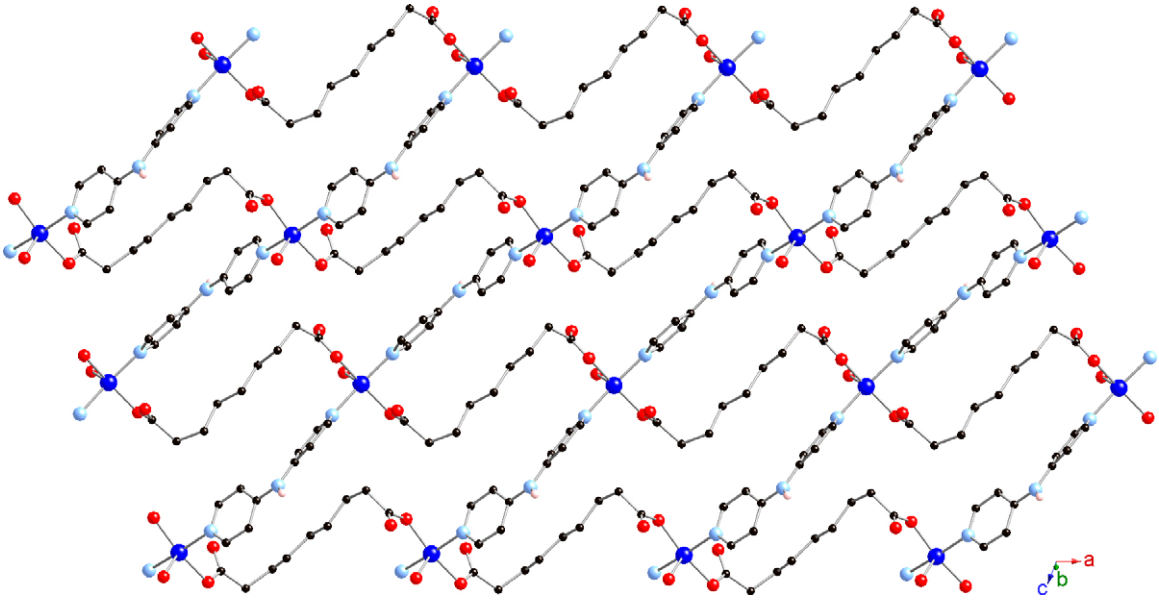

Fig. 35. The (4,4) 2D grid coordination polymer layer in **29**. Adapted from Ref. [47].

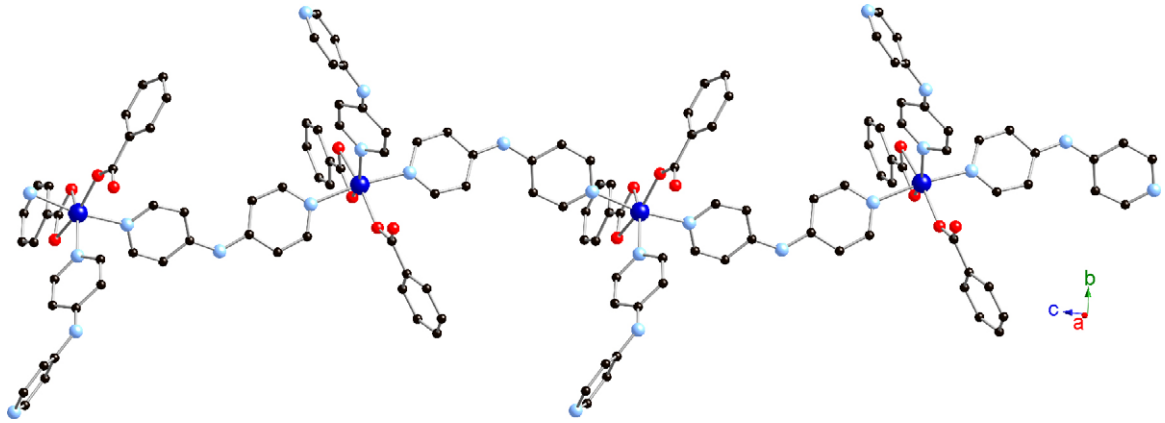

Fig. 36. The 1D chain structure of **32**. Adapted from Ref. [50].

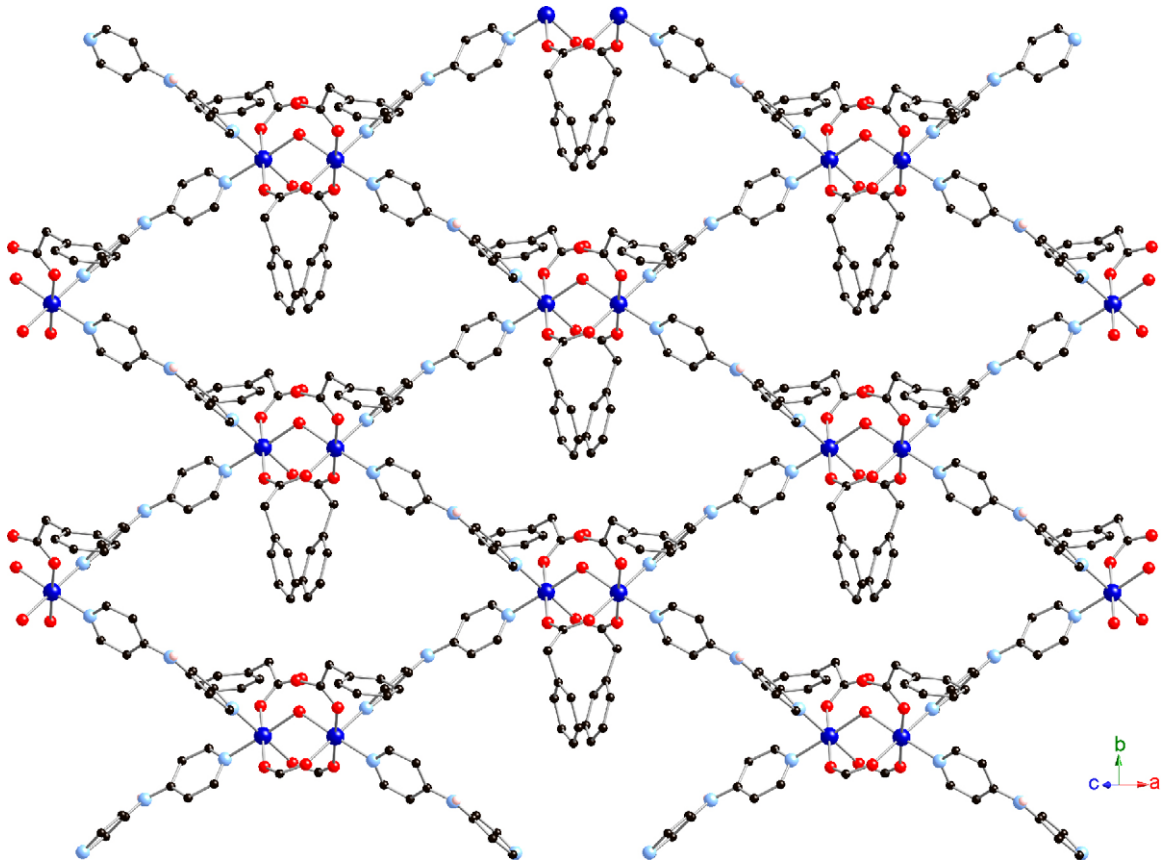

Fig. 37. A single (4,4) 2D grid coordination polymer layer in **33**. Adapted from Ref. [50].

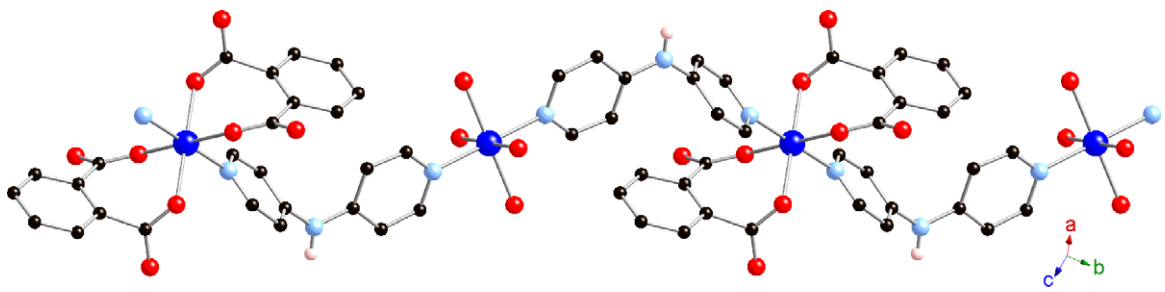

Fig. 38. The 1D chain coordination polymer structure of **34**, highlighting $[M(H_2O)_4]^{2+}$ and $[M(pht)_2]^{2-}$ ionic units linked through dpa tethers. Adapted from Ref. [53].

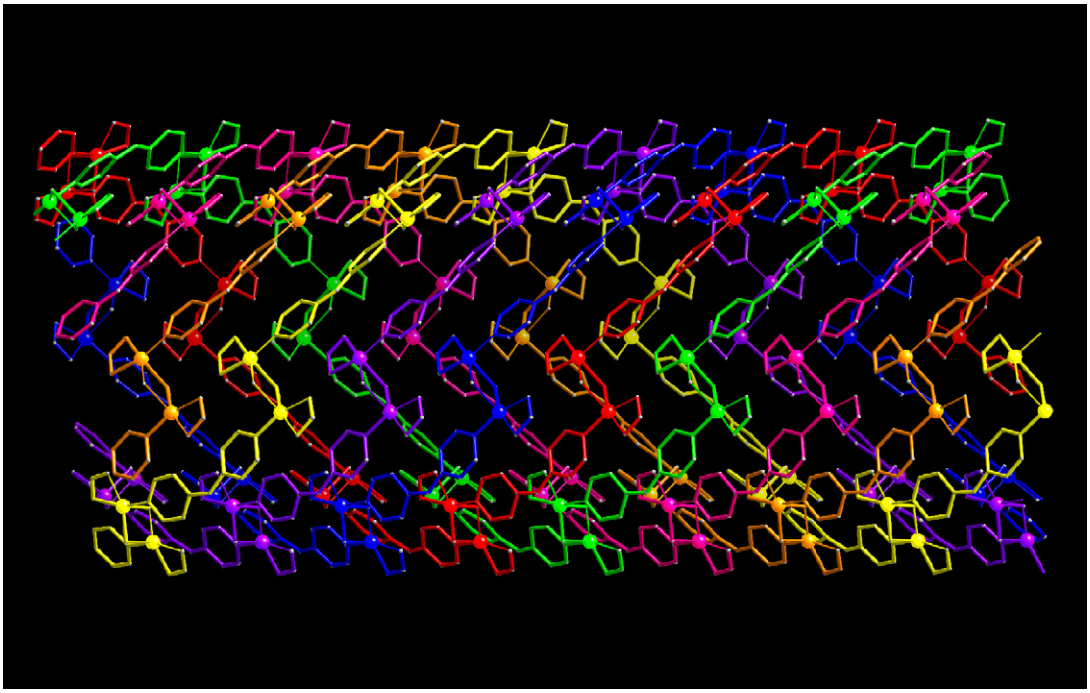

Fig. 39. Septuple right-handed $[Cu_2O_2(dpa)]_n$ helices within **35**. Adapted from Ref. [54].

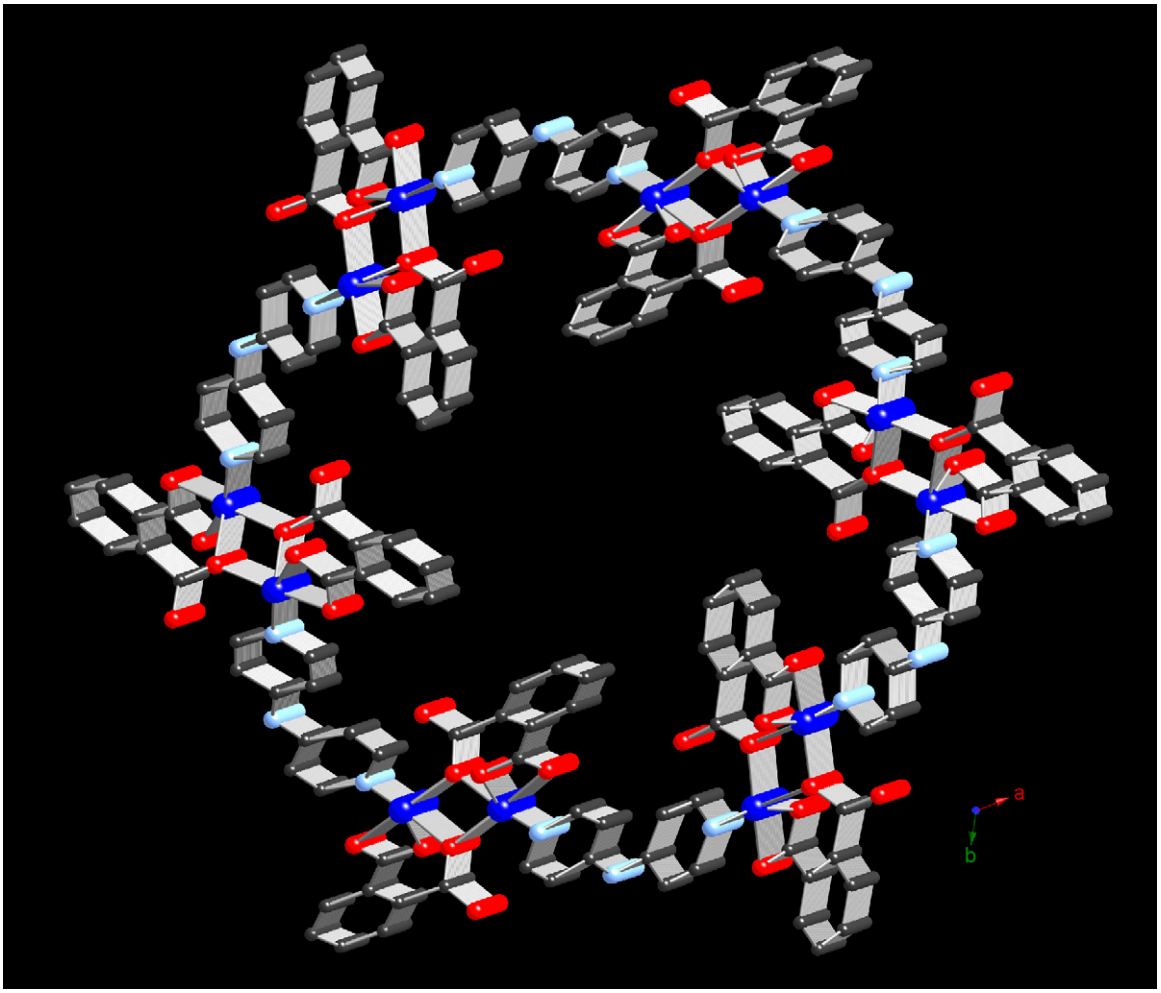

Fig. 40. A view down the *c* axis of **35**, illustrating the "star-shaped" solvent free cavity. Adapted from Ref. [54].

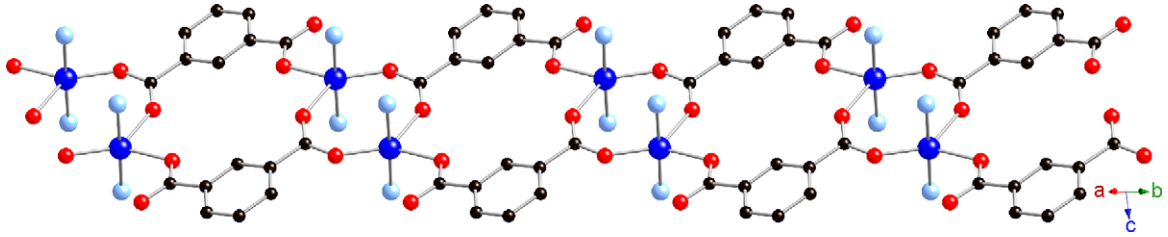

Fig. 41. One 1D $[Cu(ip)]_n$ motif within **36**. Adapted from Ref. [55].

uncommon non-interpenetrated $6^5 8$ coordination polymer topology [49].

3. Aromatic carboxylate dpa-containing coordination polymers

3.1. Aromatic monocarboxylate/dpa coordination polymers

Aromatic carboxylates have also proven useful as anionic structure directing components in transition metal/dpa coordination polymers [50]. $[Co(benzoate)_2(dpa)_2]$ (**32**) manifested dpa-linked 1D chains of cobalt atoms decorated by monodentate and chelating benzoate ligands and rarely seen monodentate dpa ligands (Fig. 36). As seen in other dpa coordination polymers in this study, the central amine units of the dpa ligands are involved in N–H···O hydrogen-bonding that connects the structural elements into higher dimensions. Hydrothermal reaction of cobalt nitrate, dpa, and phenylmalonic acid resulted in *in situ* decarboxylation and generation of $[Co_2(phac)_4(dpa)_2(H_2O)]$ (**33**, phac = phenylacetate). Complex **33** contains binuclear $[Co_2(phac)_4(H_2O)]$ units with both bridging and monodentate benzenecarboxylate ligands, which are linked into a 2D (4,4) rhomboid grid network (Fig. 37). A fit to a magnetic expression [51] for an interacting pair of $S = 3/2$ ions

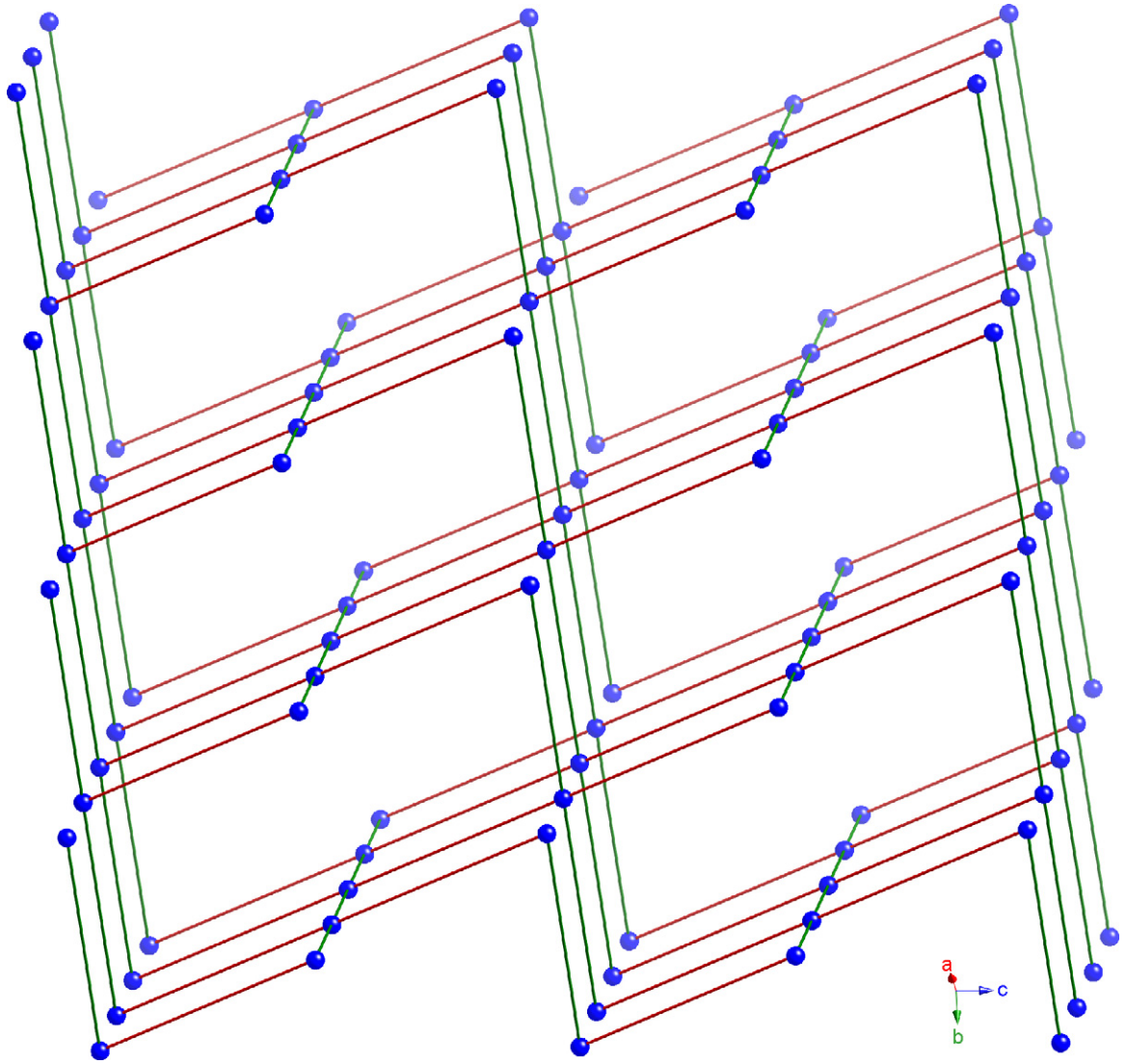

Fig. 42. Framework perspective of the non-interpenetrated $6^5 8$ topology structure of **36**. Adapted from Ref. [55].

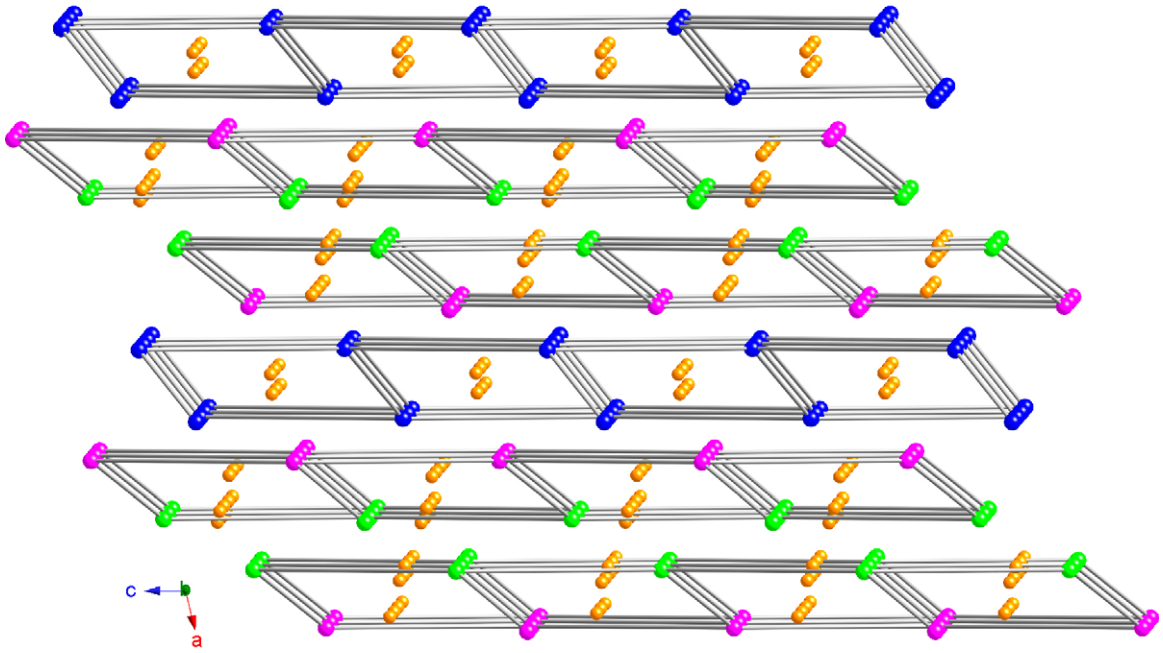

Fig. 43. *AA′B* layer stacking pattern of (6,3) herringbone grids in **37**.

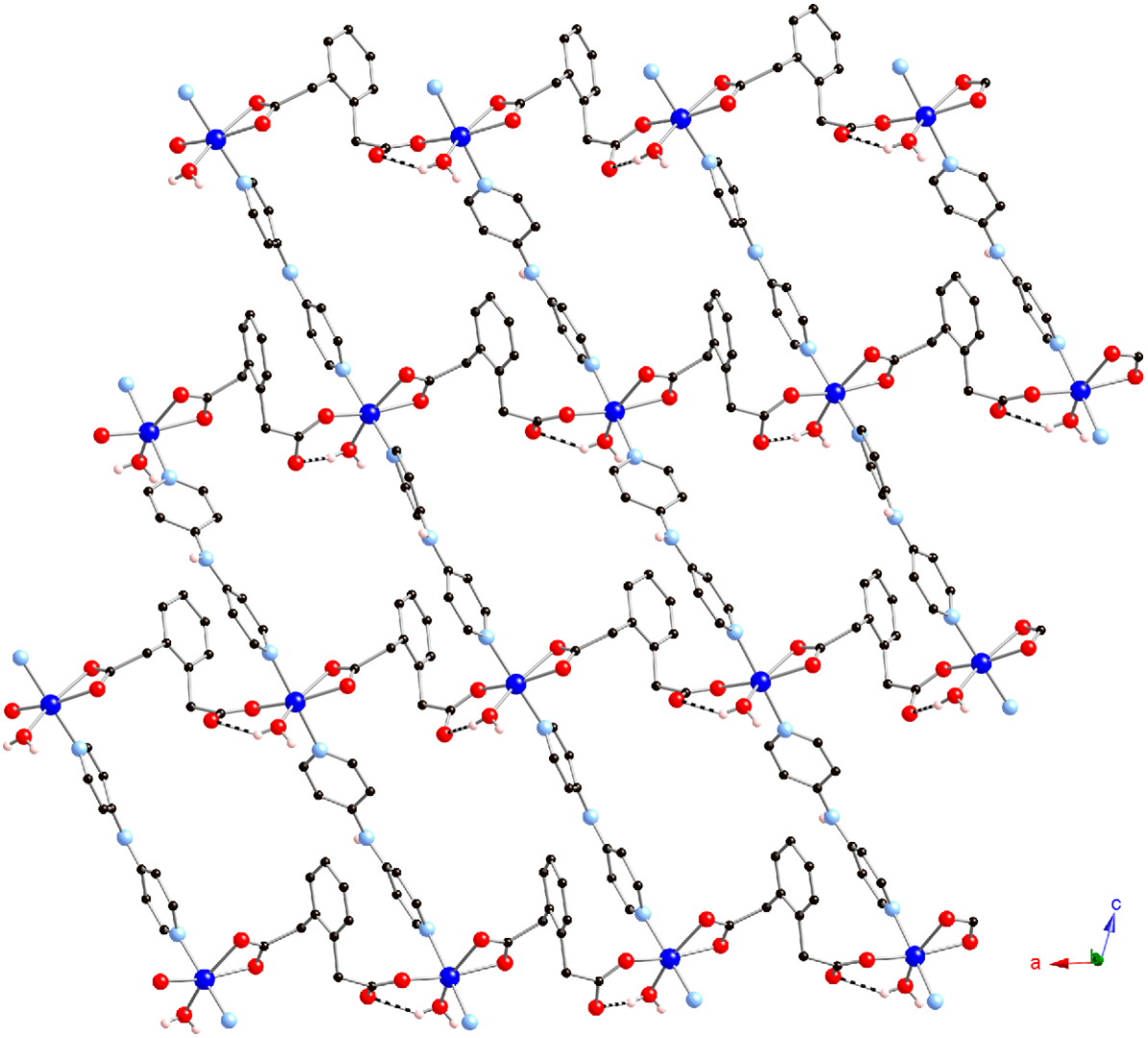

Fig. 44. A single (4,4) 2D grid in **38**. Intralayer hydrogen bonding is indicated as dashed lines.

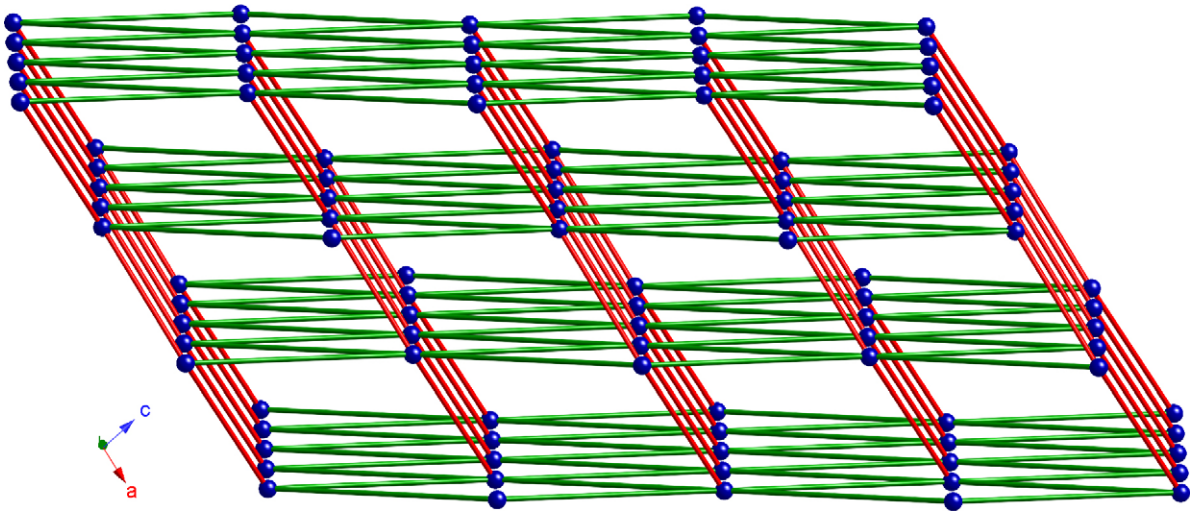

Fig. 45. Framework perspective of the canted α-Po 3D structure of **39**.

afforded $g = 2.65(3)$ and $J = -3.67(9)\,cm^{-1}$, indicative of modest antiferromagnetic coupling across the binuclear $[Co_2(phac)_4(H_2O)]$ kernels.

3.2. Aromatic dicarboxylate/dpa coordination polymers

Aromatic dicarboxylates are ubiquitous choices for the construction of coordination polymer solids because they can provide both charge balance and structural rigidity. Although numerous mixed-ligand coordination polymers incorporating both aromatic dicarboxylate isomers and 4,4′-bpy have been reported [7,52], the related chemistry based on dpa has remained unexplored until recently. The coordination polymer $\{[(pht)_2Co(dpa)Co(H_2O)_4(dpa)]\cdot H_2O\}_n$ (pht = phthalate, **34**) was the first mixed ligand aromatic dicarboxylate/dpa phase prepared in our laboratory [53]. This phase consists of alternating $[Co(H_2O)_4]^{2+}$ and $[Co(pht)_2]^{2-}$ subunits linked through dpa tethers into an undulating 1D chain (Fig. 38). Methyl group substitution at the 4-position of the phthalate ligand did not appreciably change the coordination polymer structure, dissimilar to the radical changes seen in the succinate systems discussed above.

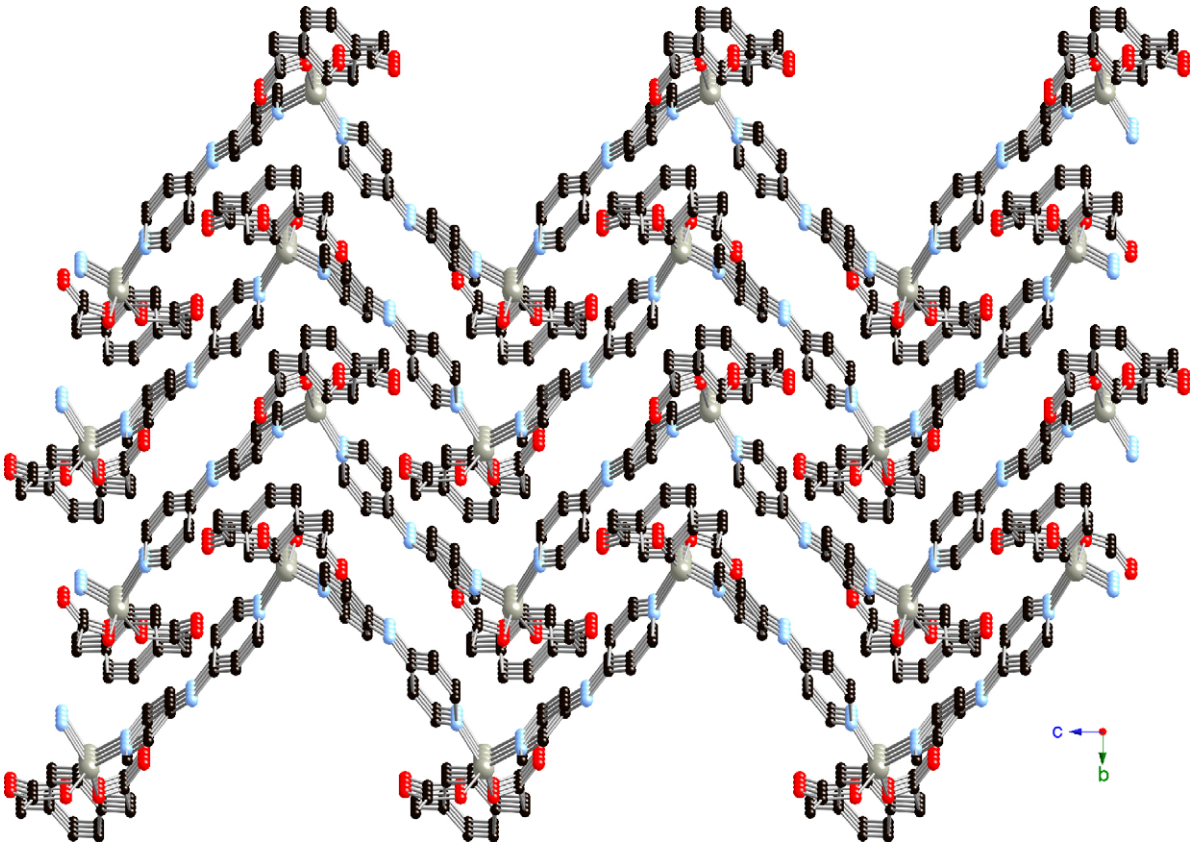

Fig. 46. The corrugated layers in **40**. Adapted from Ref. [60].

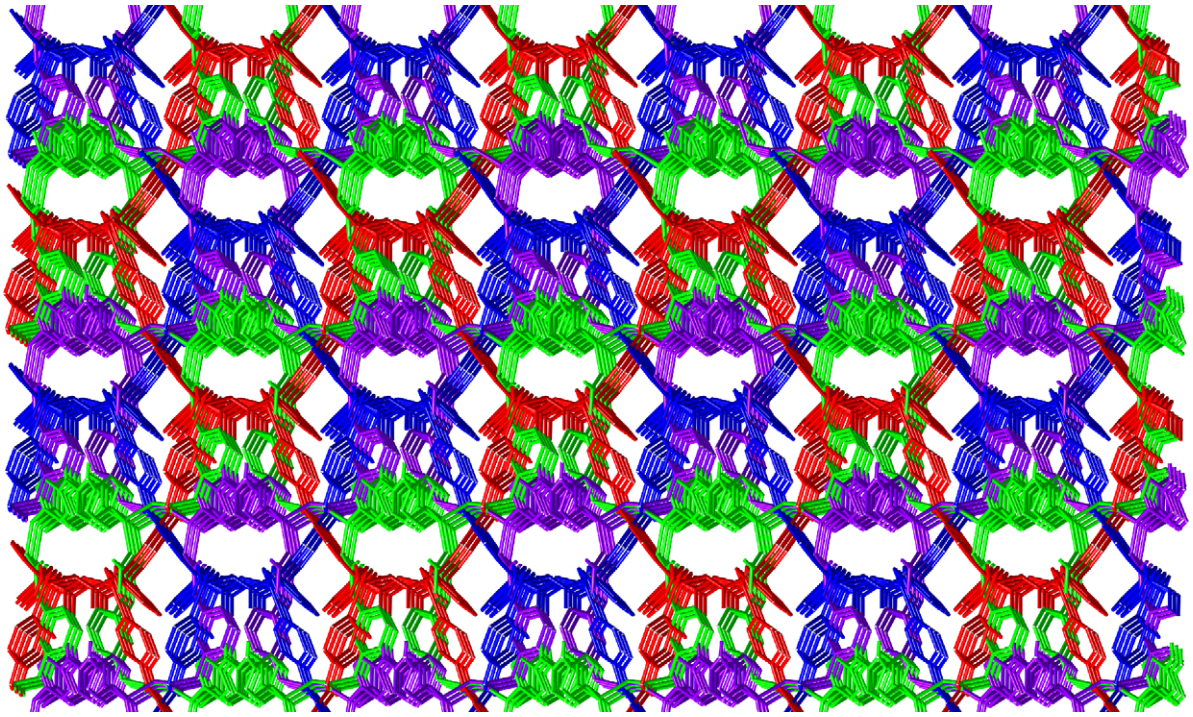

Fig. 47. The fourfold interpenetrated diamondoid network of **42**. Adapted from Ref. [60].

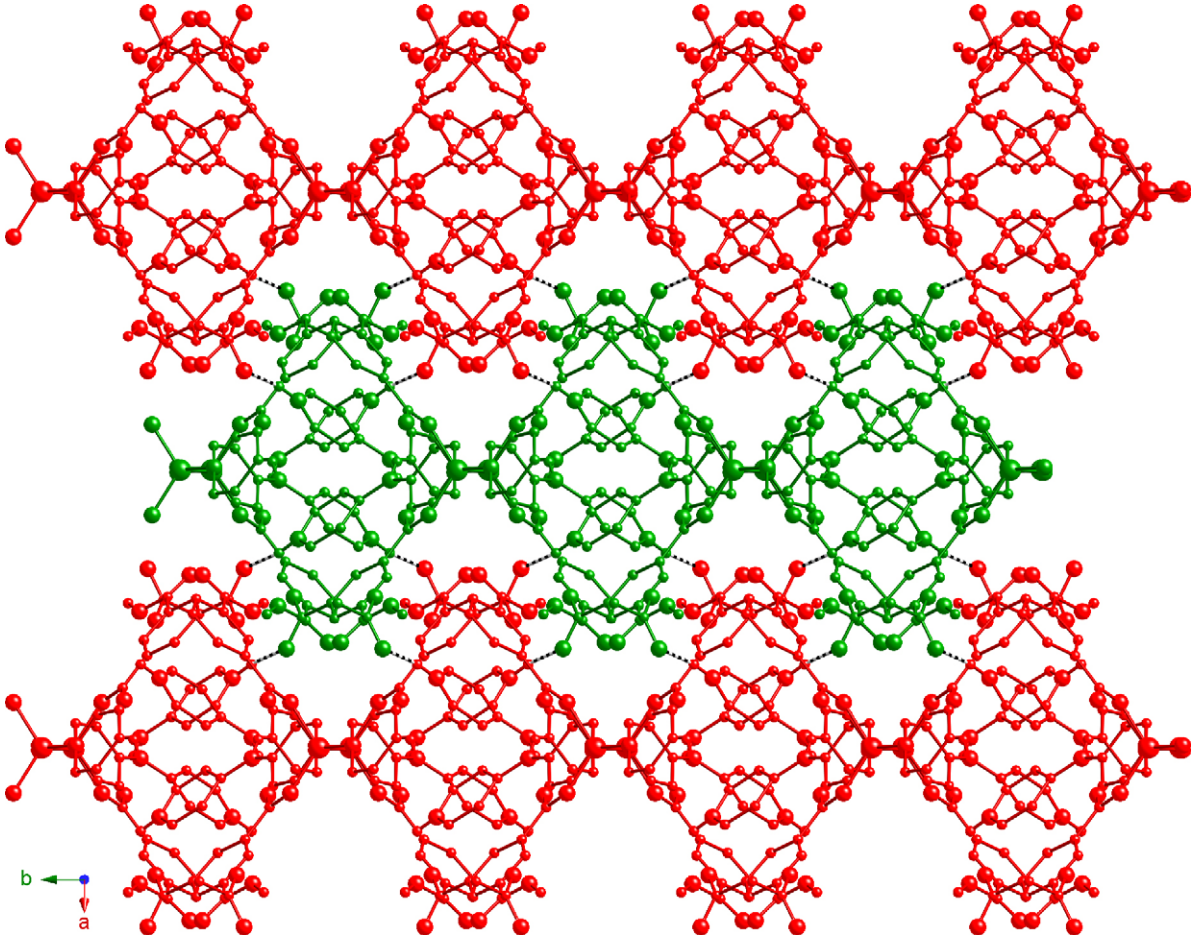

Fig. 48. Stacking of *pseudo*-2D layers in **43**.

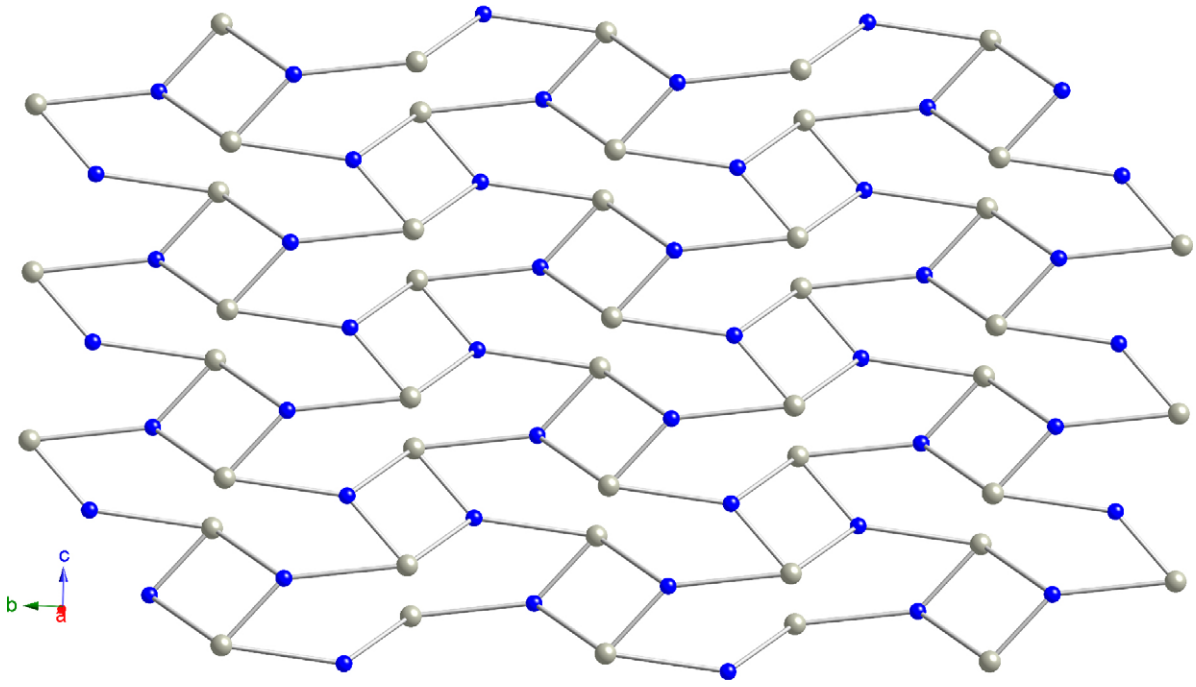

Fig. 49. The 4.8^2 topology 2D layer unit in **44**.

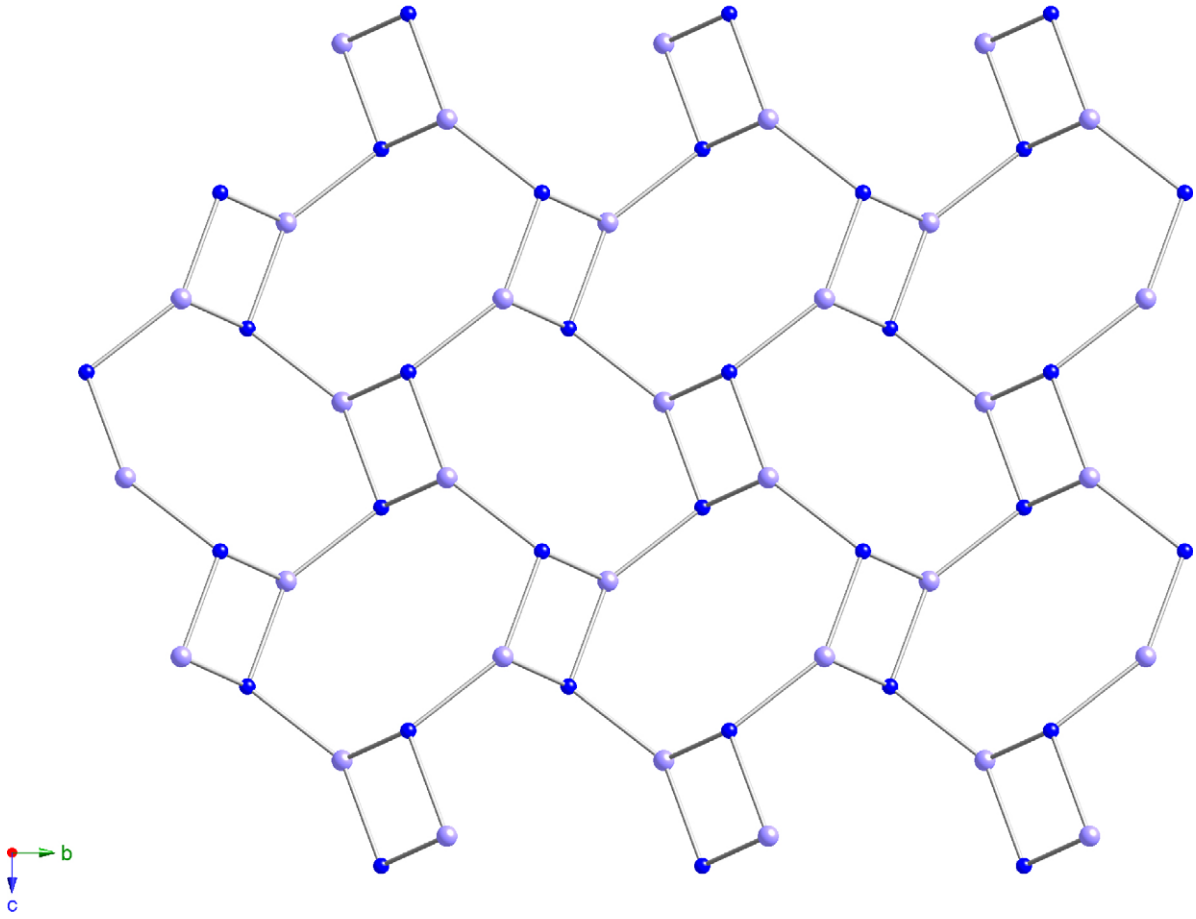

Fig. 50. The 4.8^2 topology 2D layer unit in **45**. The cavities within the layer are much larger than in **44** because of the presence of the $[Hdpa]^+$ ligands within the layer.

A crystalline copper phthalate/dpa phase also exhibited a 1D structure, but extremely different from that of **34** because of a shift from octahedral to square pyramidal coordination geometry. $\{[Cu_2(pht)_2(dpa)]\cdot H_2O\}_n$ (**35**) possesses 1D tubules formed by seven discrete "infinite" right-handed $[Cu_2O_2(dpa)]_n$ helices linked together by pht anions (Fig. 39) [54]. The aromatic rings of the pht ligands project into and away from the center of the tubule (Fig. 40). The water molecules of crystallization rest between neighboring tubules; the hydrophobic 1D "star-shaped" cavities within the ~8 Å wide tubules contain no co-crystallized species. Compound **35** exhibits hints of gas absorption selectivity. While no nitrogen or hydrogen uptake was observed at 77 K, three molar equivalents of ammonia (per Cu) were absorbed at room temperature, albeit with a concomitant partial loss of crystallinity.

Use of the isophthalate ligand in tandem with dpa resulted in a change away from 1D systems to a 3D structural morphology [55]. $\{[Cu(ip)(dpa)]\cdot 0.5H_2O\}_n$ (**36**) and its related cadmium derivative [56] contain parallel sets of identical 1D $[M(ip)]_n$ ribbons (Fig. 41) arranged orthogonally to each other. In turn these are strutted by dpa ligands to construct a non-interpenetrated 3D $CdSO_4$ structure type ($6^5 8$ topology) (Fig. 42). A fit of the variable temperature magnetic susceptibility data for **36** to the well-known Bleaney-Bowers expression [57] for an interacting pair of Cu^{2+} ions resulted in $g = 2.044(2)$ and $J = -1.93(5)\,cm^{-1}$, revealing a modicum of antiferromagnetic coupling across the eight-membered $\{CuOCO\}_2$ rings embedded within to the $[Cu(ip)]_n$ ribbons.

3.3. Flexible pendant-arm aromatic dicarboxylate/dpa coordination polymers

In contrast to the more commonly employed phthalate isomers, aromatic dicarboxylates containing flexible aliphatic carboxylate pendant-arm have seen seldom use in the design of coordination polymer solids. Reports of extended phases based on homophthalate (hmph), 1,2-phenylenediacetate (1,2-phda), 1,3-phenylenediacetate (1,3-phda) and 1,4-phenylenediacetate (1,4-phda) are very rare [58]. Recently we have reported the first coordination polymers incorporating these conformationally flexible ligands and dpa [59,60]. Synergistic structure direction on the part of metal coordination preferences, oxygen donor disposition, pendant-arm conformation and dpa-mediated hydrogen bonding permitted a very diverse collection of structural morphologies across six nickel or zinc coordination polymers.

$\{[Ni(hmph)(dpa)]\cdot 1.33H_2O\}_n$ (**37**) manifests a (6,3) herringbone style 2D coordination layer motif, in which each nickel atom is connected to three others, two through dpa, and one another through two bis(monodentate) hmph ligands [59]. Individual layers stack in an *AA′B* pattern (Fig. 43). Extension of one of the pendant arms by one methylene unit resulted in a change to the common (4,4)-grid structure of $[Ni(1,2\text{-phda})(dpa)(H_2O)]_n$ (**38**) (Fig. 44). A subsequent change in donor disposition from an *ortho* to a *meta* arrangement promoted the formation of $[Ni(1,3\text{-phda})(dpa)(\mu\text{-}H_2O)_{0.5}]_n$ (**39**), which manifests a non-interpenetrated canted primitive cubic type coordination polymer lattice (Fig. 45) constructed from dinuclear $\{Ni_2(\mu\text{-}H_2O)\}$ kernels linked into 3D through tethering 1,3-phda

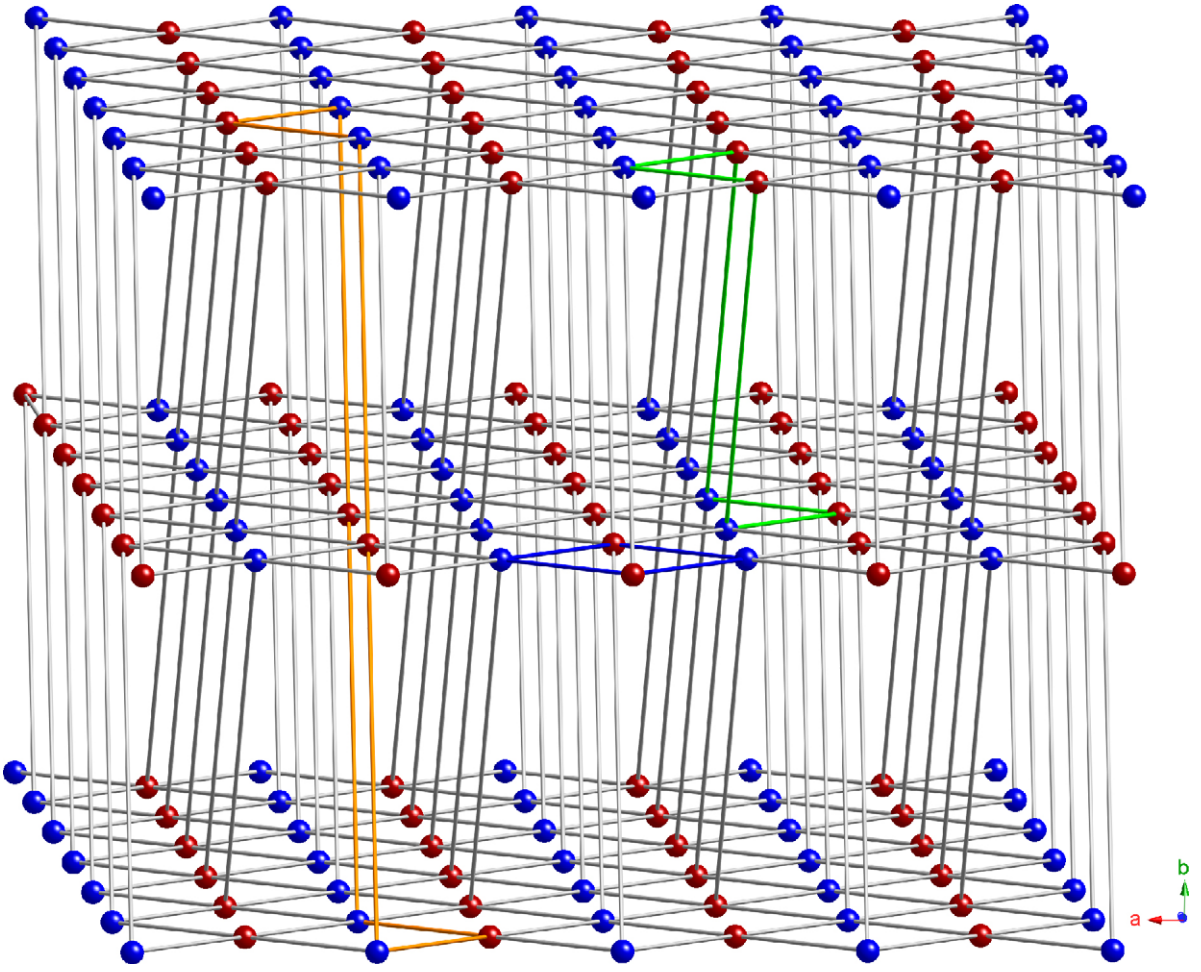

Fig. 51. The self-penetrated 6-connected $4^4 6^{10} 8$ topology supramolecular network in **46**. Four-, six-, and eight-membered circuits are highlighted. Adapted from Ref. [64].

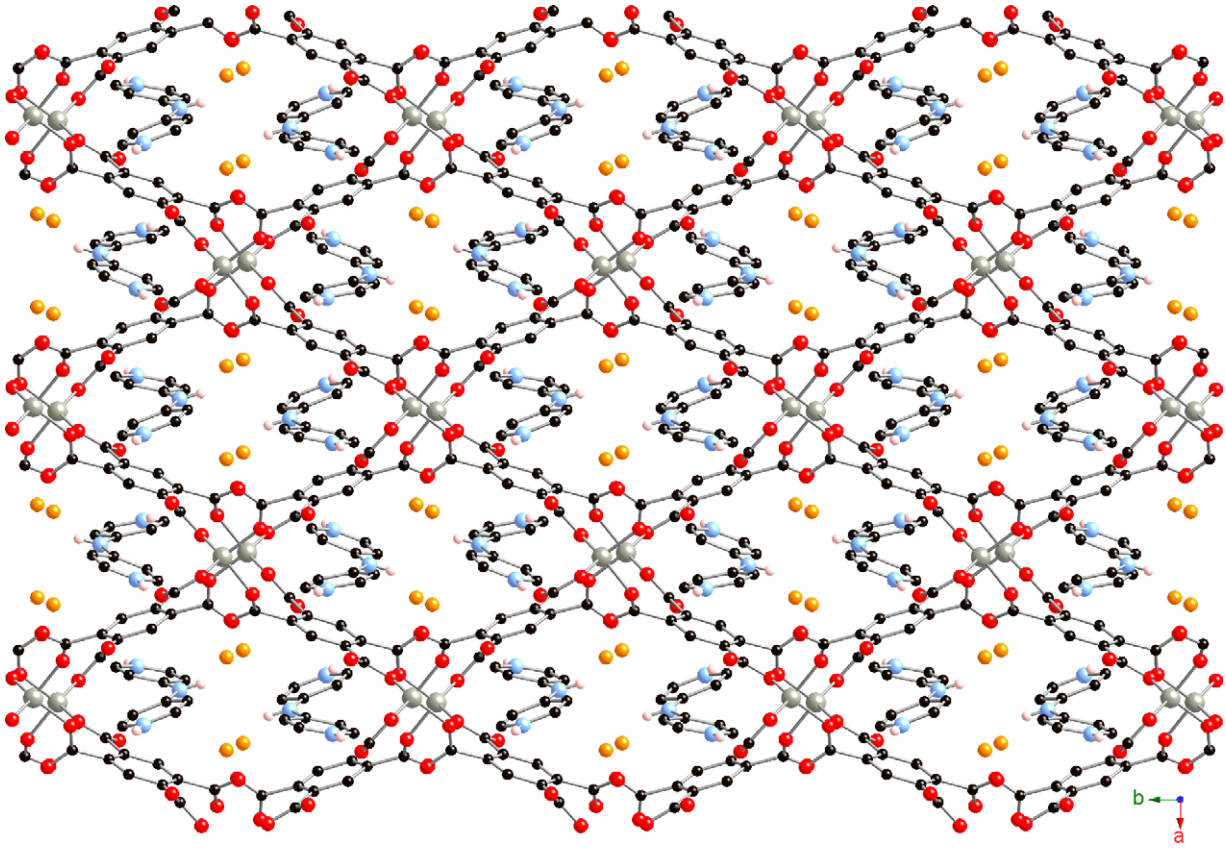

Fig. 52. The non-interpenetrated PtS network in **47**, with charge-balancing $[H_2dpa]^{2+}$ cations and unligated water molecules in the ellipsoidal cavities. Adapted from Ref. [64].

and dpa ligands. Analysis of the variable temperature magnetic susceptibility behavior of **39** indicated the presence of antiferromagnetic superexchange within its dinuclear units ($g = 2.290(2)$, $J = -4.21(2)\,cm^{-1}$).

Adjustment of the metal coordination preference from octahedral to tetrahedral afforded wholesale changes in coordination polymer morphology and dimensionality. $\{[Zn(1,4\text{-phda})(dpa)]\cdot H_2O\}_n$ (**40**) manifests a 2D corrugated layer morphology (Fig. 46) [60]. Both $\{[Zn(1,2\text{-phda})(dpa)]\cdot 2H_2O\}_n$ (**41**) and $[Zn(1,3\text{-phda})(dpa)]_n$ (**42**) contain 3D fourfold interpenetrated coordination polymer networks. However **41** possesses a $SrAl_2$ structure type similar to **7** and **10**, while the chiral material **42** adopts the diamond structure type (6^6 topology) (Fig. 47). Compound **42** is an uncommon example of a chiral diamondoid network with even-numbered interpenetration [61]. The varying morphologies thus reveal a significant structure-directing effect of the position of the acetate groups during self-assembly of these coordination polymers. Hydrogen bonding mechanisms imparted by the central amine group of the dpa ligand provide ancillary supramolecular structure-aggregating effects in all three of these cases. All three of these zinc phases **40**–**42** undergo blue-violet luminescence upon irradiation with ultraviolet light, showing intraligand π–π^* transitions similar to other d^{10} metal mixed-ligand coordination polymers.

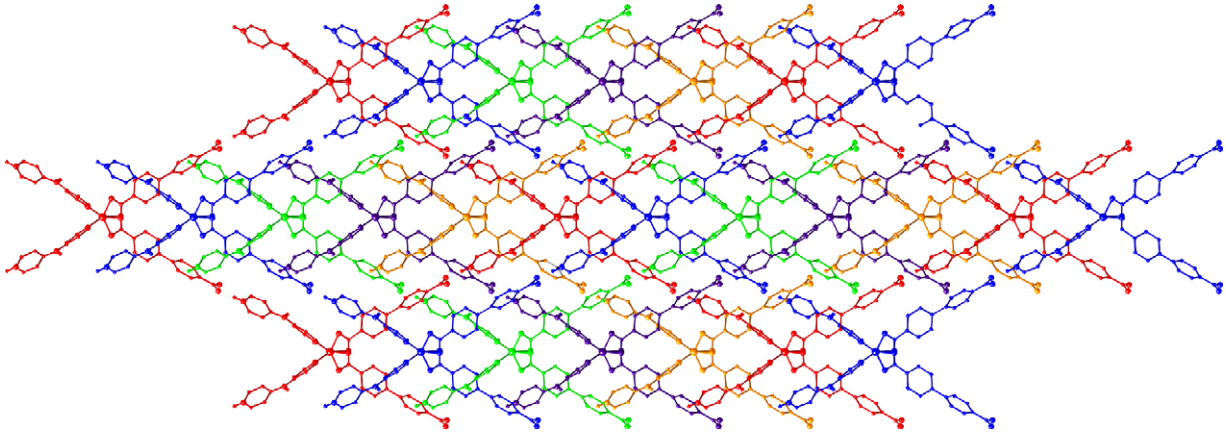

Fig. 53. Fivefold interpenetration of (4,4) supramolecular layers in **48**. Adapted from Ref. [68].

3.4. Aromatic multicarboxylate/dpa coordination polymers

Benzenetricarboxylate and benzenetetracarboxylate ligands have proven beneficial for the construction of a wide variety of coordination polymers, many of which display gas adsorptive behavior [62]. Thus we undertook to expand the scope of this genre of materials by incorporation of dpa. Depending on the pH of the reaction mixture, hydrothermal treatment of a zinc salt, dpa, and 1,3,5-benzenetricarboxylate (H_3btc) resulted in the formation of a 0D molecular species or a 2D coordination polymer [63]. Acidic conditions promoted the generation of the neutral molecular species $[Zn(Hbtc)_2(Hdpa)_2]$ (**43**), which aggregates into 2D hydrogen bonded layers (Fig. 48). Under more basic conditions, the 2D layered coordination polymer $[Zn(btc)(Hdpa)]_n$ (**44**) was obtained, which manifests covalent linkage of $[Zn(btc)(Hdpa)]_n$ serpentine chain motifs into 3-connected undulating 4.8^2 topology 2D layers (Fig. 49). $[Cd(btc)(H_2O)(Hdpa)]$ (**45**) displays a similar 4.8^2 layer topology to **44** (Fig. 50) but with significant adjustments imparted by the chelating carboxylate binding mode and aqua ligand necessitated by the preference for octahedral coordination at cadmium [63]. The extra width in the intralayer ellipsoidal cavities allows the $Hdpa^+$ ligands in **45** to lie largely within the confines of the layer, as opposed to projecting out of the layer as in **44**. The encapsulation of the sterically bulky $Hdpa^+$ ligands within the layers of **45** allow much closer interlayer contact than in **44**. All complexes in the series **43**–**45** luminescence strongly under ultraviolet exposure.

Utilization of 1,2,4,5-benzenetetracarboxylate (pyromellitate, pyro) in this system has generated one ion pair salt, $\{[Co(H_2O)_4(Hdpa)_2][pyro]\}$ (**46**), and one 3D network coordination polymer, $\{[H_2dpa][Zn(pyro)]\cdot 2H_2O\}_n$ (**47**) [64]. Complex **46** possesses individual $[Co(H_2O)_4(Hdpa)_2]^{4+}$ cations linked into supramolecular 2D (4,4) grid layers by hydrogen bonding between the aqua ligands and the unligated pyro anions. In turn these are conjoined into a 3D supramolecular lattice by charge-separated hydrogen bonding between the pendant, kinked, monodentate $Hdpa^+$ cations and pyro anions in neighboring layers. These interactions promote a supramolecular 3D structure with an exceptionally rare [65] self-penetrated 6-connected network with a $4^46^{10}8$ topology (Fig. 51). The anionic $[Zn(pyro)]_n^{2n-}$ framework in **47** creates a non-interpenetrated PtS network, with large incipient voids occupied by $[H_2dpa]^{2+}$ cations held in place via extensive hydrogen bonding pathways (Fig. 52).

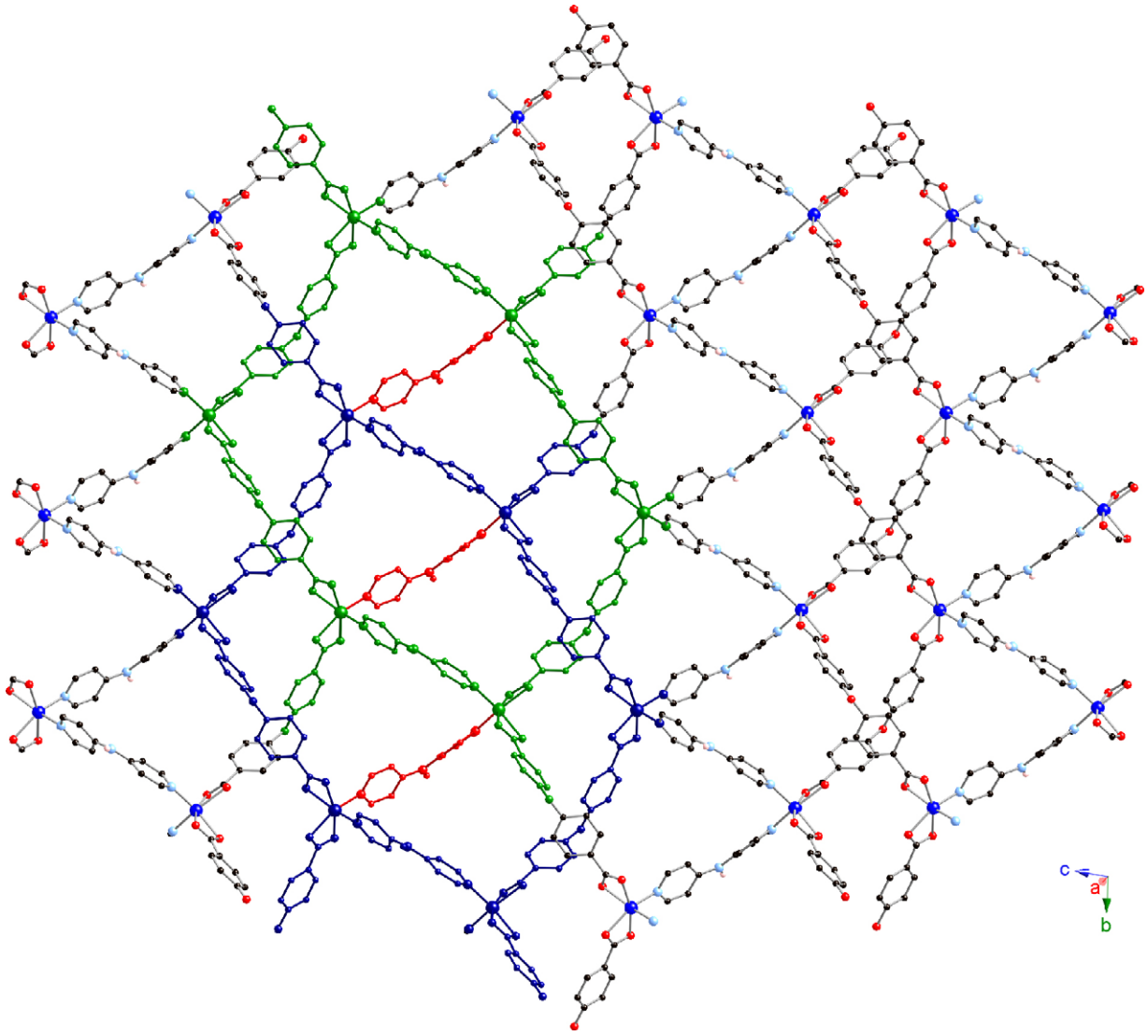

Fig. 54. The unique non-diamondoid 6^6 2D self-penetrated layer in **49** and **50**. Adapted from Ref. [69].

3.5. Diaromatic dicarboxylate/dpa coordination polymers

Several dual ligand coordination polymers with intriguing structural topologies have been prepared using the long-spanning di-aromatic dicarboxylates biphenyldicarboxylate (bpdc) [66] and oxy(bisbenzoate) (oba) [67]. Differences between the final coordination polymer structures can be ascribed to the straight (bpdc) or kinked (oba) nature of the dicarboxylate ligand. Hydrothermal combination of cobalt chloride, H_2bpdc, and dpa resulted in the neutral charge-separated complex $[Co(bpdc)_2(Hdpa)_2]$ (**48**) [68]. Individual molecules of **48** aggregate through strong $N–H^+\cdots O^-$ hydrogen bonding into parallel fivefold interpenetrated supramolecular (4,4)-grid layers (Fig. 53), representing the highest level of 2d + 2d → 2D parallel interpenetration observed to date.

$\{[Ni(oba)(dpa)]\cdot H_2O\}_n$ (**49**) and its isostructural cobalt analog (**50**) manifest a unique 2D self-penetrated lattice with a unique non-diamondoid 6^6 topology (Fig. 54) [69]. In this intriguing 4-connected network, $[Ni(oba)]_n$ double helices are linked to single strands within two other $[Ni(oba)]_n$ double helices through the dipodal dpa ligands. It appears that the kinked nature of both the oba and dpa ligands promotes the construction of the self-penetrated 2D covalent network in these materials. Both **49** and **50** exhibit extremely high-thermal robustness for 2D coordination polymers, with decomposition occurring only above 400 °C. This behavior is ascribed to the extra stability imparted by the self-entanglement of covalent bonds within their coordination polymer layers.

4. Conclusions

The use of the kinked donor disposition and hydrogen bonding capable diimine dpa instead of the standard 4,4′-bpy rigid rod tether has allowed the preparation of a wide scope of divalent metal carboxylate coordination polymer solids, many with intriguing, aesthetic, and unprecedented network topologies. Coordination geometry preferences at the divalent metal ion, conformational rigidity or flexibility and donor disposition within the multicarboxylate components, the kinked nitrogen donor arrangement within the ditopic dpa tether, and hydrogen bonding patterns provided by the central amine unit of the dpa all act together to institute the coordination polymer structures during self-assembly. In most cases, the coordination polymer topologies are significantly different from analog phases containing 4,4′-bpy. Additional steric encumbrance within the dicarboxylate components has shown to be another access point to enhanced structural diversity in this system. It is clear that the coordination polymer chemistry of dpa is far from exhausted. Efforts in this direction and synthetic explorations employing longer-spanning hydrogen-bonding capable ditopic dipyridyl ligands continue in our laboratory and will be reported in the literature in due course.

Acknowledgments

We thank Michigan State University and the donors of the American Chemical Society Petroleum Research Fund for funding this work. We acknowledge the efforts of the diligent undergraduate researchers who have worked on this project over the last 3 years: David Martin, Max Braverman, Matt Montney, Kya Brown, Lindsey Johnston, Niral Patel, Eric Shyu and Subha Mallika Krishnan. We thank Ronald Supkowski (King's College, Wilkes-Barre, PA) for thermogravimetric analysis, Rui Huang (MSU) for elemental analysis and Dr. Wayne Ouellette (Syracuse University) for gas absorption studies.

References

[1] (a) H. Li, M. Eddaoudi, M. O'Keeffe, O.M. Yaghi, Nature 403 (2000) 276;
(b) R. Matsuda, R. Kitaura, S. Kitagawa, Y. Kubota, R.U. Belosludov, T.C. Kobayashi, H. Sakamoto, T. Chiba, M. Takata, Y. Kawazoe, Y. Mita, Nature 436 (2005) 238;
(c) L. Pan, D. Holson, L.R. Ciemnolonski, R. Heddy, J. Li, Angew. Chem., Int. Ed. 46 (2006) 616;
(d) N.L. Rosi, J. Eckert, M. Eddaoudi, D.J. Vodak, J. Kim, M. O'Keeffe, O.M. Yaghi, Science 300 (2003) 1127;
(e) M. Dinca, A.F. Yu, J.R. Long, J. Am. Chem. Soc. 128 (2006) 8904;
(f) G. Ferey, M. Latroche, C. Serre, F. Millange, T. Loiseau, A. Percheron-Guegan, Chem. Commun. (2003) 2976;
(g) X. Zhao, B. Xiao, A.J. Fletcher, K.M. Thomas, D. Bradshaw, M.J. Rosseinsky, Science 306 (2004) 1012;
(h) X. Lin, J. Jia, P. Hubberstey, M. Schröder, N.R. Champness, CrystEngComm 9 (2007) 438.
[2] (a) J.S. Seo, D. Whang, H. Lee, S.I. Jun, J. Oh, Y.J. Jeon, K. Kim, Nature 404 (2000) 982;
(b) B. Chen, C. Liang, J. Yang, D.S. Contreras, Y.L. Clancy, E.B. Lobkovsky, O.M. Yaghi, S. Dai, Angew. Chem., Int. Ed. 45 (2006) 1390.
[3] (a) Q.R. Fang, G.S. Zhu, M. Xue, J.Y. Sun, S.L. Qiu, Dalton Trans. (2006) 2399;
(b) X.M. Zhang, M.L. Tong, H.K. Lee, X.M. Chen, J. Solid State Chem. 160 (2001) 118;
(c) O.M. Yaghi, H. Li, T.L. Groy, Inorg. Chem. 36 (1997) 4292.
[4] (a) N. Guillou, P.M. Forster, Q. Gao, J.S. Chang, M. Nogues, S.E. Park, A.K. Cheetham, G. Ferey, Angew. Chem., Int. Ed. 40 (2001) 2831;
(b) C.D. Wu, A. Hu, L. Zhang, W. Lin, J. Am. Chem. Soc. 127 (2005) 8940;
(c) H. Han, S. Zhang, H. Hou, Y. Fan, Y. Zhu, Eur. J. Inorg. Chem. 8 (2006) 1594;
(d) W. Mori, S. Takamizawa, C.N. Kato, T. Ohmura, T. Sato, Micropor. Mesopor. Mater. 73 (2004) 15.
[5] (a) S. Zang, Y. Su, Y. Li, Z. Ni, Q. Meng, Inorg. Chem. 45 (2006) 174;
(b) L. Wang, M. Yang, G. Li, Z. Shi, S. Feng, Inorg. Chem. 45 (2006) 2474;
(c) S. Wang, Y. Hou, E. Wang, Y. Li, L. Xu, J. Peng, S. Liu, C. Hu, New J. Chem. 27 (2003) 1144.
[6] (a) J. Tao, J.X. Shi, M.L. Tong, X.X. Zhang, X.M. Chen, Inorg. Chem. 40 (2001) 6328;
(b) J. Tao, M.L. Tong, J.X. Shi, X.M. Chen, S.W. Ng, Chem. Commun. (2000) 2043;
(c) J.C. Dai, X.T. Wu, Z.Y. Fu, C.P. Cui, S.M. Hu, W.X. Du, L.M. Wu, H.H. Zhang, R.Q. Sun, Inorg. Chem. 41 (2002) 1391;
(d) W. Chen, J.Y. Wang, C. Chen, Q. Yue, H.M. Yuan, J.S. Chen, S.N. Wang, Inorg. Chem. 42 (2003) 944;
(e) N. Hao, E. Shen, Y.B. Li, E.B. Wang, C.W. Hu, L. Xu, Eur. J. Inorg. Chem. (2004) 4102.
[7] (a) W.-G. Lu, C.-Y. Su, T.-B. Lu, L. Jiang, J.-M. Chen, J. Am. Chem. Soc. 128 (2006) 34;
(b) S. Horike, R. Matsuda, S. Kitagawa, Stud. Surf. Sci. Catal. 156 (2005) 725;
(c) C. Qin, X.-L. Wang, Y.-G. Li, E.-B. Wang, Z.-M. Su, L. Xu, R. Clerac, Dalton Trans. (2005) 2609;
(d) Y.-Q. Zheng, E.-R. Ying, Polyhedron 24 (2005) 397;
(e) S.K. Ghosh, J. Ribas, P.K. Bharadwaj, Cryst. Growth Des. 5 (2005) 623;
(f) X.Z. Sun, Y.F. Sun, B.H. Ye, X.M. Chen, Inorg. Chem. Commun. 6 (2003) 1412;
(g) K. Biradha, M. Sarkar, L. Rajput, Chem. Commun. (2006) 4169;
(h) H.W. Roesky, M. Andruh, Coord. Chem. Rev. 236 (2003) 91.
[8] (a) Y.M. Dai, E. Ma, E. Tang, J. Zhang, J.Z. Li, X.D. Huang, Y.G. Yao, Cryst. Growth Des. 5 (2005) 1313;
(b) L. Xu, G.C. Guo, B. Liu, M.S. Wang, J.S. Huang, Inorg. Chem. Commun. 7 (2004) 1145.
[9] Y.Q. Zheng, Z.P. Kong, Z. Anorg, Allgem. Chem. 629 (2003) 1469.
[10] M.J. Zaworotko, Cryst. Growth Des. 7 (2007) 4.
[11] (a) P. Ren, W. Shi, P. Cheng, Cryst. Growth Des. 8 (2008) 1097;
(b) D.T. de Lill, C.L. Cahill, Cryst. Growth Des. 7 (2007) 2390;
(c) C.C. Wang, S.C. Dai, H.W. Lin, G.H. Lee, H.S. Sheu, Y.H. Lin, H.L. Tasi, Inorg. Chim. Acta 360 (2007) 4058;
(d) C.Y. Sun, J. Zhou, L.P. Jin, J. Mol. Struct. 843 (2007) 95;
(e) J.J. Wang, L. Gou, H.M. Hu, Z.X. Han, D.S. Li, G.L. Xue, M.L. Yang, Q.Z. Shi, Cryst. Growth Des. 7 (2007) 1514;
(f) S. Wang, H. Xing, Y. Li, J. Bai, Y. Pan, M. Scheer, X. You, Eur. J. Inorg. Chem. (2006) 3041.
[12] (a) P.S. Mukherjee, S. Konar, E. Zangrando, T. Mallah, J. Ribas, N.R. Chaudhuri, Inorg. Chem. 42 (2003) 2695;
(b) J.Q. Sha, J. Peng, H.S. Liu, J. Chen, A.X. Tian, P.P. Zhang, Inorg. Chem. 46 (2007) 11183;
(c) M. Nagarathinam, J.J. Vittal, Chem. Commun. (2008) 438;
(d) X.Y. Wang, Z.M. Wang, S. Gao, Chem. Commun. (2007) 1127;
(e) M. Nagarathinam, J.J. Vittal, Angew. Chem., Int. Ed. 45 (2006) 4337.
[13] (a) C.C. Correa, R. Diniz, L.H. Chagas, B.L. Rodrigues, M.I. Yoshida, W.M. Teles, F.C. Machado, L.F.C. De Oliveira, Polyhedron 26 (2007) 989;
(b) S.M. Chu, J. Zhang, C.Z. Lu, CrystEngComm 9 (2007) 390;
(c) X. Wang, H. Lin, Y. Bi, B. Chen, G. Liu, J. Solid State Chem. 181 (2008) 556;
(d) J.Q. Liu, Y.Y. Wang, P. Liu, W.P. Wu, Y.P. Wu, X.R. Zeng, F. Zhong, Q.Z. Shi, Inorg. Chem. Commun. 10 (2007) 343.
[14] R. Horikoshi, T. Mochida, Coord. Chem. Rev. 250 (2006) 2595.
[15] K. Biradha, M. Fujita, Dalton Trans. (2000) 3805.
[16] P.J. Zapf, R.L. LaDuca, R.S. Rarig, K.M. Johnson, J. Zubieta, Inorg. Chem. 37 (1998) 3411.

[17] (a) R.L. LaDuca, R.S. Rarig, J. Zubieta, Inorg. Chem. 40 (2001) 607;
(b) D.J. Chesnut, D. Hagrman, P.J. Zapf, R.P. Hammond, R. LaDuca, R.C. Haushalter, J. Zubieta, Coord. Chem. Rev. 192 (1999) 737.
[18] R.L. LaDuca, R.C. Finn, J.A. Zubieta, J. Chem. Soc., Chem. Commun. (1999) 1669.
[19] D. Hagrman, C.J. Warren, R.C. Haushalter, C. Seip, C.J. O'Connor, R.S. Rarig, K.M. Johnson, R.L. LaDuca, J. Zubieta, Chem. Mater. 10 (1998) 3294.
[20] R. La Duca, M. Laskoski, J. Zubieta, J. Chem. Soc., Dalton Trans. (1999) 3467.
[21] D.B. Cordes, L.R. Hanton, M.D. Spicer, Cryst. Growth Des. 7 (2007) 328.
[22] D.B. Cordes, L.R. Hanton, M.D. Spicer, J. Mol. Struct. 796 (2006) 146.
[23] D.B. Cordes, L.R. Hanton, M.D. Spicer, Inorg. Chem. 45 (2006) 7651.
[24] M.R. Montney, R.M. Supkowski, R.L. LaDuca, Polyhedron 27 (2008) 2997.
[25] Y. Rodriguez-Martin, M. Hernandez-Molina, J. Sanchiz, C. Ruiz-Perez, F. Lloret, M. Julve, Dalton Trans. (2003) 2359.
[26] M.E. Lines, J. Phys. Chem. Solids 31 (1970) 101.
[27] M.R. Montney, R.L. LaDuca, Inorg. Chem. Commun. 10 (2007) 1518.
[28] A.W. Addison, T.N. Rao, J. Chem. Soc., Dalton Trans. (1984) 1349.
[29] H.-Y. Bie, J.-H. Yu, K. Zhao, J. Lu, L.-M. Duan, J.-Q. Xu, J. Mol. Struct. 741 (2005) 77.
[30] Y. Rodriguez-Martin, M. Hernandez-Molina, F.S. Delgado, J. Pasan, C. Ruiz-Perez, J. Sanchiz, F. Lloret, M. Julve, CrystEngComm 4 (2002) 440.
[31] G.A. Baker, G.S. Rushbrooke, H. Gilbert, Phys. Rev. A 135 (1964) 1272.
[32] J. Pasan, F.S. Delgado, Y. Rodriguez-Martin, M. Hernandez-Molina, C. Ruiz-Perez, J. Sanchiz, F. Lloret, M. Julve, Polyhedron 22 (2003) 2143.
[33] M.R. Montney, S. Mallika Krishnan, N.M. Patel, R.M. Supkowski, R.L. LaDuca, Cryst. Growth Des. 7 (2007) 1145.
[34] R.S. Rarig, R.L. LaDuca, J. Zubieta, Inorg. Chim. Acta 292 (1999) 131.
[35] E. Shyu, R.L. LaDuca, Polyhedron 28 (2009), doi:10.1016/j.poly.2008.12.026, in press.
[36] L.-S. Long, Y.-R. Wu, R.-B. Huang, L.-S. Zheng, Inorg. Chem. 43 (2004) 3798.
[37] K.A. Brown, D.P. Martin, R.M. Supkowski, R.L. LaDuca, CrystEngComm 10 (2008) 846.
[38] E.M. Lyons, M.A. Braverman, R.M. Supkowski, R.L. LaDuca, Inorg. Chem. Commun. 11 (2008) 858.
[39] W. Hiller, J. Strähle, A. Datz, M. Hanack, W.E. Hatfield, L.E. ter Haar, P. Gutlich, J. Am. Chem. Soc. 106 (1984) 329.
[40] K.A. Brown, D.P. Martin, R.M. Supkowski, R.L. LaDuca, CrystEngComm 10 (2008) 1305.
[41] M.R. Montney, R.J. Staples, R.M. Supkowski, R.L. LaDuca, J. Solid State Chem. 182 (2009) 8.
[42] D.P. Martin, M.R. Montney, R.M. Supkowski, R.L. LaDuca, Cryst. Growth Des. 8 (2008) 3091.
[43] M.R. Montney, S. Mallika Krishnan, R.M. Supkowski, R.L. LaDuca, Inorg. Chem. 46 (2007) 7362.
[44] E. Shyu, R.L. LaDuca, Cryst. Growth Des., submitted for publication.
[45] S. Mallika Krishnan, M.R. Montney, R.L. LaDuca, Polyhedron 27 (2008) 821.
[46] L. Infantes, S. Motherwell, CrystEngComm 4 (2002) 454.
[47] S. Mallika Krishnan, R.M. Supkowski, R.L. LaDuca, J. Mol. Struct. 891 (2008) 423.
[48] S. Mallika Krishnan, R.M. Supkowski, R.L. LaDuca, Cryst. Growth Des. 9 (2009) 358.
[49] E. Shyu, R.L. LaDuca, Polyhedron, submitted for publication.
[50] L.L. Johnson, K.A. Brown, D.P. Martin, R.L. LaDuca, J. Mol. Struct. 882 (2008) 80.
[51] O. Khan, Molecular Magnetism, VCH Publishers, New York, 1993.
[52] X.-Z. Sun, Y.-F. Sun, B.-H. Ye, X.-M. Chen, Inorg. Chem. Commun. 6 (2003) 1412.
[53] M.A. Braverman, R.M. Supkowski, R.L. LaDuca, Inorg. Chim. Acta 360 (2007) 2353.
[54] M.A. Braverman, R.L. LaDuca, Inorg. Chem., submitted for publication.
[55] P.J. Szymanski, M.A. Braverman, R.L. LaDuca, Inorg. Chim. Acta, submitted for publication.
[56] E. Shyu, M.A. Braverman, R.M. Supkowski, R.L. LaDuca, Inorg. Chim. Acta 362 (2009), doi:10.1016/j.ica.2008.10.015, in press.
[57] B. Bleaney, K.D. Bowers, Proc. R. Soc. Lond., Ser. A 214 (1952) 451.
[58] (a) L. Pan, K.M. Adams, H.E. Hernandez, X. Wang, C. Zheng, Y. Hattari, K. Kaneko, J. Am. Chem. Soc. 125 (2003) 3062;
(b) Y.-F. Zhou, R.-H. Wang, B.-L. Wu, R. Cao, M.-L. Hong, J. Mol. Struct. 697 (2004) 73;
(c) J. Zhou, C. Sun, J. Linpei, J. Mol. Struct. 832 (2007) 55.
[59] M.A. Braverman, R.J. Staples, R.M. Supkowski, R.L. LaDuca, Polyhedron 27 (2008) 2291.
[60] M.A. Braverman, R.L. LaDuca, Cryst. Growth Des. 7 (2007) 2343.
[61] O.R. Evans, W. Lin, Acc. Chem. Res. 35 (2002) 511.
[62] (a) M. Eddaoudi, H. Li, O.M. Yaghi, J. Am. Chem. Soc. 122 (2000) 1391;
(b) O.M. Yaghi, H. Li, T.L. Groy, J. Am. Chem. Soc. 118 (1996) 9096;
(c) O.M. Yaghi, C.E. Davis, G. Li, H. Li, J. Am. Chem. Soc. 119 (1997) 2861;
(d) Q. Fang, G. Zhu, M. Xue, J. Sun, F. Sun, S. Qiu, Inorg. Chem. 45 (2006) 3582;
(e) H. Kumagai, K.W. Chapman, C.J. Kepert, M. Kurmoo, Polyhedron 22 (2003) 1921;
(f) Y.-H. Wen, Q.-W. Zhang, Y.-H. He, Y.-L. Feng, Inorg. Chem. Commun. 10 (2007) 543;
(g) A. Majumber, V. Gramlich, G.M. Rosair, S.R. Batten, J.D. Masuda, M.S. El Fallah, J. Ribas, J.-P. Sutter, C. Desplanches, S. Mitra, Cryst. Growth Des. 6 (2006) 2355;
(h) C. Ruiz-Perez, P. Lorenzo-Luis, M. Hernandez-Molina, M.M. Laz, F.S. Delgado, P. Gili, M. Julve, Eur. J. Inorg. Chem. (2004) 3873.
[63] M.A. Braverman, R.M. Supkowski, R.L. LaDuca, J. Solid State Chem. 180 (2007) 1852.
[64] M.A. Braverman, R.L. LaDuca, CrystEngComm 10 (2008) 117.
[65] H.-L. Sun, S. Gao, B.-Q. Ma, S.R. Batten, CrystEngComm 6 (2004) 579.
[66] (a) S.H. Kim, H.S. Huh, S.W. Lee, J. Mol. Struct. 841 (2007) 78;
(b) L.J. Zhou, Y.Y. Wang, C.H. Zhou, C.J. Wang, Q.Z. Shi, S.M. Peng, Cryst. Growth Des. 7 (2007) 300.
[67] X.L. Wang, C. Qin, E.B. Wang, Y.-G. Li, Z.-M. Su, L. Xu, L. Carlucci, Angew. Chem., Int. Ed. 44 (2005) 5824.
[68] M.R. Montney, R.M. Supkowski, R.L. LaDuca, CrystEngComm 10 (2008) 111.
[69] D.P. Martin, R.M. Supkowski, R.L. LaDuca, Inorg. Chem. 46 (2007) 7917.